DEPARTAMENTO DE CIÊNCIAS DA VIDA

FACULDADE DE CIÊNCIAS E TECNOLOGIA
UNIVERSIDADE DE COIMBRA

Ataxin-3 aggregation and its impact on membrane destabilization

João Carlos Ribas de Almeida

2010

DEPARTAMENTO DE CIÊNCIAS DA VIDA

FACULDADE DE CIÊNCIAS E TECNOLOGIA
UNIVERSIDADE DE COIMBRA

Ataxin-3 aggregation and its impact on membrane destabilization

Dissertação apresentada à Universidade de Coimbra para cumprimento dos requisitos necessários à obtenção do grau de Mestre em Biologia Celular e Molecular. O trabalho foi realizado sob a orientação científica da Professora Doutora Sandra de Macedo Ribeiro (Instituto de Biologia Molecular e Celular) e supervisão da Professora Doutora Maria Conceição Pedroso Lima (Universidade de Coimbra).

João Carlos Ribas de Almeida

2010

(…) a verdadeira fecundidade de um poeta não consiste no número dos seus versos, mas bem mais na extensão dos seus efeitos.

Paul Valéry

Agradecimentos

Gostaria de começar por agradecer à minha orientadora, Professora Doutora Sandra de Macedo-Ribeiro, por me ter acolhido no seu grupo de investigação, por me ter ensinado boa parte do que aprendi, por exigir de mim sempre mais e melhor, o que me fez crescer ao longo deste percurso. Não poderia deixar também de agradecer à Professora Doutora Conceição Pedroso-Lima, minha co-orientadora, assim como ao Professor Doutor Henrique Faneca, pelos contributos valiosos e pela disponibilidade em me receber no seu laboratório. Colaborações são, na minha opinião, o futuro da ciência, e por isso agradeço-vos. Agradeço também ao Professor Doutor Pedro Pereira, co-líder do grupo de Cristalografia de Proteínas, por toda a ajuda fornecida.

Durante o ano o trabalho foi imenso e desgastante, mas todos os dias foram repletos de momentos que não esquecerei. Muito obrigado a todas as pessoas com quem trabalhei pela boa disposição, conversas e por simpaticamente aturarem as minhas parvalheiras, em especial Isabel Abreu, Tatiana Barros, Diana Pires, Ana Figueiredo, Joana Santos, Simon Lee, Bruno Almeida, Alexandra Marques e Maria Macedo. Não me esquecerei, no entanto, de agradecer à Doutora Gabriela Mazovek pela confiança que depositou em mim e por me fazer não ter medo de sujar as mãos.

Pela grande simpatia e preciosa ajuda técnica, gostaria de agradecer ao Doutor Frederico Silva e Dr. Rui Fernandes.

Gostaria também de agradecer a toda a malta do Mestrado em Biologia Celular e Molecular, pela amizade, pelas noitadas e jantaradas, e por darem às noites de Coimbra o brilho que tantos estudantes falam! Um agradecimento especial também para quem me acolheu de boa vontade quando trabalhei em Coimbra, e para aqueles a quem as palavras não chegariam.

Um muito obrigada à minha Avó Emília, ao meu tio Manuel e minha tia Manuela, por todos os dias me meterem um prato na mesa, e deixarem os meus

colegas de laboratório verdadeiramente cheios de inveja por não almoçarem também a comidinha da avó!

Aos meus pais, Joaquim e Isabel, ao meu irmão Daniel e à Mónica agradeço todo o apoio... e espero em breve ter um sobrinho! Agradeço também ao meu tio/primo Manuel, pela grande prenda que é um Mac, e que em bastante ajudou a minha produtividade!

Agradeço às forças da Natureza por me proporcionarem umas belas ondas durante o ano, e me fazerem esquecer, por momentos, todos os problemas!

Finalmente, Sofia, obrigado por (...), e tudo e tudo e tudo!

Table of Contents

Abbreviations

aa	amino acid
Aβ	amyloid beta
AD	Alzheimer's disease
AFM	Atomic Force Microscopy
Atx3	Ataxin-3
bp	base pairs
CAG	three nucleotides (Cytosine, Adenine, Guanine)
CD	circular dichroism
Cfu	colony-forming unit
Chol	cholesterol
CKII	casein kinase II
CR	Congo red
CRM1	chromosome region maintenance 1
DMPC	L-α-dimuristoylphosphoglycerolcholine
DPH	1-6-diphenyl-1,3,5-hexatriene
DRPLA	dentatorubral-pallidolusyian atrophy
DTT	dithriothreitol
EDTA	Ethylenediamine tetraacetic acid
EM	electron microscopy
FRET	Fluorescence resonance energy transfer
GndHCl	guanidine hydrochloride
HD	Huntington's disease
HMM	high molecular mass
Hsp	heat shock protein
IPTG	β-D-1-thiogalactopyranoside
LUV	large unilamellar vesicles

MJD	Machado Joseph disease
NES	nuclear export signal
NI	nuclear inclusion
NLS	nuclear localization signal
PC	phosphatidylcholine
PE	phosphatidylethanolamine
PMSF	phenylmethanesulfonylfluoride
polyQ	polyglutamine
PS	phosphatidylserine
PVDF	polyvinilidene fluoride
ROS	reactive oxygen species
SBMA	spinal and bulbar muscular atrophy
SCA 1/2/3/6/7/17	spinocerebellar ataxia 1/2/3/6/7/17
SDS	sodium dodecyl sulphate
SDS-PAGE	SDS-polyacrylamide gel electrophoresis
SEM	scaning electron microscopy
siRNA	small interference RNA
SUV	small unilamellar vesicles
TEM	transmission electron microscopy
TEV protease	tobacco etch virus protease
ThT	thioflavin-T
UCH	ubiquitin C-terminal hydrolases
UIM	ubiquitin interacting motif
UPP	ubiquitin proteasome pathway
USP	ubiquitin specific proteases

Resumo

A doença de Machado Joseph, também conhecida como ataxia espinocerebelar tipo 3 (SCA3), é uma doença neurodegenerativa autossómica dominante. Pertence a um grupo mais alargado de desordens designadas por doenças de poliglutaminas (polyQ), caracterizado por uma repetição do codão CAG no gene responsável, codificando uma sequência de glutaminas. A expansão de glutaminas provoca *misfolding* e agregação da proteína, principalmente no núcleo de neurónios afectados, formando inclusões nucleares (NIs). Na MJD, uma expansão de polyQ na proteína ataxina-3 (atx3) provoca agregação e formação de fibras de amilóide. Apesar da função biológica da atx3 permanecer por esclarecer, várias pistas, como a sua actividade desubiquitinante e motivos de interacção com ubiquitina (UIMs), sugerem um papel na via da ubiquitina-proteassoma (UPP). Em relação ao mecanismo de patogénese, um crescente número de provas sugere que oligómeros na via de formação de amilóide estarão na origem da toxicidade. Os mecanismos moleculares responsáveis por esta toxicidade são desconhecidos, porém, há pistas que indicam que estas espécies poderão interagir com membranas celulares e bicamadas lipídicas, perturbando a sua permeabilidade e normal homeostase celular.

Produzimos diferentes variantes da atx3, contendo diferentes domínios proteicos, nas formas monomérica e oligomérica. A atx3 completa agregou em condições fisiológicas, formando oligómeros, como já tinha sido previamente caracterizado. Avaliamos a cinética de oligomerização das diferentes variantes da atx3 usando tioflavina-T (ThT), detectando diferenças na cinética. Estas diferenças foram correlacionadas com a presença ou ausência de diferentes domínios proteicos das variantes da atx3. Uma proteína contendo um terceiro UIM (1-1N), agregou mais rápido que as restantes variantes enquanto que o domínio Josefina (J1) foi o mais lento a agregar. Em alguns casos, a J1 mostrou também uma diferente cinética de

agregação. Baixo pH e maior força iónica mostraram aumentar a taxa de agregação, de acordo com outros trabalhos publicados. Imagens de microscopia electrónica (EM) das variantes 1-1N, 1A e D1 mostraram que estas formam fibras após incubação a 37ºC, enquanto que a variante J1 mostrou apenas agregados amorfos. Precipitados das variantes 1-1N e J1 mostraram também birrefringência após coloração com vermelho de Congo, o que para a J1 é uma nova característica.

Preparamos também grandes vesículas unilamelares (LUVs; liposomas) contendo fosfatidilserina (PS), fosfatidilcolina (PC), fosfatidiletanolamina (PE) e colesterol (Chol) (num rácio 1:1:1:1), e testamos a capacidade das variantes monoméricas da atx3 e oligómeros da variante 1-1N para destabilizar membranas membranas celulares (usando liposomas como seu modelo). Observamos que os resultados exibiam uma grande variabilidade. Os monómeros da atx3 não destabilizaram membranas lipídicas, tanto a pH 7 como a pH 5 (o que aumenta o número de espécies parcialmente *unfolded*), e demonstrou-se que os oligómeros da variante 1-1N interferiam com a fluorescência da sonda. Apesar disso, imagens de EM revelaram uma grande proximidade entre liposomas e agregados, observando-se o que parecem ser agregados a penetrar a membrana do liposoma.

Em suma, os nossos resultados distinguem uma diferente influência dos domínios proteicos da atx3 na sua agregação em condições fisiológicas, e sublinharam a possível importância dos oligómeros na destabilização membranar. A continuação deste trabalho será necessária para descobrir (i) o mecanismo para destabilização membranar por oligómeros, (ii) como um interface lipídico pode modular a oligomerização, e ainda (iii) a influência de domínios proteicos específicos da atx3 na sua agregação.

Palavras-chave: Ataxina-3; doença de Machado-Joseph; Amilóide; Oligomerização; Destabilização membranar.

Abstract

Machado Joseph's Disease (MJD), also known as spinocerebellar ataxia type 3 (SCA3), is an autosomal dominant neurodegenerative disorder. It belongs to a wider group of disorders termed CAG repeat disorders that are characterised by a CAG three-nucleotide repeat encoding a polyglutamine stretch (polyQ). The expansion of glutamine repeats causes protein misfolding and aggregation, mainly in the nucleus of affected neurons, commonly forming nuclear inclusions (NIs). In MJD, expansion of polyQ stretch in ataxin-3 (atx3) causes the protein to aggregate and form amyloid fibrils. Even though, atx3 protein biological function is still unknown, several clues, as its deubiquitinating activity and ubiquiting interacting motifs (UIMs), suggest a role in the ubiquitin proteasome pathway (UPP). Regarding the mechanism of pathogenesis, it remains unknown, but a growing body of evidence suggest that oligomers in the path of amyloid formation are the source of toxicity. The molecular mechanisms for amyloid oligomer toxicity are still unclear, but several lines of evidence indicate that these species might interact with cellular membranes and lipid bilayers, perturbing normal cell homeostasis.

We have produced different atx3 variants, containing different protein domains, in monomeric and oligomeric forms. The full-length atx3 aggregated in physiological conditions, forming oligomers, as it had been already characterized. We evaluated the kinetics of oligomerization of the different atx3 variants using thioflavin-T (ThT) and detected differences in aggregation kinetics. These differences were correlated with the presence or absence of different protein domains in the atx3 variants. A protein containing a third UIM (1-1N) aggregated faster than the remaining variants, while Josephin domain alone (J1) was the slowest to aggregate. In some cases, J1 alone showed also different kinetics of aggregation. Lower pH and increased ionic strength was shown to increase the aggregation rate, in accordance with other published works.

Electron micrographs of 1-1N, 1A and D1 atx3 variants showed that they form fibrils upon incubation at 37ºC whereas J1 forms amorphous aggregates. Also, 1-1N and J1 pellets exhibited Congo red apple-green birefringence, which for J1 is a newly found characteristic.

We have prepared large unilamellar vesicles (LUVs; liposomes) containing phosphaditylserine (PS), phosphatidylcholine (PC), phosphatidylethanolamine (PE) and cholesterol (Chol) (1:1:1:1 ratio) and tested the ability that monomeric variants of atx3 or oligomers of 1-1N have to destabilize cell membranes (using the liposomes as a membrane model). We observed a high variability in the results. Monomers did not destabilize cell membranes at both pH 7.4 and pH 5 (which increases partially unfolded species) and oligomers of 1-1N were shown to interfere with the fluorescence probes. Even though, electron micrographs showed close proximity between liposomes and aggregates, and it appears that these aggregates penetrate the liposome membrane.

Together, our results recognized the different influence of atx3 protein domains on its aggregation under physiological conditions, and highlighted a possible importance of oligomers in membrane destabilization. Further assays are required to unveil the mechanism for membrane destabilization by oligomers, how lipid interface might modulate oligomerization, and the influence of specific atx3 domains on protein aggregation.

Keywords: Ataxin-3; Machado-Joseph disease; Amyloid; Fibrillogenesis; Membrane destabilization

Chapter 1 Introduction

1.1. – Protein misfolding

In 1958, Francis Crick first published the idea of the central dogma of biology (Crick, 1958). It stated that information was sequentially transmitted from DNA to RNA (transcription) and from RNA to protein (translation). Proteins are the last messengers in living organism's chain of information, and thus they are responsible of expressing that information, in what we know as phenotype.

Proteins require a correct and functional structure to properly work. After the translation process, a protein has to acquire a specific three-dimensional structure by being correctly folded, either by the interactions of self-residues or by the aid of molecular chaperones. Protein folding is, therefore, a critical step on obtaining a functional working protein, and an unfolded or partially folded state often cause cellular problems. The transition between an unfolded to a folded protein is not a binary event. Several studies have been performed along the years in order to clarify these protein un/folding mechanisms. Nowadays, a protein's search for a folded state is viewed as an energy landscape (Fig. 1), where proteins search for a more stable state down a funnel-like energy profile (Jahn and Radford, 2005; Jahn and Radford, 2008). Hence, un/folding processes are viewed as dynamic. Although small single domain polypeptides reach the native state in a sub-second timescale, larger proteins (>100 residues) have a longer time span, a rougher energy landscape and form relatively stable intermediates *en route* to the native state. These intermediates may possess structural conformations that make them thermodynamically more stable, being unlikely for them to fold back into the native structure without a major reorganization. Furthermore, proteins that are partially folded on this landscape (intermediates) might have structural conformations that expose aggregation prone regions, playing, therefore, an important role in protein-misfolding diseases (Jahn and Radford, 2005; Chiti and Dobson, 2006; Jahn and Radford, 2008).

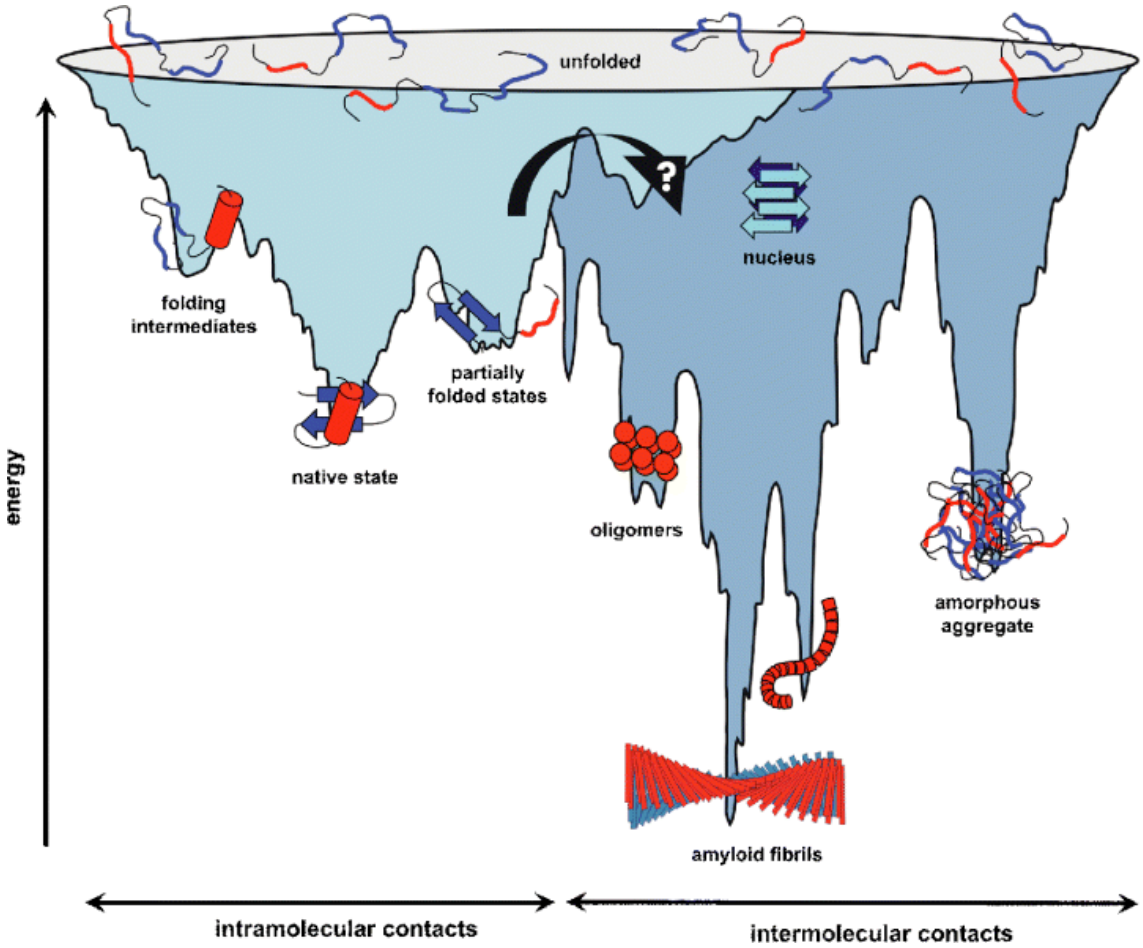

Figure 1 – Energy landscape schematics for protein aggregation. Multiple conformations can be seen in the landscape, tunnelling towards the most stable structure. When there is an increase in partially folded states, a protein can reveal hidden regions that might promote intermolecular contacts (and can be aggregation prone), leading to the right part of the scheme. In this part, protein forms oligomers, amorphous aggregates or amyloid fibrils in a favourable energy gradient, and can also act as a nucleus, recruiting native protein to the aggregates. Also, these structures are more stable, which renders the reversibility to the native state improbable. (From Jahn and Radford, 2005).

1.1.2. – Protein-misfolding diseases

Protein-misfolding diseases occur because of the failure of a peptide or protein to fold or maintain its native structure. Misfolded proteins may arise by several factors including decreased folding efficiency, post translational processes or improper trafficking, which will led to a reduction in normal protein (Chiti and Dobson, 2006). In

spite of that, the largest group of misfolding diseases is associated with the formation of protein aggregates into highly organized fibrillar aggregates – amyloid fibrils. Neurodegenerative misfolding diseases include Alzheimer's disease (AD) with the aggregation of amyloid-β peptide (Aβ-peptide), Parkinson with the aggregation of α-synuclein, Huntington disease (HD) and spinocerebellar ataxias (SCAs) with the aggregation of huntingtin and ataxins, respectively (Chiti and Dobson, 2006).

1.1.3. – Machado-Joseph Disease

Machado Joseph disease (MJD), also known as spinocerebellar ataxia type 3 (SCA3), is an autosomal dominant neurodegenerative disorder. It was firs described by Nakano *et al.* (1972) on descendents of a Portuguese immigrant from Azores islands. The disease is characterized by degeneration of the spinocerebellar, dentate, pontine, and vestibular nuclei as well as extra pyramidal structures such as substantia nigra, locus coeruleus and pallidolusyian complex. Clinical manifestations include ataxia, progressive external ophtalmoplegia, pyramidal and extra pyramidal signs, dystonia with rigidity and distal muscles atrophies. MJD is also the most common dominantly inherited ataxia worldwide (Nakano *et al.*, 1972; Maciel *et al.*, 1995; Ichikawa *et al.*, 2001).

The gene responsible for the disease (MJD1) is mapped to chromosome 14q31.1 (Kawaguchi *et al.*, 1994). The disease is associated with an unstable expansion of the CAG trinucleotide repeat in the coding region, which leads to a protein containing multiple glutamines (Ichikawa *et al.*, 2001). Throughout literature it indeed varied in the population, and the number of glutamines in the normal and expanded polyglutamine (polyQ) tract ranged between 12-40 and 61-84, respectively (Ranum *et al.*, 1995; Paulson *et al.*, 1997).

MJD is part of a wider group of diseases: CAG repeat disorders, or polyQ expansion disorders, which are caused by a CAG repeat in the coding region of each respective disease gene. In this group is also included the above-mentioned HD as

well as dentatorubral pallidolusyian atrophy (DRPLA), spinal and bulbar muscular atrophy (SBMA) and all spinocerebellar ataxias (SCA1, SCA2, SCA3, SCA6, SCA7, SCA17) (Gusella and MacDonald, 2000; Yamada *et al.*, 2008).

Compiled data from literature shows a relation between age at onset and CAG repeat length – age of the person at neurological onset decreases with the increase in polyQ length (Gusella and MacDonald, 2000; Orr, 2001). It is thought that the gain of toxic function, as a result of mutations, might play a role in pathogenesis of MJD (Yamada *et al.*, 2008), while loss of function seems less feasible, since ataxin-3 (atx3) knockout mice do not reveal gross differences compared to normal mice (Schmitt *et al.*, 2007).

1.2. – Ataxin-3 protein

1.2.1. – Structure

Atx3 consists of a globular deubiquitinating N-terminal – Josephin domain (amino acids 1-170) – and a flexible C-terminal tail (Masino *et al.*, 2004). The longest splice variant contains 376 residues and has an approximate molecular weight of 42kDa. The C-terminal tail contains two ubiquitin-interacting motifs (UIM) and a polyQ region. An alternative splice variant has a third UIM at the C-terminus (Fig. 2) (Burnett *et al.*, 2003; Albrecht *et al.*, 2004).

In the coding region of atx3 protein its found a nuclear localization signal (NLS) upstream polyQ region (Macedo-Ribeiro *et al.*, 2009) and a potential site for casein kinase II (CKII) phosphorylation. Comparisons with nuclear export signal profile sequences also suggest the existence of a nuclear export signal (NES) (Albrecht *et al.*, 2004). The allegedly NES was recently confirmed by Macedo-Ribeiro and co-workers, that have also detected CRM1-dependent and –independent pathways to nuclear export of atx3 (Macedo-Ribeiro *et al.*, 2009).

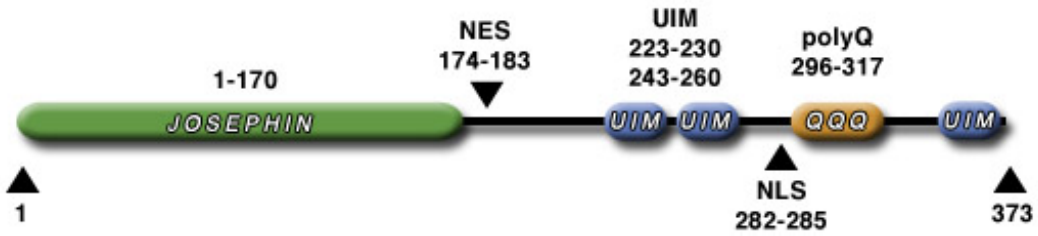

Figure 2 - Ataxin-3 protein architecture, including the Josephin domain, ubiquitin-interacting motifs (UIMs), polyglutamine region (polyQ), nuclear export signal (NES) and nuclear localization signal (NLS). The numbers represent the amino acids chain length in the different protein regions. Adapted from Albrecht *et al.*, 2004.

1.2.2. – Subcellular localization

Atx3 has a predominantly cytoplasmatic distribution, but also localizes in the nucleus and a recent study reported localization in the mitochondria (Pozzi *et al.*, 2008). The major difference verified between normal and affected individuals brains is the strong immunostaining of atx3 within the nuclei of the neurons, observed in brain regions that are known targets of MJD (Paulson *et al.*, 1997; Tait *et al.*, 1998; Pozzi *et al.*, 2008). Neuron intranuclear inclusions (NIIs) were found selectively in those brain regions. It was also shown that expanded glutamine repeats recruited full-length normal and expanded protein to form insoluble complexes (Paulson *et al.*, 1997). This was one of the first clues that polyQ might have an important role in the disease pathogenesis, by means of initializing or catalyzing the aggregation in the nucleus (Paulson *et al.*, 1997).

Recent work by Bichelmeier and colleagues revealed that nuclear localization of atx3 is required for the manifestation of neuropathological symptoms (Bichelmeier *et al.*, 2007). Transgenic mouse models of SCA3 were generated to evaluate the influence of polyQ length and subcellular localization on the phenotype and neuropathological manifestations. Different polyQ lengths were tested. 15 CAG repeats showed no neurological damage as expected. 70 CAG repeats revealed a milder phenotype (compared to a 148 CAG repeat) with a large number of NI, while 148 CAG

repeats revealed the strongest phenotype with extremely reduced survival. In order to further study the influence of subcellular localization on phenotype, constructs were created with 148 CAG repeats and an exogenous NES or a NLS. Mice with NES showed mild phenotype with very low NIs whereas mice with NLS accelerated and intensified the phenotype even more, and the number of aggregates increased significantly. Although the data obtained from these mice models offered new insights about MJD/SCA3 pathology, it should be validated for human patients (Bichelmeier *et al.*, 2007).

1.2.3. – Cellular function

Although there are a considerable number of articles concerning atx3 protein and probable function, its definitive specific physiological role remains unclear. Still, the strongest evidences point to a role in the ubiquitin proteasome pathway (UPP) (Chai *et al.*, 2004; Mao *et al.*, 2005).

Atx3 has the ability to bind ubiquitin chains containing four or more ubiquitins in a UIM-dependent way, and the Josephin domain has a catalytic site for lysine-linked (K-linked) polyubiquitin chains (such as K63 and K48-linked chains), being a deubiquitinating enzyme (Burnett *et al.*, 2003; Mao *et al.*, 2005). The catalytic site of the Josephin domain shows homology with the ones present in the ubiquitin C-terminal hydrolases (UCH) and ubiquitin specific proteases (USP) (Scheel *et al.*, 2003). Moreover, atx3 binds a broad range of ubiquitinated proteins, which accumulate when the proteasome is inhibited (Berke *et al.*, 2005). Ubiquitination of atx3 enhances the ubiquitin chain cleavage, but mutating its catalytic site induces an accumulation of ubiquitinated proteins in the cell (Berke *et al.*, 2005; Todi *et al.*, 2009). Further evidences come from atx3 protein interactors, as Rad23, that can translocate proteins for proteasomal degradation, and valosin containing protein (VCP/p97), which has, among other several cellular roles, an involvment in the proteasomal degradation

pathways (Dai *et al.*, 1998; Doss-Pepe *et al.*, 2003). Together, these evidences, strongly suggest a role for atx3 protein in the UPP.

It was thought that a non-expanded atx3 could address expanded atx3 for degradation, since it mitigated neurodegeneration in a Drosophila and mouse model of SCA3 (Warrick *et al.*, 2005), still, a double transgenic mouse model with normal and expanded protein does not shown mitigation of SCA3 (Hubener and Riess, 2010). The absence of atx3 in human cell lines induces cytoskeletal disorganization and a decrease in adhesion-related molecules, suggesting that atx3 might also have a role on the organization of the cytoskeleton (Rodrigues *et al.*, 2010).

The activity and cellular role of ataxin-3 might be important to explain its pathogenicity in MJD, since the ubiquitin plays several functions, including targeting proteins for proteasomal degradation, and the dysregulation of those processes might be important for the disease development and progression. Also, the range of post-translation modifications atx3 can possibly undergo, might modulate its function and can also be part of the explanation on how it selectively affects brain regions.

1.3. – Ataxin-3 aggregation and pathogenesis

1.3.1. – Amyloid fibrils

PolyQ expansion disorders are linked to the formation of extracellular amyloid deposits or intracellular inclusions with amyloid-like characteristics.

Amyloid fibrils have specific features, and can be characterized by: (a) can be imaged by transmission electron microscopy (TEM) or atomic force microscopy (AFM), (b) possess a cross-β-sheet structure X-Ray diffraction pattern and (c) bind specific dyes such as thioflavin-T (ThT) and Congo red (CR). A curious observation is that virtually any protein sequence can form amyloid fibrils in the right conditions, suggesting that amyloid forming propensity is an inherent characteristic of the polypeptide chain (Dobson, 2004; Chiti and Dobson, 2006; Rousseau *et al.*, 2006a;

Jahn and Radford, 2008). A large amount of experiments involving kinetics of aggregation and physico-chemical properties of amino acids, resulted in the development of computer algorithms capable of identifying aggregation prone-regions in proteins (Rousseau *et al.*, 2006a). Noteworthy is the TANGO algorithm, with 90% accuracy for 176 experimentally validated proteins (Fernandez-Escamilla *et al.*, 2004). Bioinformatics tools as these are a valuable resource, and made possible to Rousseau and co-workers to study the aggregation of 28 full proteomes (*in silica*), figuring out a clear evolutionary pressure to minimize the aggregation propensity of the sequences analysed. They also proposed the existence of gatekeeper residues as an evolved strategy to minimize aggregation (Rousseau *et al.*, 2006b).

1.3.2. – Fibril formation pathways

As discussed above, MJD is a protein misfolding disease that results from atx3 protein aggregation. In order to fully comprehend the complexity of aggregation it is necessary to isolate and identify the conformational states and oligomeric structures, as well as determine specific parameters as thermodynamics and kinetics (Chiti and Dobson, 2006).

In these aggregation disorders, proteins go from a monomeric structure to oligomeric and fibrillar ones. A growing body of evidence suggests that the structures responsible for cytotoxicity are the oligomers and not the mature fibrils (Bucciantini *et al.*, 2002; Kayed *et al.*, 2003; Demuro *et al.*, 2005; Xue *et al.*, 2009). In this context, the study of oligomers is of special interest, since there is a crescent awareness that these species might play a key role in MJD pathogenicity, as well as in another polyglutamine diseases. However, the mechanism of toxicity remains to be elucidated (Chiti and Dobson, 2006; Rousseau *et al.*, 2006a).

Protein aggregation has been an extensively studied subject. In order for a native protein to aggregate, it usually must be destabilised. Alterations that might have that effect include addition of denaturants, low pH, high temperature, truncations or

mutations. The importance of these destabilisations is on the fact that they will increase the partially folded states, which might expose sequence regions prone to aggregation, increasing the probability of intramolecular interactions (Chiti and Dobson, 2006).

Hypothesized by Perutz, and now widely established, is the idea that glutamine expansions are responsible for cell damage by an aggregation via nucleation. These findings were based on the fact that in each glutamine expansion disease there is a correlation between the repeat length and age at onset (Perutz, 1999; Perutz and Windle, 2001). An expansion of glutamines is, therefore, the logical primary suspect of causing aggregation and neural death. In addition, evidences show that an increased polyQ tract forms fibrils faster and exhibits a worst phenotype (Chiti and Dobson, 2006; Bichelmeier *et al.*, 2007). However, studies have also proven that the native non-expanded protein forms fibrils, although in a slower way (Gales *et al.*, 2005). Even though an expanded polyQ tract was thought to destabilise native atx3 (Bevivino and Loll, 2001), Chow and co-workers verified no alteration of un/folding kinetics, meaning that the expansion does not destabilise native protein (Chow *et al.*, 2004). These findings made possible to elaborate a hypothesis in which the un/folding of the protein and the misfolding events are separate (Chow *et al.*, 2004). The polyQ did not affect the un/folding events, but could lower the energetic barrier for the formation of misfolded protein.

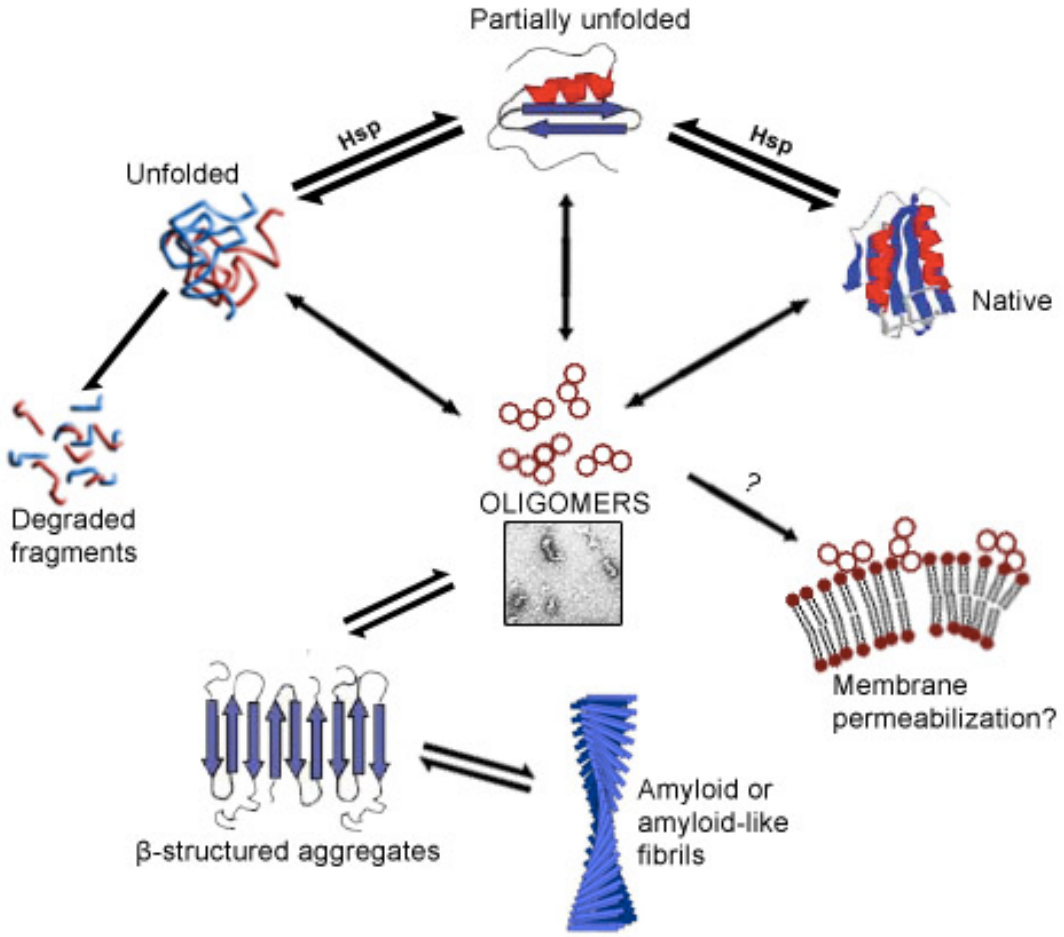

Figure 3 – Schematic representation of the different pathways a protein may take. The folding of proteins is aided by molecular chaperones (as heat-shock proteins – Hsp). Under native, unfolded or partially folded state, a protein can aggregate, forming, in a first step, oligomers. These oligomers are thought to destabilize cell membranes. The formation of β -structure aggregates (e.g. protofibrils) follows the oligomer formation, and as these aggregates grow, they form amyloid or amyloid-like fibrils. Adapted from Chiti and Dobson, 2006; Jahn and Radford, 2008.

Measurements with of ThT fluorescence and other techniques reveal that the polymerisation kinetics mechanism has characteristics of a nucleated growth, showing a sigmoidal-type time-response. It is typically observed a lag phase followed by a rapid exponential growth, in which the lag phase is alleged to correspond to nuclei formation (Chiti and Dobson, 2006). Gales and colleagues revealed by gel filtration chromatography the existence of both monomeric and oligomeric species in a native ataxin-3 (14 glutamine residues) purified protein, proving that a normal length

polyglutamine tract also shows propensity to aggregate in physiological conditions. Additionally, circular dichroism (CD) demonstrates a β-sheet increase, suggesting that oligomerization either induces or is a product of a conformational change in the secondary structure of the protein. Moreover, assays of aggregation kinetics using small amounts of dimmers and oligomers as pre-formed nuclei showed a less extensive lag phase, suggesting a seeding effect in the aggregation process and a proof of a nucleated growth model (Gales *et al.*, 2005).

1.3.3. – Sequence influence in amyloid fibril formation

The capacity to form amyloid structures is an intrinsic property of polypeptide chains – almost every protein, given the right conditions, can form amyloid. However, specific amino acid sequences facilitate this process. How do specific sequences promote aggregation? As mentioned above, different computer algorithms have been designed to predict the propensity of specific protein sequences to form amyloid fibrils (by predicting the cross-β aggregation propensity), such as Zyggregator, TANGO and Aggrescan algorithms (Fernandez-Escamilla *et al.*, 2004; Rousseau *et al.*, 2006a; Conchillo-Sole *et al.*, 2007; Tartaglia and Vendruscolo, 2008). Although these algorithms offer new ways to predict amyloid formation, other criteria has to be taken in account, such as the protein physical-chemical properties. The study of these property alterations might contribute to our understanding of protein aggregation, especially amyloid fibril formation, at a molecular level (Chiti and Dobson, 2006; Rousseau *et al.*, 2006a).

Despite the fact that protein sequence plays an important role in the way it aggregates, the scope of different proteins causative of amyloid formation, which have different sizes and properties, advocate that sequence may not be the key factor in cellular toxicity. A growing body of evidence supports the idea that the state of aggregation, rather than a specific amino acid sequence is the answer to explain the

toxicity. Findings on different amyloid forming proteins suggest, therefore, a common mechanism of toxicity (Bucciantini *et al.*, 2002; Glabe, 2006).

1.3.4. – Toxicity of amyloid intermediates

The similarities observed among different polyQ disorders, as for instance, the formation of oligomers and fibrils, suggest a common mechanism of toxicity, as was already mentioned. Even thought there are several studies regarding this question, the mechanism by which amyloid intermediates cause toxicity remains unknown. The strongest evidences addresses the toxicity of these intermediates to the destabilization of lipid bilayers, leading to cell dysfunction by perturbing normal cell homeostasis (Glabe, 2006).

Three important questions have been discussed more recently, (a) what kind of intermediates cause toxicity, (b) how protein-lipid interaction can modulate amyloid fibril formation and (c) how are cell membranes destabilized.

Aggregate toxicity depends on protein concentration and length of exposure in aggregation conditions, but it is reduced when amyloid fibres are formed. Toxicity is more pronounced for the rapidly formed non-fibrillar aggregates than for highly organized fibrillar structures – proof that intermediate species might be the primary responsible for toxicity (Bucciantini *et al.*, 2002). An AD study showed that oligomer specific antibodies inhibited oligomer toxicity *in vitro* (Kayed *et al.*, 2003). Moreover, the antibody positive deposits are distinct from ThT-positive ones, proof that the oligomers identified are non-fibrillar and that they might precede the development of fibrillar plaques (Kayed *et al.*, 2003).

In order to study fibril length correlation with toxicity, experiments were conducted with amyloid fibrils using constant stirring to fragment growing fibrils. The fragmented fibrils had an increase ability to disrupt membranes and decrease cell viability. Fragmented fibrils resemble oligomeric species and are proof of enhanced toxicity compared to non-fragmented amyloid fibres (Xue *et al.*, 2009; Xue *et al.*, 2010).

A polyQ aggregation study in living cells done by fluorescence resonance energy transfer (FRET) followed the formation of oligomers and inclusion bodies starting from monomers. A survival assay of neuronally differentiated cells showed that cells with oligomer species died faster, in what is another proof of higher toxicity of these species compared to monomers and fibrils (Takahashi *et al.*, 2008).

In addition to these evidences of oligomer toxicity as a common feature in polyQ disorders, an increase in membrane permeability and intracellular calcium concentration is known to be associated with amyloid toxicity (Glabe, 2006). However, the mechanism underlying this increase is not yet clear; nevertheless several hypotheses have been discussed such as ion channels and membrane pores (Quist *et al.*, 2005; Singer and Dewji, 2006). It has been observed that extracellular applications of oligomeric forms from different amyloidogenic proteins cause a rapid increase in cytosolic free calcium, while soluble monomers and fibrils do not have a noticeable effect. The calcium influx observed is not due to alterations in the existing calcium channels, since the use of cobalt (calcium channel inhibitor) shows no alteration (Demuro *et al.*, 2005). In coherence with these results it is also observed a release of fluorescent dyes such as fluo-3AM and calcein from cells (leakage assay). Together, these results suggest that oligomeric species destabilize cell membranes and that calcium dysregulation might have an important role in toxicity by either its importance in membrane gradients or intracellular signalling (Demuro *et al.*, 2005).

The permeabilization of cellular membranes might represent the first primary common mechanism of amyloid pathogenesis and it can initiate a variety of downstream events. These events may include alterations in signalling processes (Saitoh *et al.*, 1993; Mattson, 1995), production of reactive oxygen species (ROS)(Schubert *et al.*, 1995), mitochondria dysfunction (Shoffner, 1997; Hashimoto *et al.*, 2003) and autophagy and cell death (Ravikumar *et al.*, 2004).

1.3.5. – Lipid-protein interaction

As discussed above, the main cytotoxic effect of amyloid fibril formation is due to prefibrillar aggregates. Numerous studies committed to reproduce the aggregation *in vitro* showed that lipid membrane interface promotes protein misfolding, whereas cytotoxicity studies revealed a destabilization of cell membranes (Demuro *et al.*, 2005; Gorbenko and Kinnunen, 2006; Takahashi *et al.*, 2008; Relini *et al.*, 2009). The protein-lipid interaction is considered a two-fold aspect, recalling the above-mentioned questions (section 1.3.4) on (b) how protein-lipid interaction can modulate amyloid fibril formation and (c) how are cell membranes destabilized by protein aggregates (Relini *et al.*, 2009).

Lipidomics is an emergent research area, since awareness is rising that lipid-protein interactions play key roles in a variety of different cellular processes. There is an incredible diversity of lipids than compose the cellular membrane, each with different chemical and physical properties, which can affect protein function and organization. Since lipids do not have an inherent catalytic activity most studies focus on the secondary effects on *in vitro* reconstituted processes (Dowhan *et al.*, 2004). The different lipidic composition of cellular membranes gives them specific properties such as its phase state, bilayer curvature and elasticity, surface charge and degree of hydration, while each specific lipid carries an intrinsic chemical nature that also plays a role in a complex and dynamic protein-lipid interaction (Jensen and Mouritsen, 2004).

The specific role of protein-lipid interaction and its influence on protein aggregation has been studied recently. There are evidences for lipid-aided protein folding for some proteins (Dowhan *et al.*, 2004). The strongest evidence comes from *E. coli* integral membrane associated lactose permease that requires phosphaditylethanolamine in the cell membrane to be fully functional, and together with other data, introduces the idea of lipid chaperones – lipochaperones (Bogdanov and Dowhan, 1995). Although these effects are seen on membrane proteins, it is suggestive of the influence of lipids or lipid environment on protein conformation.

Several studies point to the lipid bilayer as an effective catalyst of fibrillogenesis (Sparr *et al.*, 2004; Stefani, 2004; Zhao *et al.*, 2004; Hebda and Miranker, 2009). The studies on α-synuclein (Lee *et al.*, 2002; Zhu *et al.*, 2003), Aβ peptide (Bokvist *et al.*, 2004), islet amyloid polypeptide (Sparr *et al.*, 2004), lysozyme, transthyrethin, cytochrome c, insulin, myoglobin, and endostatin (Zhao *et al.*, 2004) demonstrate a membrane-responsible fibril formation enhancement. This formation varies with different types of lipids and in different ways, indicating that these properties are not specific to a certain lipid class, but to a certain composition. Nevertheless, the molecular mechanism of protein-lipid interaction may depend also on the structural characteristics of the protein implicated. Collectively, these studies reveal that lipid membranes can modulate amyloid fibril formation by specific and non-specific protein-lipid interactions. The evidences support the idea that lipid interaction might lower the activation energy barrier for unfolding, which together with a higher propensity to form β-sheet structures might cause protein aggregation (Gorbenko and Kinnunen, 2006; Hebda and Miranker, 2009; Relini *et al.*, 2009).

The studies done so far on the process of amyloid fibril formation modulated by membranes reveal the existence of different steps. Initially the protein binds to the lipid bilayer by electrostatic attraction, followed by a structural transformation of the bound protein into a partially folded conformation that can expose aggregation-prone regions. Then, the oligomerization of the membrane bound protein occurs by addition of monomers, producing fibre formation and growth (Gorbenko and Kinnunen, 2006). In some studies with membrane induced fibril formation, the fibril even reveals lipid inclusions, a proof that it can extract lipids from the membrane (Sparr *et al.*, 2004; Zhao *et al.*, 2004). Another probable mechanism of membrane assisted fibril formation might occur by a local increase in protein concentration. Such can occur by adsorption of protein molecules to oppositely charged surfaces as, for instance, an anionic lipid surface, which can increase the concentration up to two orders of magnitude (Gorbenko and Kinnunen, 2006). In the other hand, although a higher concentration

promotes a faster aggregation, molecules adsorbed at lipid surfaces are less labile and diffuse slower, which can conduct to a decrease rate of fibril formation.

Membranes can also be viewed as a template for protein aggregation, and the model lipid systems can give different results depending on their dimensionality. Monolayers or liposomal bilayers, for instance, even though using the same chemical composition for both, they behave differently (Zhu *et al.*, 2002). These facts have to be taken in account when choosing a model for lipid-protein interaction, since bulk solutions of lipid will not represent the structures seen *in vivo*. An increasing number of studies have being using different lipid-protein interaction models, such as large or small unilamellar vesicles (LUVs or SUVs), micelles or monolayers. One should bear in mind that in such models there is the influence of lipid composition, charge and phase, as well as the influence of a specific three-dimensional structure formed by lipids. Another interesting fact is that different cellular membrane have a different lipidic composition, as shown on Table 1 for different rat cellular membranes (Kleinig, 1970). Furthermore, in rat liver nuclear membranes, it is seen that older rats (60 days) have a different lipidic composition compared to younger ones (6 days) (Albi *et al.*, 1997). In what way these facts influence the development of amyloid forming disorders, whose mechanism of pathogenicity is thought to be related to cell membranes, is still unclear, but should be a point of focus in a near future. Moreover, these evidences can be part of the explanation on (a) why are these diseases late onset disorders and (c) why they affect different regions of the brain, although the last one might have more to do with specific protein-protein interactions.

Table 1 – Lipidic composition of different cellular membranes from rat. Adapted from Kleinig, 1970.

Lipid	Rat liver nuclear membrane	Rat Golgi membrane	Rat plasma membrane
PC	61.4	45.3	39.9
PE	22.7	17.0	17.8
PS	3.6	4.2	3.5

(PC, phosphaditylcholine; PE, phosphatidylethanolamine; PS, phosphatidylserine)

Recent studies point to the cell membrane as a target of disease related amyloids (as Aβ or polyQ). It has been shown that oligomers from Aβ42, prion, islet amyloid polypeptide and polyQ and not the monomers or fibrils, greatly increase the intracellular calcium (Ca^{2+}) (Demuro *et al.*, 2005). Also Aβ42 increases membrane permeability, since its oligomers cause a leakage of dyes such as calcein or fluo-3AM from within cells (Demuro *et al.*, 2005). Calcein leakage from liposomes is also seen with yeast prion Ure2p, in which a significant release from negatively charged phosphatidylserine vesicles contrasts with minor release from zwitterionic phosphatidylcholine ones. Moreover, cholesterol enriched membranes were observed to be protected against permeabilization. Polymerisation of Ure2p was speeded up by phosphatidylserine, into oligomers and fibrils similar the Ure2p assemblies arising in free solution, suggestive of the lipid influence on protein aggregation (Pieri *et al.*, 2009). Another study, but about the influence of metal ions on atx3 aggregation, used 1-6-diphenyl-1,3,5-hexatriene (DPH) dye to load small unilamelar vesicles of L-α-dimyristoylphosphoglycerolcholine (DMPC) and measured interactions of atx3 with lipid membrane models. The results reveal that oligomers of atx3 can perturb the membrane, and the changes observed are prominent when in the presence of aluminium (Al^{3+}) and zinc (Zn^{2+}) metal ions, probably because these ions increase the oligomerization state of atx3 (Ricchelli *et al.*, 2007).

1.3.6. – Ataxin-3 aggregation mechanism

Although there are several mechanisms proposed regarding amyloid formation, the nature of the process is not completely clear. The process of initiation might occur via, (a) kinetically or thermodynamically unfavourable conversion of a monomer to a nucleus, (b) collision between two monomers that converts one or both to an amyloid competent conformation or (c) association of a monomer to a non-structured oligomer, and its conversion to a structured oligomer. The mechanism of fibril growth may include (a) addition of a non-amyloid monomer to a pre-existing structure aggregate (followed by conformation conversion), (b) indefinite self-association of amyloid-competent monomers or (c) association of oligomers into larger aggregates (Murphy, 2007).

When looking to the mechanism of atx3 aggregation we have to take in account the protein properties, the involvement of the polyQ tract, the influence of the different domains and regions of the protein, the protein-protein interactions, post-translational modifications and the influence of lipid membranes.

Since the finds of Paulson an Perez (Paulson *et al.*, 1997; Perez *et al.*, 1998) on nuclear inclusions and nuclear localization signal of atx3, Bevivino (Bevivino and Loll, 2001) firstly showed the aggregation of the expanded form of atx3 *in vitro*. The polyQ region was thought to be the responsible for aggregation, but the Josephin domain would reveal itself to be also important. Work done to characterise the Josephin domain of atx3 revealed that the domain alone aggregated in heat-induced conditions (Masino *et al.*, 2004), and the electron micrographs revealed the presence of unbranched fibrils, similar to those of the expanded full length atx3 (Shehi *et al.*, 2003). Masino and colleagues proposed a model to explain the influence of the Josephin domain and polyQ tract on aggregation. Known as induced misfit model, it states that a protein with normal polyQ length will interact normally with other proteins, while expanded polyQ tract will not interact normally thus leaving the protein exposed to solvent. The increased exposition will increase the probability of conformational

changes, leading to a β-sheet rich structure that together with the expanded polyQ region initiates the process of aggregation.

Normal length polyQ atx3 was also proven to aggregate under high pressure and temperature (Marchal *et al.*, 2003), yet Gales and colleagues proved the aggregation of a non-expanded polyQ atx3 in near physiological conditions (Gales *et al.*, 2005). It was also shown a seeding effect by adding to the aggregation assays small dimmers or high molecular mass (HMM) oligomer, a proof of a nucleated growth for atx3 aggregation.

The most accepted model for atx3 aggregation comes from Ellisdon and co-workers. Work done with normal and expanded polyQ tract atx3 showed a two-stage aggregation mechanism (Fig. 4): a nucleation step independent of the polyQ length followed by a second step observed only in expanded atx3 (polyQ dependent) (Ellisdon *et al.*, 2006). Moreover, the aggregation process starts from the formation of a thermodynamic nucleus, which is the less stable structure of the aggregation pathway (Fig. 4). Once it is formed, the aggregation proceeds down a free energy gradient. Several lines of evidence point to the Josephin domain as a nucleating core, since it forms fibrils alone and it undergoes structural rearrangement upon fibrillisation in full length atx3 (Masino *et al.*, 2004; Ellisdon *et al.*, 2006; Ellisdon *et al.*, 2007).

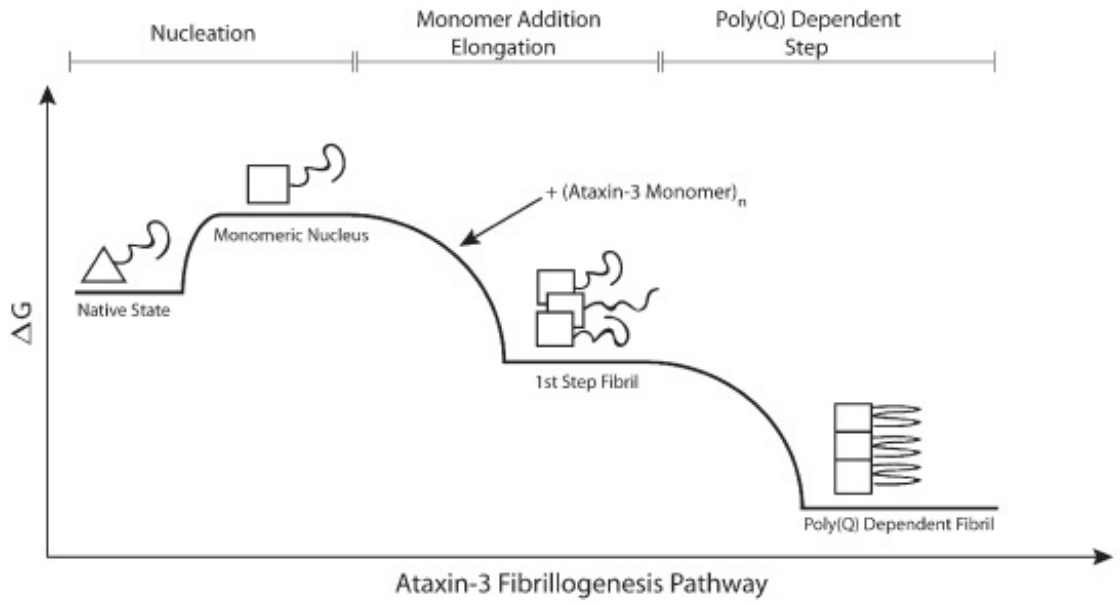

Figure 4 – Hypothesised mechanism of ataxin-3 amyloid fibril formation. In the ataxin-3 native state, Josephin domain is represented as a triangle with the polyQ tract as a predominantly random-coil tail. Fibril formation is instigated by a monomeric thermodynamic nucleus, and this nucleating event is represented by structural changes in the non-polyQ regions of the protein. The first-step of ataxin-3 elongation occurs down an energy gradient, by the addition of ataxin-3 monomers to the growing fibril. Only expanded ataxin-3 undergoes a second aggregation stage, with the involvement of the polyQ tract, which produces large and SDS-resistant aggregates. Adapted from (Ellisdon *et al.*, 2007).

In conjunction with previous results that show membrane destabilization upon incubation with atx3 (Macedo-Ribeiro, S. and Pedroso-Lima, C., unpublished data), these evidences from several amyloid-like forming proteins point to an effective interaction between the protein and the lipid membranes. Whether these interactions lead to or aid protein aggregation, or if these protein aggregates conclusively destabilize cellular membranes in a toxic manner should be further studied. We proposed to unveil the different influences of non-expanded atx3 domains on protein aggregation and whether monomers or oligomers cause any destabilization in a cellular bilayer membrane model – liposome.

Chapter 2 Material and Methods

Material and Methods

2.1. – Protein expression and purification

Commonly used media:

Luria-Bertani broth medium (LB): 1% (w/v) tryptone, 1% (w/v) sodium chloride and 0.5% (w/v) yeast extract.

Luria-Bertani broth medium without sodium chloride (LB-ON): 1% (w/v) tryptone and 0.5% (w/v) yeast extract.

Super Optimal broth with Catabolite repression (SOC): 2% (w/v) bacto-tryptone, 0.5% (w/v) bacto-yeast extract, 10mM NaCl, 2.5mM KCl, 10mM $MgCl_2$ and 20mM glucose.

Commonly used buffers:

Histrap buffer: pH 7.5, 20mM sodium phosphate, 500mM NaCl and 10mM imidazole.

Cell lysis buffer: histrap buffer plus 50µg/mL lysozime, 5µg/mL DNASE I and 10mM $MgCl_2$.

Gel filtration buffer: pH 7.5, 20mM sodium phosphate, 200mM NaCl, 1mM EDTA, 1mM DTT and 5% (v/v) glycerol.

Liposome assay buffer: pH 7.4, 10mM sodium phosphate and 140mM NaCl.

2.1.1. – Preparation of competent cells

BL21(DE3) and BL21(DE3)SI competent cells (Invitrogen Corporation, USA) were prepared according to Inoue et al. method (Inoue *et al.*, 1990). This method results from several experiments that uncovered the best conditions of temperature, time of growth, and buffer composition among others, for an optimal cell competency. Cell competency was assessed with pUC19 and atx3 J1 plasmids by transformation on the prepared cells, and calculating the colonies formed per µg of plasmid used.

2.1.2. – Transformation

Transformation method was based on the ability of divalent cations (specifically, Ca^{2+} and Mg^{2+}) to render cells able to take up DNA. Normally, 100ng of plasmid were added for 50µL of competent cells and incubated on ice for 30 minutes. After that time, a small heat-shock treatment on a 42ºC water bath for 60-90 seconds followed by a cold-shock, 3 minutes on ice, which makes the DNA efficiently enter the cell.

Cells were then incubated on 1mL of super optimal broth with catabolite repression (SOC: 2% (w/v) bacto-tryptone, 0.5% (w/v) bacto-yeast extract, 10mM NaCl, 2.5mM KCl, 10mM $MgCl_2$ and 20mM glucose) for 1 hour at 37ºC. After that, 100-200µL of the previously grown cells were incubated overnight at 37ºC on a Luria-Bertani broth medium (LB: 1% (w/v) tryptone, 1% (w/v) sodium chloride and 0.5% (w/v) yeast extract) or Luria-Bertani broth medium without sodium chloride (LB-ON: 1% (w/v) tryptone and 0.5% (w/v) yeast extract) agar plate (15g/L of agar), with 50µg/mL ampicillin (Sigma-Aldrich, USA).

2.1.3. – Plasmid preparation

Plasmids for 1-1N, 1A, D1 1-1Nb and J1b were prepared from existing pDEST17 plasmids with NZY Tech Miniprep kit (NZY Tech Genes and Enzymes, Portugal). DH5α cells were transformed according to the supplied kit protocol. In order to verify the integrity of the plasmids, restriction analysis was performed through digestion and double digestion with XbaI and EcoRI (Fermentas, Canada), previously determined by restriction mapping using EnzymeX software (http://mekentosj.com/science/enzymex/). Digestion was performed at 37ºC for 1h, using FastDigest® and Tango™ buffers (Fermentas, Canada) for EcoRI and XbaI, respectively.

A 1% agarose gel stained with 0.02 ‰ ethidium bromide was run, and viewed under UV light. Plasmidic DNA was quantified by spectroscopy, using the absorbance

at 260nm to determine concentration, and the ratio 260:280 for DNA purity assessment.

2.1.4. – Protein expression tests

Protein expression tests require a factorial number of experiments in order to verify what condition suits the best for optimal protein expression. Since it will give rise to an elevated number of experiments, which requires time and is expensive, another approach was thought. An incomplete factorial approach was used to save time and use less laboratory reagents. The available on-line tool used for the purpose, was the Simulated Annealing and Backtracking (SAmBA) method (http://igs-server.cnrs-mrs.fr/samba/), originally created to elaborate incomplete factorial approaches on crystallization conditions (Audic *et al.*, 1997). Since the basic principle on incomplete factorial approach is the same, we used it on protein expression tests so that each variable's influence on bacterial growth and expression could be identified.

A total of nine and six experiments were performed for atx3 1-1N variant in two individual tests. The first test varied the strains BL21(DE3)pLysS (Invitrogen Corporation, USA), BL21(DE3) and BL21(DE3)star, the growth temperature of 30ºC and 25ºC and glucose concentrations of 0,5%, 2,5% and 5%. However, the growth rate of the BL21(DE)star were too slow, preventing the completion of the experiment within a reasonable time. Thus, the experiment was repeated using two *E. coli* strains BL21(DE3) and BL21(DE3)pLysS, three growth temperatures (37ºC, 30ºC and 25ºC) and just one concentration of glucose (1%). We tested also for all conditions different expression times (2 and 3 hours). The media used was LB and expression induction was achieved with 0.4mM Isopropyl β -D-1-thiogalactopyranoside (IPTG; Sigma-Aldrich, USA).

For the analysis of expression 1mL of culture samples were harvested for t_0 (time before induction), t_2 (two hours after induction) and t_3 (three hours after induction). The cell samples were lysed with cell lysis buffer (20mM sodium phosphate

pH 7.5, 500mM NaCl, 10mM imidazole, 50µg/mL lysozime, 5µg/mL DNASE I and 10mM $MgCl_2$) and centrifuged at 10000g (Eppendorf centrifuge 5415R, Eppendorf, Germany) to separate the soluble and insoluble fractions. A 12.5% acrylamide gel was run and stained with coomassie blue (Fermentas, BioPortugal, Portugal). The gels were scanned with a Molecular Image GS800 Calibrated Densitometer (Bio-Rad, USA) and the band densities were analysed with Quantity One software (Bio-Rad, USA). Only 1-1N variant was screened, and the best conditions were selected by higher soluble/insoluble ratio, having also in mind the total amount of protein (total band density).

2.1.5. – Protein expression

The 1-1N, 1A, D1 and 1-1Nb hexahistidine proteins were expressed in *E. coli* BL21(DE3) cells, J1 and J1b hexahistidine proteins were expressed in *E. coli* BL21(DE3)SI cells. Typically 100ng of plasmid were transformed in 50µL of competent BL21(DE3) or BL21(DE3)SI cells, plated on LB or LB-ON plates overnight at 37ºC. For the pre-inoculum, two to three colonies were picked from the plate and incubated overnight at 37ºC on 200mL of the correspondent media with 50µg/mL ampicillin. BL21(DE3) cells were grown at 37ºC in LB medium or LB-ON for BL21(DE3)SI, and in both cases with 4% pre-inoculum, 50µg/ml ampicillin and 2% (w/v) glucose. Expression was induced at 30ºC after cultures reached an absorbance at 600nm of 0.5-0.7, with IPTG to a final concentration of 0.4mM for BL21(DE3) strain or with 300mM NaCl for the BL21(DE3)SI strain. After 2h/3h induction the cells were harvested by 20 min centrifugation at 4500g on an Avanti J26 XPI (Beckman Coulter, USA) ultracentrifuge. The cell pellet (2L or 3L) was resuspended in cell lysis buffer (20mL per litre of cell culture pelleted) and frozen at -20 ºC. Samples of t_0 and t_2 or t_3 were analysed by SDS-PAGE for expression verification, as previously described.

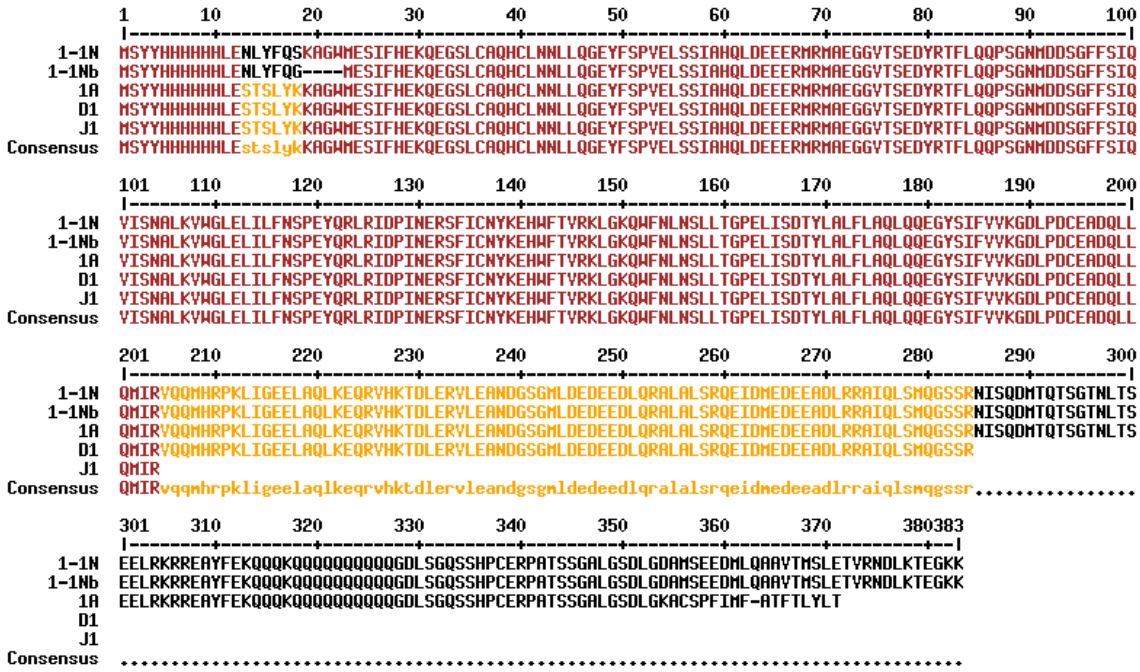

Figure 5 – Sequence alignment of ataxin-3 variants performed with MultAlin tool (http://multalin.toulouse.inra.fr/multalin/cgi-bin/multalin.pl). All constructs have a purification tag with 6 histidine residues (1-23). The 1-1N and 1-1Nb variants have a TEV protease cleavage site, however the one from 1-1Nb has an improved site, and after cleavage it will only leave a glycine residue before ataxin-3 sequence. 1A differs from 1-1N in the C-terminal (from lysine residue 354), and it lacks the third ubiquitin-interacting motif (UIM). D1 has the Josephin domain a two UIMs, but lacks the polyQ tract, since it finishes at arginine residue 284. J1 has only the Josephin domain, and J1b (not represented) is equal to J1 but with the N-terminal equal to 1-1Nb.

2.1.6. – TEV protease cleave assay

The full-length atx3 (1-1Nb and J1) has a cleavage site (Fig. 6) for recombinant tobacco etch virus protease (TEV protease). In order to find a best condition for the cleavage of the tag, a set of three different conditions were prepared. In each condition three concentrations of TEV protease were used: (i) 0.5µg, (ii) 1µg and (iii) 2µg to 10µg of 1-1Nb protein. The conditions were (1) overnight at 4ºC, (2) 4h at 4ºC and (3) 2h at 20ºC and the cleavage was performed on gel filtration buffer. The TEV protease was supplied by Bruno Almeida in buffer containing 25mM sodium phosphate pH 8, 200mM NaCl, 10% (v/v) glycerol, 2mM EDTA and 10mM DTT, and at 2mg/mL concentration.

Buffer exchange to gel filtration buffer of the purified protein from affinity chromatography was made by consecutive dilutions followed by ultrafiltration. After the cleavage, another buffer exchange was made, but to histrap buffer. The cleaved products were loaded to a Histrap HP affinity chromatography column. Cleaved protein was eluted with histrap buffer, and uncleaved, as well as TEV (the used TEV protease has an hexahistidine tag), was eluted with histrap buffer with 500mM imidazole. After this step, the production went in the same way as for the other proteins, beginning in the preparative size exclusion chromatography.

Figure 6 – Tag from the 1-1Nb protein. The green sequence refers to the hexahistidine tag, the red sequence is the TEV protease recognition sequence and with a yellow arrowhead it's indicated the site of cleavage. Blue represents the beginning of the ataxin-3 protein sequence.

2.1.7. – Protein purification

Re-suspended pellets were stored at -20ºC. Before starting purification, the pellet was thawed and 1mM phenylmethanesulfonylfluoride (PMSF, serine protease inhibitor), 5µg/mL DNASE I and 10mM $MgCl_2$ were added. Cell rupture was achieved by 1-2h agitation with a magnetic stirrer in an ice bath. The lysed cell extract was centrifuged for 40 minutes at 16000 rpm and 4ºC on an Avanti J26 XPI centrifuge (Beckman Coulter, USA). The supernatant was filtered through a 0.22µm pore Polyvinilidene fluoride (PVDF) membrane (Millipore, USA) and then applied to a HisTrap HP 5mL column (GE Healthcare Life Sciences, Sweden) previously loaded with a nickel sulphate solution (1M $NiSO_4$) and equilibrated with histrap buffer (pH 7.5, 20mM sodium phosphate, 500mM NaCl and 10mM imidazole). Elution was performed on an AKTAprime Plus (GE Healthcare Life Sciences, Sweden) in three steps with

histrap buffer with 50, 250 and 500mM imidazole. Fractions from the 250mM peak were selected for preparative size exclusion chromatography. These fractions were applied to a Hiprep 26/60 Sephacryl S-200 High Resolution column (GE Healthcare Life Sciences, Sweden) equilibrated with gel filtration buffer (pH 7.5, 20mM sodium phosphate, 200mM NaCl, 1mM EDTA, 1mM DTT and 5% (v/v) glycerol). Elution was performed with a 0.5ml/min flow rate at 4ºC. Fractions from size exclusion chromatography were analysed by SDS-PAGE and analytical size exclusion chromatography on an AKTA Purifier (GE Healthcare Life Sciences, Sweden) in a Superdex 200 10/300GL (GE Healthcare Life Sciences, Sweden).

Table 2 – Physicochemical properties of the ataxin-3 produced variants, based on amino acid sequence analysis with Protparam tool.

Protein	Length (aa)	Size (kDa)	Extinction coefficient ($M^{-1}cm^{-1}$)
1-1N	383	44055.1	36900
1A	370	42594.6	38390
D1	284	32980.1	35410
J1	204	23767.8	35410
1-1Nb	362	41307.0	26930
J1b	183	21092.8	25440

1-1Nb and J1b are the same as 1-1N and J1, but without the hexahistidine tag. (aa, amino acids)

The final selected fractions were concentrated by ultrafiltration on an Ultra 15 concentrator[1] MWCO 10kDa (Amicon Ultra Centrifugal Devices, Millipore, USA). An aliquot of the concentrated protein was analysed by SDS-PAGE and analytical size

[1] Membrane passivation was performed by incubation overnight at 4ºC with 5% (w/v) polyethilenoglycol (PEG) compound (Sigma-Aldrich, USA).

exclusion chromatography. The protein concentration was determined by measuring the absorbance at 280nm (Nanodrop ND-1000, Thermo Scientific, USA), using extinction coefficients (Table 2) calculated with Protparam tool (Gasteiger *et al.*, 2005).

2.1.8. – Ataxin-3 oligomerization

A sample protein of 1-1N and J1 variants (20μM) was incubated at 37ºC for ≈120h in order to obtain oligomers. Samples were collected at different time points and analysed by analytical size exclusion chromatography and electron microscopy. Prior to size exclusion chromatography, proteins were filtered through a 0.22μm pore PVDF-membrane centrifugal filters to avoid having precipitates entering the chromatographic column.

2.2. – Protein stability analysis

2.2.1. – Melting temperature

Thermofluor assay was performed using sypro orange dye (Sypro® Orange Protein Gel Stain, Sigma-Aldrich, USA). A master mix was prepared with 20μM protein and a 20x concentration of sypro orange. An opaque 96-well plate was used and four replicates of each condition were made (20μL/well). The thermofluor assay was carried out with increments of 0.5ºC each 15 seconds on an IQ™5 Multicolor Real-Time PCR detection system (Bio-Rad, USA).

2.2.2. – Chemical denaturation profiles

The red shift of intrinsic tryptophan fluorescence was measured by excitation at 295nm and the emission spectrum was acquired from 300-450nm at 25ºC on a Horiba Fluoromax-4 fluorimeter (Jobin Yvon, France). The monomeric form of ataxin-3 1-1N protein spectra was compared to its oligomeric form, as to J1 alone (Josephin domain). The protein denaturation was obtained by diluting the protein in increasing

concentrations of guanidine hydrochloride (GndHCl, 0-6M) on liposome assay buffer, and incubating them for at least 1 hour at 25ºC as described by (Masino *et al.*, 2004). GndHCl was prepared on liposome assay buffer (10mM sodium phosphate pH 7.4, 140mM NaCl) at 6M concentration and diluted in the same buffer. Protein concentration used was 2μM in a volume of 150μL of denaturing agent. A graph was plotted with the wavelength of the fluorescence peak as function of GnHCl concentration.

2.2.3. – Theoretical analysis of ataxin-3 aggregation propensity

In order to assess the aggregation propensity of protein regions, available on-line tools as TANGO (Fernandez-Escamilla *et al.*, 2004), Zyggregator (Tartaglia and Vendruscolo, 2008) and Aggrescan (Conchillo-Sole *et al.*, 2007) were used. These algorithms calculate the aggregation propensity for a protein to form amyloid fibrils by analysing its sequence, revealing regions of high β-sheet formation propensity. The results from each tool were compared for the 1-1N variant.

2.3. – Analysis of the kinetics of amyloid fibril formation

Thioflavin-T (Sigma-Aldrich, USA) solution was prepared in water and its concentration was determined by measuring the absorbance at 411nm, using as extinction coefficient $2{,}2 \times 10^4 M^{-1} cm^{-1}$. Two different buffers were used in the assay, buffer A (20mM sodium phosphate, 200mM NaCl, 1mM EDTA, 1mM DTT and 0,01% (v/v) sodium azide) and buffer B (10mM sodium phosphate, 140mM NaCl and 0,01% (v/v) sodium azide). Proteins were pre-diluted to 200μM in gel filtration buffer (the buffer in which they are stored), so that the final glycerol concentration in the assay was 0.5%. A master mix was made for each condition, with final ThT and protein concentrations of 30μM and 20μM, respectively. In each assay, 6, 8 or 10 replicates were done in an clear 96-well plate, with 20μL/well; also 10μL of paraffin oil (Hampton Research, USA) were added in the top of the wells to minimize evaporation.

Fluorescence was recorded with a Fluodia T70 PTI® (Photon Technology International, USA) at 37ºC, excitation an emission wavelengths were 385nm and 445nm respectively. The plate was read with 30-minute cycles and 3 second agitation before each reading for approximately 2 weeks. The data from the ThT assays was fitted, when possible, to a Boltzmann sigmoidal curve equation.

2.4. – Membrane destabilization assay

Liposomes were prepared from chloroform stock solutions of phosphatidylserine (PS), phosphaditylethanolamine (PE), phosphatidylcholine (PC) and cholesterol. A 1:1:1:1 (PS:PE:PC:Chol) molar relation was mixed from these stock solutions and chloroform was evaporated under a gentle nitrogen flow. The lipid film obtained was hydrated with 80mM calcein (Sigma-Aldrich, USA) in 50mM HEPES and 1mM EDTA (pH 7.4), followed by a 3-minute sonication, and passed 21 times through a 100nm pore polycarbonate membrane (Nuclepore Track-Etch Membrane, Whatman®, GE Healthcare Life Sciences, Sweden) on an extruder (Avestin®, Germany) to form large unilamellar vesicles (LUV). The liposomes were separated from free calcein by loading the liposome preparation onto a Sephadex™ G-75 column (prepared by dissolving G-75 media in liposome assay buffer – 10mM sodium phosphate, 140mM NaCl, pH 7.4). Liposome preparation was then stored at 4ºC and protected from light. Phosphate concentration was measured by Bartlett modified Fiske-Subbarow method (Bartlett, 1958).

Liposome leakage assays were performed on a 96-well opaque plate. The monomer and oligomer concentrations used were 1, 2 and 5 μM and liposome concentration was 7.5μM (phosphate concentration). For each concentration three replicates were done and two independent assays were performed. The kinetics of leakage of calcein was followed at 37ºC for 20 minutes on a SpectraMax Gemini EM fluorimeter (Molecular Devices, USA); excitation and emission wavelengths were 490nm and 520nm respectively.

2.5. – Fibril visualization

2.5.1. – Electron microscopy

Samples of protein (5µL) were applied to a formvar carbon film on 400 square mesh copper grids (Aname, Spain) and were negatively stained with 1% uranyl nitrate solution previously filtered through a 0,22µm pore cellulose membrane. The grids were viewed with a Zeiss 902A (Zeiss, Germany) transmission electron microscope (TEM) operating at 80kV.

2.5.2. – Congo red staining

Pellets of protein incubated at 37ºC were placed to dry on a slide previously coated with 3-aminopropyltriethoxy silane (APES; Sigma-Aldrich, USA). A solution of 80% ethanol with saturated sodium chloride and 0,01% sodium hydroxide was applied to the slide for 20 seconds and then dried out. After this, a solution with 80% ethanol (also with saturated sodium chloride), 1% Congo-Red (CR) and 0,01% sodium hydroxide was placed on the slide for 20 seconds and dried out. Slides were then coated with Entellan®, covered with a cover slip and were kept protected from light. The slides were observed under polarized light on a Olympus BX50 (Olympus Corporation, Japan).

2.6. – Data analysis and structural images

All statistical tests and fittings were made on Graphpad Prism 5 software (GraphPad software, USA).

Structural images of the Josephin domain were obtained with PyMOL Molecular Graphics System, Version 1.0, Schrödinger, LLC; PDB ID:1YZB (Nicastro *et al.*, 2005).

Chapter 3 Results and Discussion

3.1. – Ataxin-3 protein domains reveal different stabilities

We have expressed and purified atx3 and obtained monomers and oligomers of different domains. The purified proteins exhibit different stabilities, which were measured by thermal and chemical denaturation.

We will hereby describe the process of obtaining the monomeric atx3 variants, as well as oligomers from 1-1N variant.

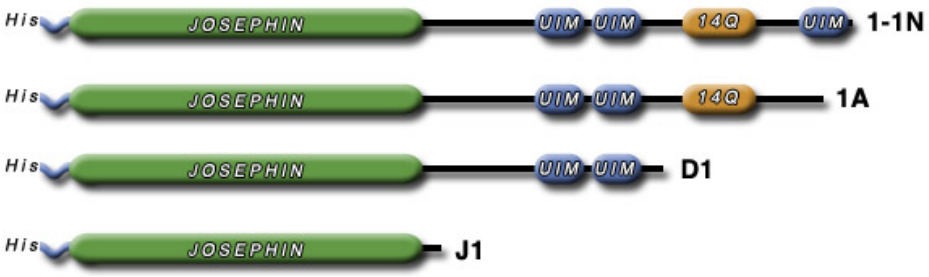

Figure 7 – Different ataxin-3 variants purified.

The different variants of atx3 purified have different domains (Fig. 7). Josephin domain is present in all variants. 1-1N variant has three UIMs, while 1A variant just has two, but both have the 14 polyQ tract, while D1 variant lacks it. By working with these different atx3 variants we were able to study the influence of different domains, as the Josephin domain alone, the polyQ tract and the third UIM, in both the aggregation process and the ability to destabilize lipid bilayer membranes.

3.1.1. – Preparation of plasmid DNA

Protein was produced after transforming the plasmids on BL21(DE3) or BL21(DE3)SI cells (cell competency was $4.8x10^4$ and $3.9x10^4$ cfu/µg for pUC19 plasmid). Plasmids for expression of atx3 variants were prepared using the NZY Tech Miniprep kit. Accordingly to restriction map analysis (Fig. 8, A) it is expected a fragment of ≈5700 base pairs (bp) on the single digestion (XbaI), and two fragments of ≈4500bp and ≈1200bp on the double digestion (EcoRI), which were confirmed on the agarose gel (representative for all plasmids) (Fig. 8, B).

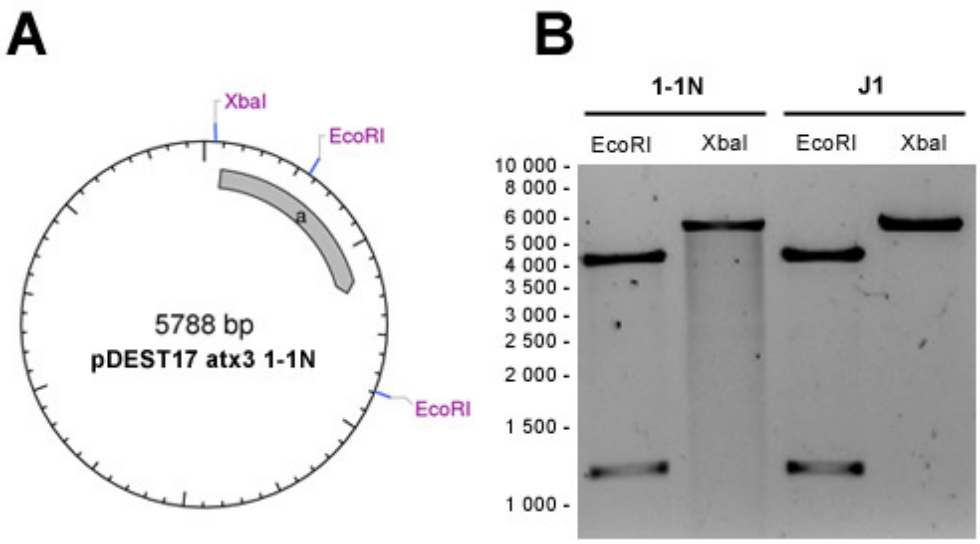

Figure 8 – Restriction analysis of 1-1N and J1 plasmids. **A** – restriction map for pDEST17 plasmid with atx3 1-1N sequence (represented by *a*), and the respective enzymatic digestion sites (XbaI and EcoRI). **B** – 1% agarose gel for 1-1N and J1 plasmid digestions.

Although it seems that 1-1N plasmid might be degraded (Fig. 9, A, 1-1N - XbaI lane), the digestion with EcoRI reveals that it is not, since the smearing is not observable there. Plasmidic DNA quantified by spectroscopy revealed a typical yield of 100ng/µL, and the ratio 260:280 was always higher than 1.8.

3.1.2. – Optimization of expression conditions

For optimization of the expression conditions, the *E. coli* strain, temperature and expression time variables were tested in an incomplete factorial experiment.

Protein expression was obtained using the best conditions of the expression tests (Fig. 9), BL21(DE3) strain, 30ºC and 2h induction. SDS-PAGE analysis on the protein expression (Fig. 10) reveals that 1-1N protein shows a high amount of soluble protein. We have used the same conditions to express the other atx3 variants (with exception for J1, in which we used BL21(DE3)SI *E. coli* strain, since previous experiments showed a higher soluble expression). In spite of that, the yields in soluble protein for those variants were smaller, maybe because of intrinsic differences in

protein stability and aggregation propensity. Nevertheless, the expression was optimized only for 1-1N variant, and the best conditions for the other variants will not necessarily be the same.

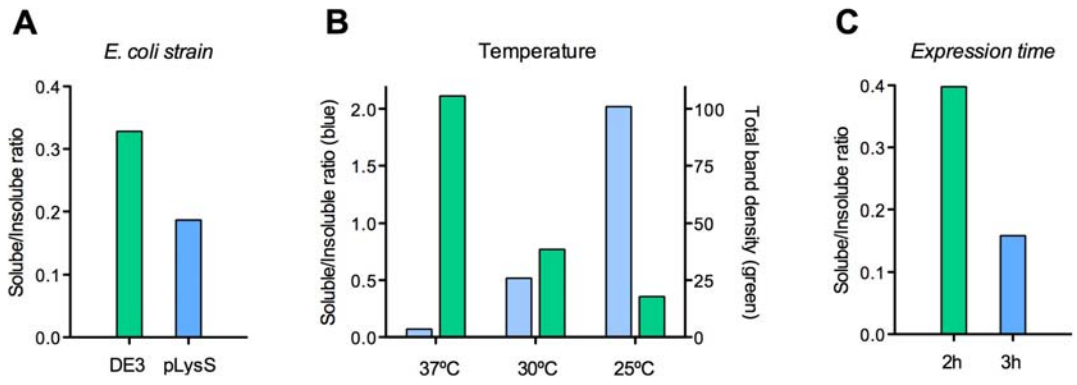

Figure 9 – Results for the expression test show that BL21 DE3 has a higher yield of soluble protein (**A**). Although a higher soluble/insoluble ratio is observed for 25ºC, the total band density is half of the 30ºC one, meaning that total protein is lesser at 25ºC (**B**). Concerning expression time, 2 hours reveal the best ratio (**C**).

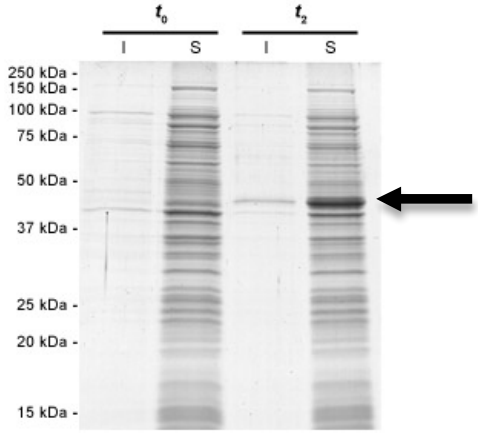

Figure 10 – SDS-PAGE analysis of 1-1N expression stained with coomassie blue. (I, insoluble; S, soluble; t_0, sample collected before induction; t_2, sample collected after 2 hours induction)

3.1.3. – Purification reveals both monomeric and oligomeric protein

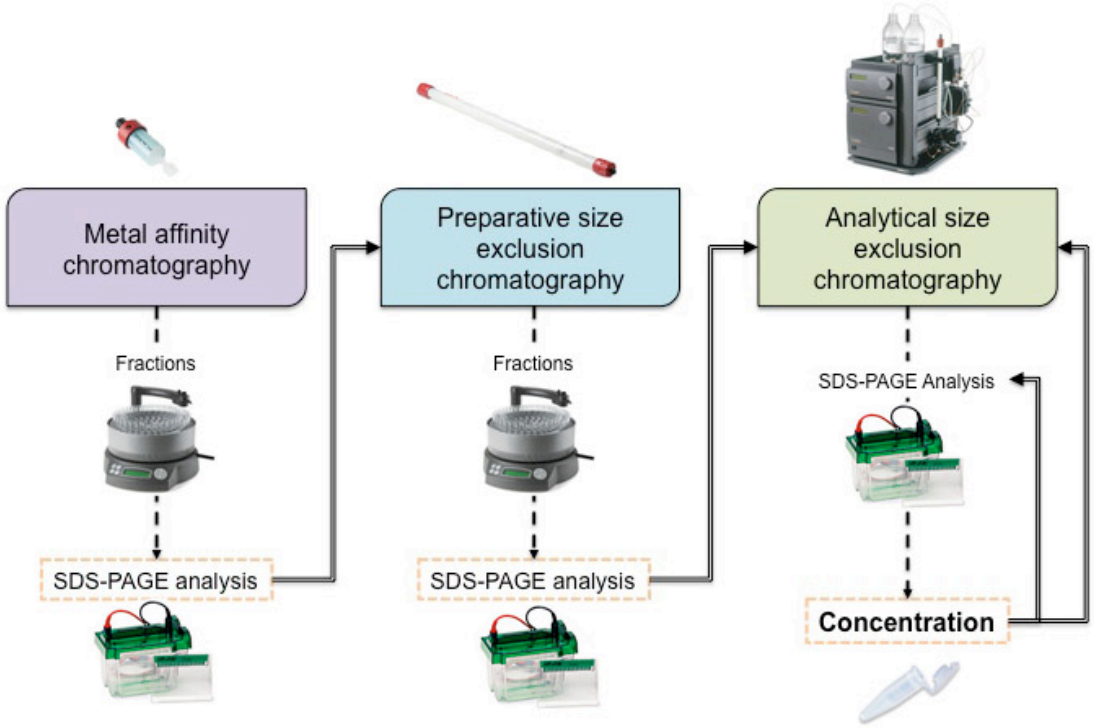

Figure 11 – Flowchart of the different experimental procedures for protein purification.

Protein was purified according to a previously described protocol (Gales *et al.*, 2005), with some minor changes. A flowchart illustrates the different experimental steps for atx3 purification (Fig. 11). Briefly, the protein extract obtained after cell lysis and centrifugation was applied to a metal affinity column loaded with nickel (Histrap HP, GE Healthcare Life Sciences, Sweden), and eluted stepwise with increasing concentrations of imidazole (50mM, 250mM and 500mM, Fig. 12). Pure protein eluted from the 250mM imidazole peak (Fig. 12, B; cleavage of the purification tag of 1-1Nb was performed with TEV protease [Appendix section I, Fig. 48]). This purification protocol differs from the previously published one (Gales *et al.*, 2005) because the protein was eluted in a 250mM imidazole step on the metal affinity chromatography, instead of a 100mM peak. The major difference observed, was that when using 100mM imidazole step, the following 500mM imidazole step exhibited a peak containing atx3 (data not shown). Furthermore, when the fractions from a 250mM imidazole step are

applied to a size exclusion chromatography, they exhibit a higher oligomeric peak (data not shown).

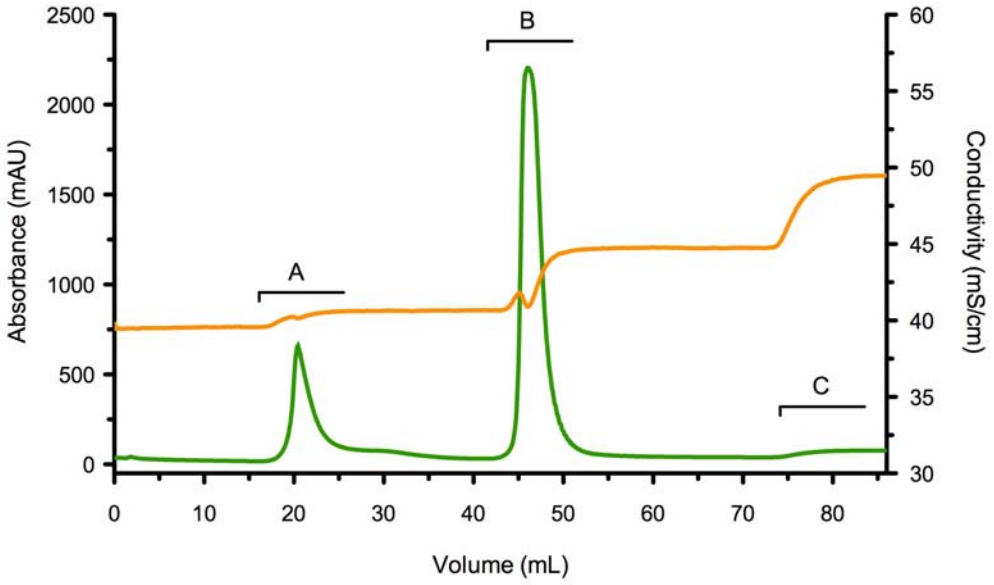

Figure 12 - Chromatogram for 1-1N metal affinity step, showing the three step elution with 50mM imidazole (A), 250mM imidazole (B) and 500mM imidazole (C). (Green line, absorbance at 280nm; Orange line, conductivity.)

After metal affinity chromatography, the fractions were analysed by SDS-PAGE (Fig. 13, A) and applied (fractions Pb, Fig. 13, A) to a preparative size exclusion chromatographic column (Hiprep 26/60 Sephacryl S-200 High Resolution column, GE Healthcare Life Sciences, Sweden). The size exclusion chromatography apparatus was maintained at 4ºC, and elution was performed at a 0.5mL/min rate. The buffer used was different from the previously described protocol, since we used 20mM sodium phosphate instead of 20mM HEPES buffer. The size exclusion chromatography performed for selected fractions exhibited two peaks (Fig. 14), both containing atx3 protein as seen on SDS-PAGE analysis (Fig. 13, B, fractions G1 and G2), closely resembling the atx3 gel filtration profile from Gales and colleagues (Gales *et al.*, 2005).

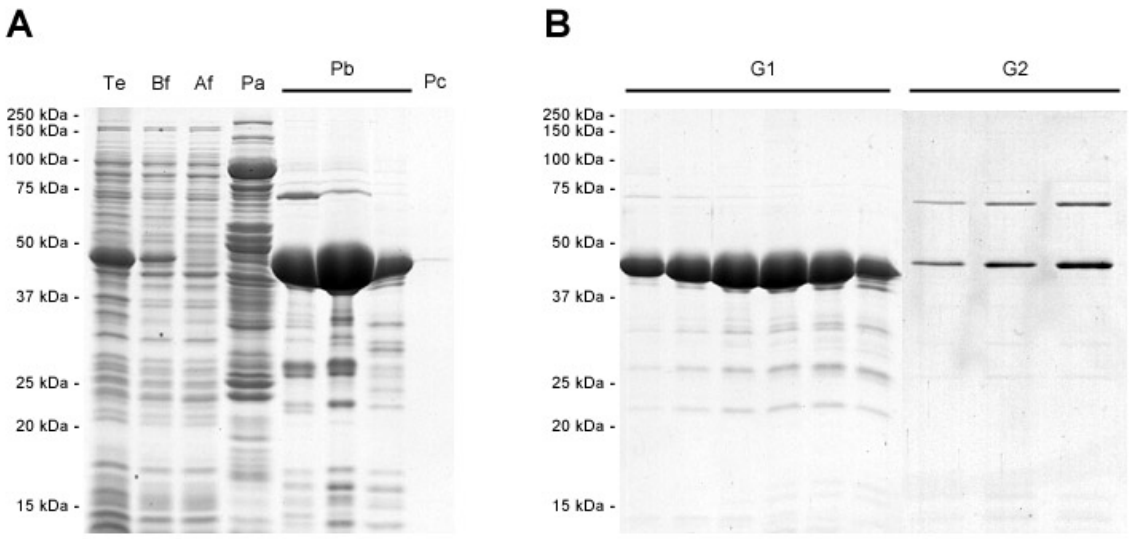

Figure 13 – SDS-PAGE analysis on fractions from affinity chromatography (**A**) and size exclusion chromatography (**B**). Fractions represented by Pb were selected for size exclusion chromatography. The first four fractions from G1 were pooled and concentrated and all fractions from G2 were pooled and concentrated separately. (**A**, Te, total lysed extract; Bf, filtered extract before loading to Histrap column; Af, flow-through Histrap with 10mM imidazole; Pa, elution with 50mM imidazole; Pb, elution with 250mM imidazole; Pc, elution with 500mM imidazole. **B**, G1 and G2, fractions from peaks A and B, Fig. 10, respectively.)

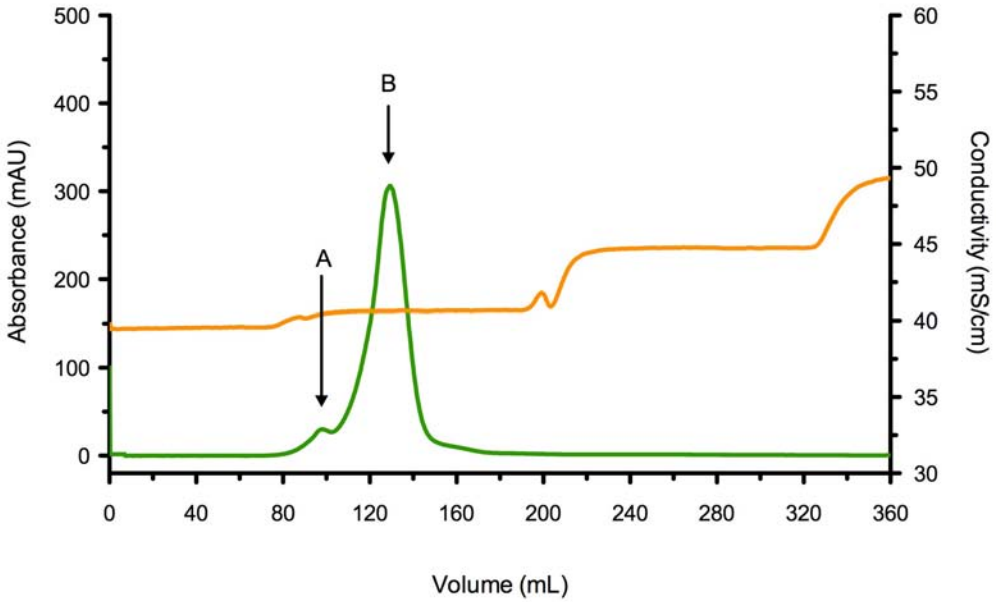

Figure 14 – Preparative size exclusion chromatogram for 1-1N variant. It is possible to see two distinct peaks: peak A, containing mostly oligomers and peak B, monomeric protein.

The fractions from preparative size exclusion chromatography (both peaks) were analysed by SDS-PAGE (Fig. 13, B) and each fraction was also analysed by analytical size exclusion chromatography.

For the monomeric protein preparation (Fig. 14, peak B), fractions exhibiting a single peak on the chromatographic profile (data not shown) and no contaminants on the acrylamide gel (Fig. 13, B) were pooled and concentrated by ultrafiltration. For the oligomeric fractions, since the total amount was always smaller, all fractions were pooled and concentrated.

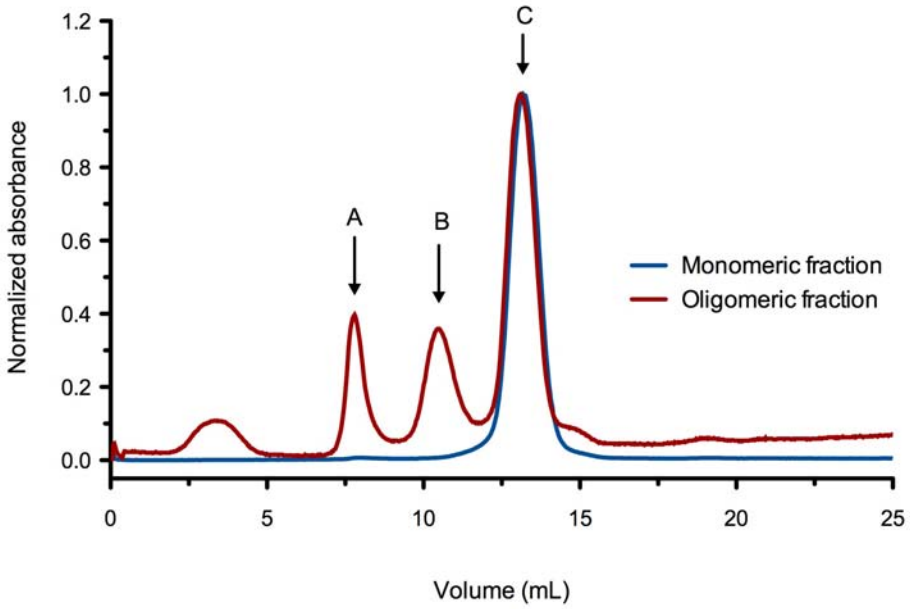

Figure 15 – Analytical size exclusion chromatograms of concentrated monomeric and oligomeric fractions of 1-1N. The monomeric form (blue) exhibits only one peak (C), while the oligomeric form (red) exhibits three peaks. Peak A corresponds to high molecular mass oligomers (HMM), peak B oligomers and peak C monomeric protein.

An aliquot of concentrated protein was analysed again by analytical size exclusion chromatography (Fig. 15) and SDS-PAGE (Fig. 16). The chromatographic profile for the monomeric protein reveals a single peak (Fig. 15, blue line) and no contaminants (Fig. 16, 1-1N batch 2) while the oligomeric fraction has three distinct peaks (Fig, 15, A, B and C). The peak A elutes in the void volume of the column and

corresponds to high molecular mass oligomers (HMM), peak B represents oligomers to a size up to 440kDa (accordingly to size exclusion markers elution profile), while peak C represents the monomeric protein. Previously work done by Gales and colleagues (Gales *et al.*, 2005) showed by gel filtration chromatography the existence of a predominant monomeric peak for atx3, but also two small overlapping peaks – oligomeric contaminants. In our experiment, we were only able to see the existence of a monomeric peak and one single oligomeric peak for the preparative size exclusion chromatography. However, the analytical size exclusion chromatography reveals one monomeric peak and two distinct oligomeric peaks that represent different subunit compositions. The peak that elutes in the void volume of the column (Fig. 15, A) represents high molecular mass oligomers, while the second peak (Fig. 15, B), represents a mixture of multimers of different subunit composition.

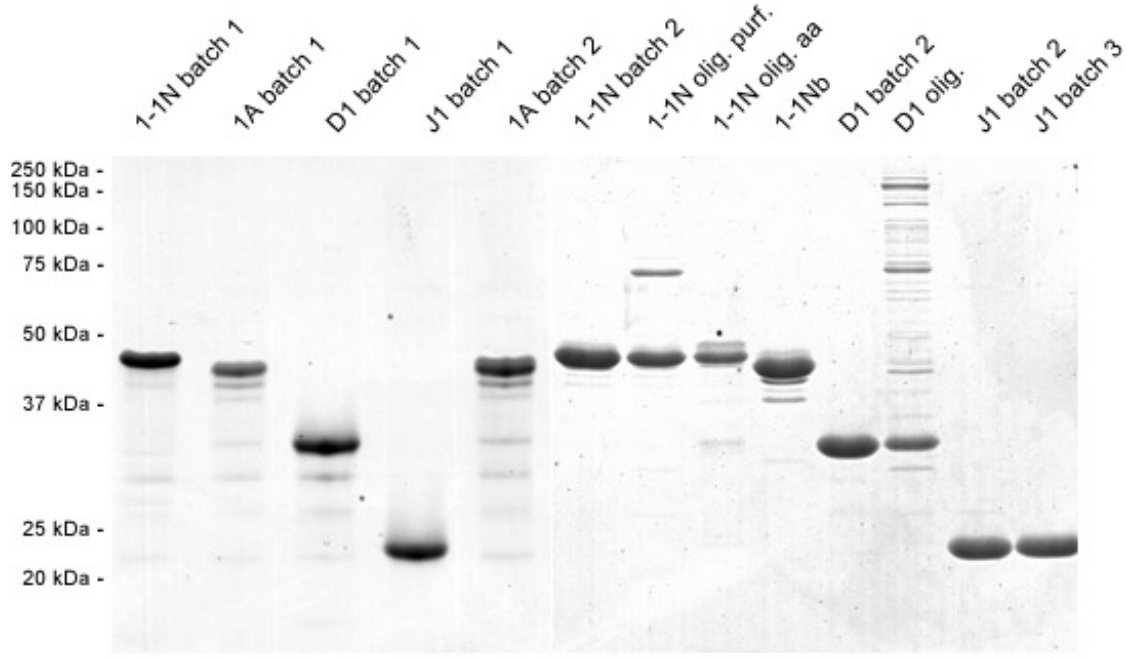

Figure 16 – SDS-PAGE analysis of purified proteins from different batches, monomeric and oligomeric forms. (The label “olig. purf.” refers to oligomers obtained from the purification process above-mentioned, whether “olig. aa” refers to oligomers that were obtain throw an oligomerization assay. Further details on section 3.1.4)

As atx3 has a high propensity to aggregate, the quality control of protein was a very important aspect. The fractions for preparative size exclusion chromatography were selected always by SDS-PAGE analysis, and the fractions from it were only concentrated after analytical size exclusion chromatography and SDS-PAGE analysis.

Atx3 was successfully purified in a monomeric form at a required yield and without major contaminants. After this step we had the necessary working material for oligomerization assays, in order to obtain oligomers for liposome leakage assays. On the Appendix section III, it is possible to consult each protein's analytical size exclusion chromatographic profile, concentration and protein yield.

3.1.4. – Monomeric 1-1N forms oligomers under near physiological conditions

The yield of oligomers obtained by the purification processes was scarce for the amount of experiments they were needed for. Having that in mind, we proceeded to an *in vitro* aggregation assay, with the intention of obtaining oligomers ready to use in the liposome leakage assays.

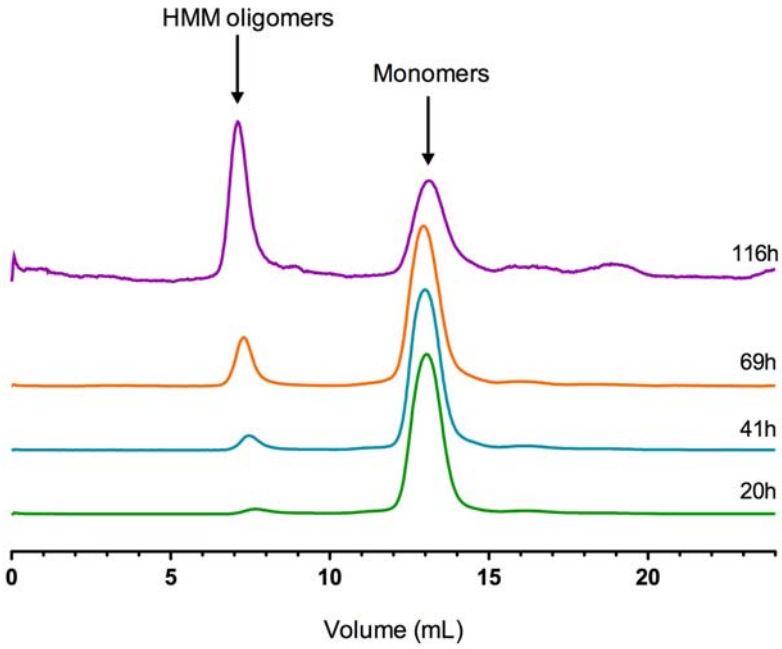

Figure 17 - Analytical size exclusion chromatography analysis of samples from 1-1N oligomerization assay at different time points.

In order to produce protein aggregates similar to oligomers we incubated monomeric protein at 37ºC (in liposome leakage assay buffer, pH 7.4) and followed the aggregation kinetics by collecting samples at different time points, and running them on an analytical size exclusion chromatography (Fig. 17), as well as viewing them with electron microscopy (Fig. 18). The total volume of the assay was approximately 5mL, with protein at 20μM. Aliquots of 100μL were analysed by analytical size exclusion chromatography (Fig. 17).

The elution profiles from the size exclusion chromatography allowed us to quantify (in percentage) the amount of aggregates at a given time point (Table 3).

The chromatographic elution profiles (Fig. 17) clearly show a decrease in the monomeric form of the protein and a concomitantly increase of oligomeric form, while the electron micrographs (Fig. 18) show an evolution of aggregate morphology. At 45h we only have 5% HMM oligomers, but they present mostly small-oligomer morphology, while at 116h we have 50% HMM oligomers, but they exhibit an increased number of small fibrils. The morphology of the obtained oligomers is very similar to other atx3 oligomers from other studies (Gales *et al.*, 2005; Ellisdon *et al.*, 2006). Curiously though, size exclusion profiles of samples from this assay did not reveal a peak corresponding to the second peak (peak B, Fig. 15) for oligomers obtained during the purification procedure.

Table 3 - Percentage of HMM at different time points (calculated by peak integration).

Time (hours)	HMM oligomers (%)
20	2.02
41	5.85
69	15.93
116	50.98

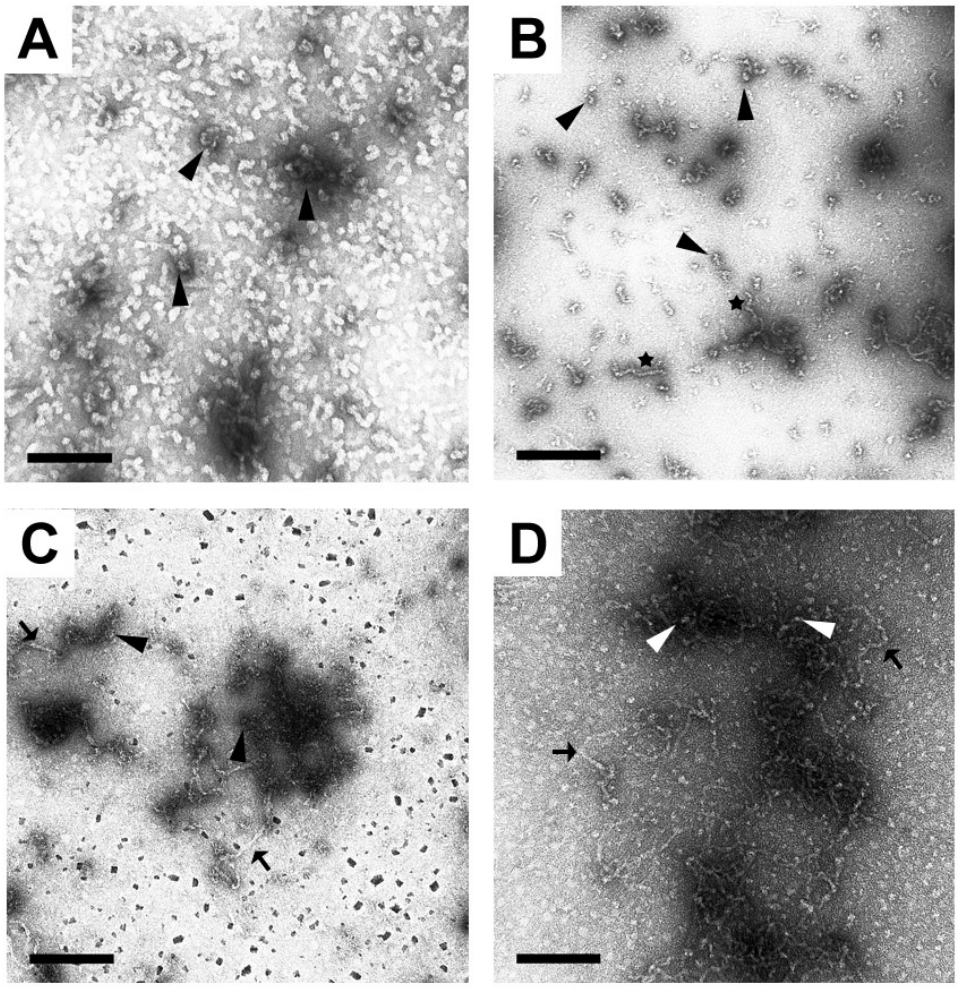

Figure 18 – Oligomerization of 1-1N followed by electron microscopy. Electron micrographs from samples collected during the aggregation assay stained with 1% uranyl. **A**, 20h aggregation, it is possible to see small oligomers (arrowhead). **B**, 45h aggregation showing several oligomers (arrowhead) and small fibrils (star). **C**, 69h aggregation, were it is possible to see much longer fibrils (arrow) and small oligomers (arrowhead). **D**, 116h aggregation exhibits even longer fibrils (arrow) and also oligomers (arrowhead). Scale bar represents 200nm.

The same assay, but for the Josephin domain (J1), shows that either it precipitates in the centrifugal filtering procedure before size exclusion chromatography, or if incubated for long periods of time. The size exclusion profiles did not reveal the presence of oligomers and clean electron microscopy images could not be obtained. The reason why the size exclusion profile did not reveal an oligomeric peak might indicate that the formed precipitate could contain oligomers, and as consequence, they

could have not entered the size exclusion column, not being detected. Nonetheless, the precipitates were stained with Congo red in search for signs of amyloid-like properties, and the results will be presented at 3.2.1 section.

The aggregates obtained by this method are a mixture between small fibrils and oligomers, as the electron micrograph shows for 116h incubation (Fig. 18). The current hypothesis we are leaning to, is that oligomers, and not fibrils, may destabilize cell membranes (Bucciantini *et al.*, 2002; Kayed *et al.*, 2003; Demuro *et al.*, 2005; Xue *et al.*, 2009). The ideal would be having the same amount obtained with 116h, but with the morphology of the 45h incubation, i.e. more small oligomers and less small fibrils. In order to overcome this setback we could adopt a proceeding similar to Xue and colleagues, constantly stirring the protein in the aggregation conditions, fragmenting the growing fibril in small oligomers (Xue *et al.*, 2009; Xue *et al.*, 2010).

Having obtained the monomers and oligomers we started looking at the intrinsic physico-chemical protein properties of (1) different atx3 variants and (2) 1-1N monomers *versus* oligomers.

3.1.5. – Ataxin-3 variants have different stabilities and monomers/oligomers are structurally distinct

Within the scope of comparing the different produced proteins stabilities, we have made thermal and chemical denaturation assays, determining their melting temperature and establishing their chemical denaturation profile.

A thermofluor assay was performed to measure the different melting temperatures of atx3 protein variants 1-1N, 1A, D1, J1, and oligomers of D1 and 1-1N. D1 oligomers started already with a high fluorescence signal and didn't exhibit a normal melting curve, being impossible do determine its melting point (data not shown), and probably because the protein was already unfolded. The reason why oligomers of D1 could be completely unfolded is not clear, but it might be due to longer exposure at room temperature, the freeze-thaw process of stored protein (although we

only made one cycle), or the influence of contaminants in that preparation, as seen on the SDS-PAGE analysis (Fig.16, D1 olig.).

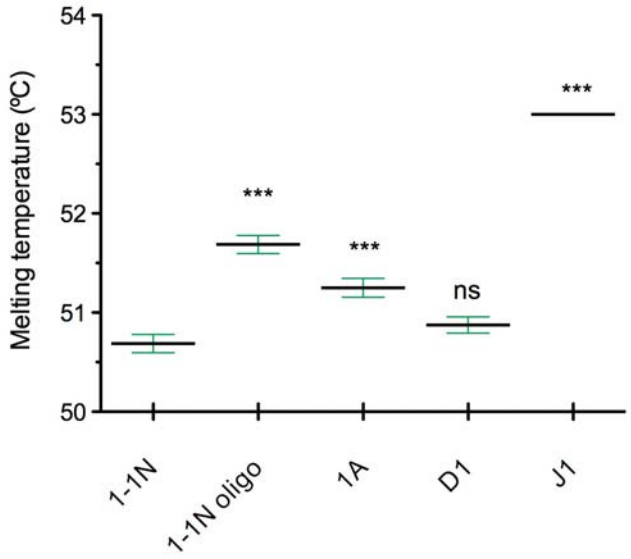

Figure 19 – Melting temperatures determined by a thermofluor assay. 1A and J1 are significantly different from 1-1N (P<0.001), while D1 does not vary significantly (ns, not significant).

The results show the differences between the different atx3 variants and the 1-1N variant. One-way analysis of variance (one-way ANOVA) revealed that the melting temperatures are significantly different (P<0.0001). Despite the small difference between 1-1N and 1A atx3 variants sequence, they exhibit a significantly different melting point. The divergences between the two are on the C-terminal, as they differ after glycine residue 353, as well as in size (1A is 13 residues shorter), and the 1A variants lacks the third UIM (Fig. 7; Chapter 2, point 2.1.5, Fig. 5). The reason behind the stability difference is unkown. It is unlikely that 1A variant increased stability could be due to the presence of oligomers, since that the fluorescence detected at the beginning was similar to all monomeric variants, and different from both D1 and 1-1N oligomers (data not shown). Having the two variants (1-1N and 1A) approximately the same size, it seems that the presence of a third UIM (in 1-1N) does not improve protein

stability, but decreases it. Furthermore, D1 variant, that has two UIMs (but lacks the polyQ tract), does not show a significant increase in stability from the 1-1N variant, possibly showing that the third UIM, may account for decreased stability. Curiously, comparing the D1 and J1 variants, being that J1 does not have UIMs, J1 exhibits a higher stability.

Josephin domain (J1) reveals to be thermically more stable (almost 2.5ºC apart in melting temperatue) than the other atx3 variants, which might correlate with the differences observed on fibril morphologies and kinetic of aggregation followed by ThT. Furthermore, J1 stability may influence on how it aggregates. Amyloid characteristics for J1, as electron micrograph fibril morphology, were shown when using high temperatures (Masino *et al.*, 2004), and in our case, a pellet formed by an ultrafiltration step which exhibited apple-green birefringence (Fig. 24; point 3.2.2), a classical characteristic of amyloid fibrils. However, J1 pellets formed under incubation at 37ºC revealed negative Congo red staining (data not shown) and amorphous aggregates on electron micrographs (Fig. 25). Overall, since the roles of UIMs and polyQ on protein thermal stability are unknown, one should bear in mind that the discussed causes for divergences might be highly speculative.

Having determined the melting temperatures of the different atx3 variants we were interested on seeing if the relative stabilities were similar, when followed by tryptophan fluorescence upon denaturation with guanidine hydrochloride (GnHCl). Taking advantage on the fact that our protein has tryptophan (W) residues, and especially because they are on the Josephin domain, which allows us to use any of our atx3 variants, we carried out a chemical denaturation assay based on the intrinsic tryptophan (W) fluorescence. One tryptophan residue is located in the purification tag, but other three are located on the Josephin domain (Fig. 20). Two of them are accessible at the surface of the protein (W87 and W130), while the other one (W120) is positioned in an inner and less accessible part (Fig. 20, B). The increase exposure of these tryptophan residues to the solvent will shift their emission maximum (red-shift),

and makes it a valuable resource to measure changes in protein structure without the need of probes and possible associated problems (as, for instance, probe influence on protein structure).

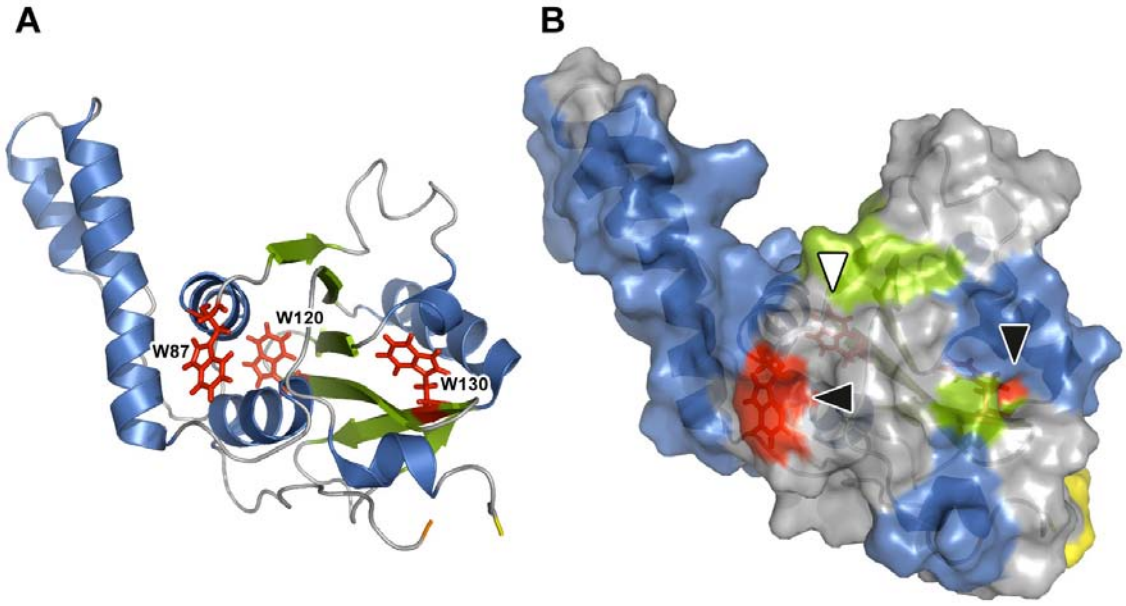

Figure 20 - Structure of the Josephin domain exhibiting the different tryptophan (W) residues. **A**, in the Josephin domain there are two tryptophan residues more accessible (W87 and W130) and one hidden (W120). **B**, Josephin protein surface exhibiting in red the surfaces corresponding to W87 and W130 (black arrowheads) and the inner W residue (white arrowhead). (PDB ID: 1YZB; Nicastro et al., 2005)

This technique has been widely used to assess protein structure alterations, inclusively on normal and expanded atx3 (Chow et al., 2004) and Josephin domain (Masino et al., 2004). The denaturation profiles of 1-1N (monomeric) and J1 are very similar, and the proteins denature at approximately the same GndHCl concentration (Fig. 21). Monomers from 1-1N and J1 exhibit sigmoidal curves, which can be fitted onto a Boltzmann sigmoidal type with R^2>0.97 (data not shown). In the other hand, oligomeric 1-1N has a completely different profile and does not exhibit a typical sigmoidal curve. Instead, it starts in a stage with emission maximum very similar to the one observed for denatured monomeric form, but finishes at the same fluorescence peak observed for monomeric protein.

1-1N and J1 variants show very similar chemical unfolding profiles, in quite resemblance to the work of Masino and colleagues (Masino *et al.*, 2004), although the denaturation is achieved at ≈2.2M GndHCl against the 2.7M from Masino (which might correlate to differences in buffers). On the other hand, oligomers show a completely different profile, meaning that in its native state, oligomers are structurally different from monomers. Furthermore, changes induced by the increased denaturing agent show a modest red-shift until a concentration of 2.5M, and only from them a larger increase. Although oligomers are structurally unkown species, one could speculate that the first part of the denaturation profile (until 2.5M GndHCl) might correspond to a structural conformation that fully exposes the outer tryptophan residues, while from there till 6M could correspond to the exposure of the hidden one (Fig. 20, W120). We should bear in mind that these are only speculations, since the structure of the oligomers might alter significantly the position of the tryptophan residues mentioned.

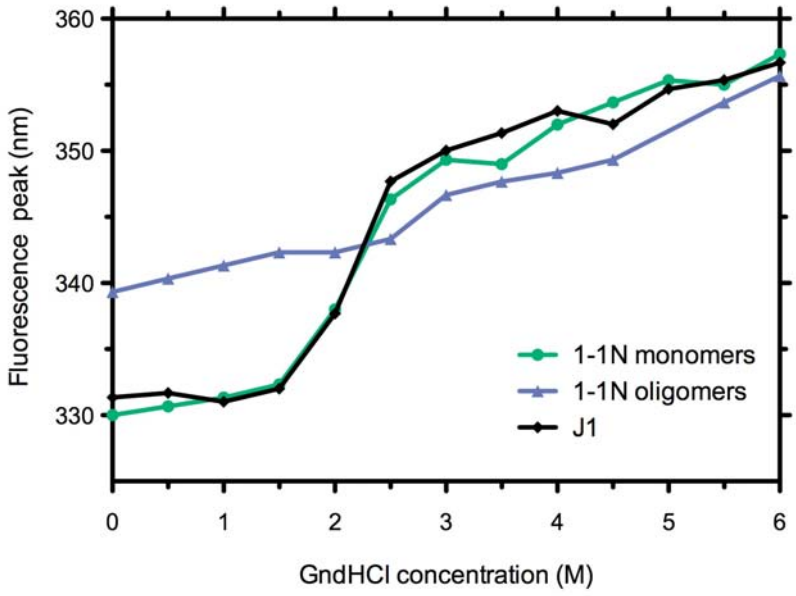

Figure 21 – Chemical unfolding profiles of monomeric and oligomeric 1-1N as well as monomeric J1 obtained by increasing concentrations of guanidine hydrochloride (GndHCl).

The finding that oligomers are structurally different from monomers, and that they resemble partially denatured protein is a very important aspect, since they support

the idea that partially folded protein are part of the process of protein misfolding that leads to aggregation (Bucciantini *et al.*, 2002; Jahn and Radford, 2005; Rousseau *et al.*, 2006a). Furthermore, the structural rearrangement that oligomers present, might expose protein regions that are normally hidden on the monomeric form, especially regions that can be aggregation prone (as we will discussed at section 3.2.1), which can, therefore, lead to an increase aggregation.

3.2. – Ataxin-3 vaiants aggregate differently but form amyloid-like fibrils

So far we have highlighted the differences in thermal and chemical stabilities of different atx3 variants and oligomers and we were now interested on how the atx3 domains behaved on different fibril formation conditions (by using the different variants). There are a few published works on different atx3 domain's influence on aggregation, and only Ricchelli and colleagues (Ricchelli *et al.*, 2007) compared a full-length atx3 with different polyQ sizes and Josephin domain alone. The main differences verified concerned the curve shape, where for the full-length atx3 with 26 glutamines had a sigmoidal-type shape and for J1 a plain increase (Ricchelli *et al.*, 2007). Previous work from our group, gives directions on the influence of pH on fibril formation rate and we thereby studied the different profiles (the modality of the curve) and rates of aggregation (faster or slower aggregation) and the ability of the different atx3 domains to form amyloid-like fibrils or have amyloid-like characteristics.

3.2.1. – Ataxin-3 amino acid sequence regions are predicted to form β-aggregates

Awareness is rising that specific amino acid sequences may have an instrinsic propensity to form amyloid aggregates, and might play an important role on protein aggregation (Tartaglia *et al.*, 2008).

We therefore analysed the aggregation propensity of atx3 1-1N variant (that has a purification tag with 22 residues) with three available algorithms: TANGO,

Zyggregator and Aggrescan. Aggrescan is an algorithm that predicts aggregation prone regions of proteins, based on an aggregation-propensity scale of natural amino acids derived form *in vivo* experiments (Conchillo-Sole *et al.*, 2007). Zyggregator algorithm is based on the role of physico-chemical properties on the aggregation rate, and involves hydrophobicity, charge and propensity to adopt α -helical or β -sheet structures on the algorithm equation (Tartaglia and Vendruscolo, 2008). TANGO algorithm is also based on physico-chemical properties to calculate the β -sheet formation propensity (Fernandez-Escamilla *et al.*, 2004). All the algorithms calculate the propensity of an unfolded peptide to form amyloid fibrils, except the Zyggregator Z_{tox} that calculates the propensity of oligomer formation by native protein.

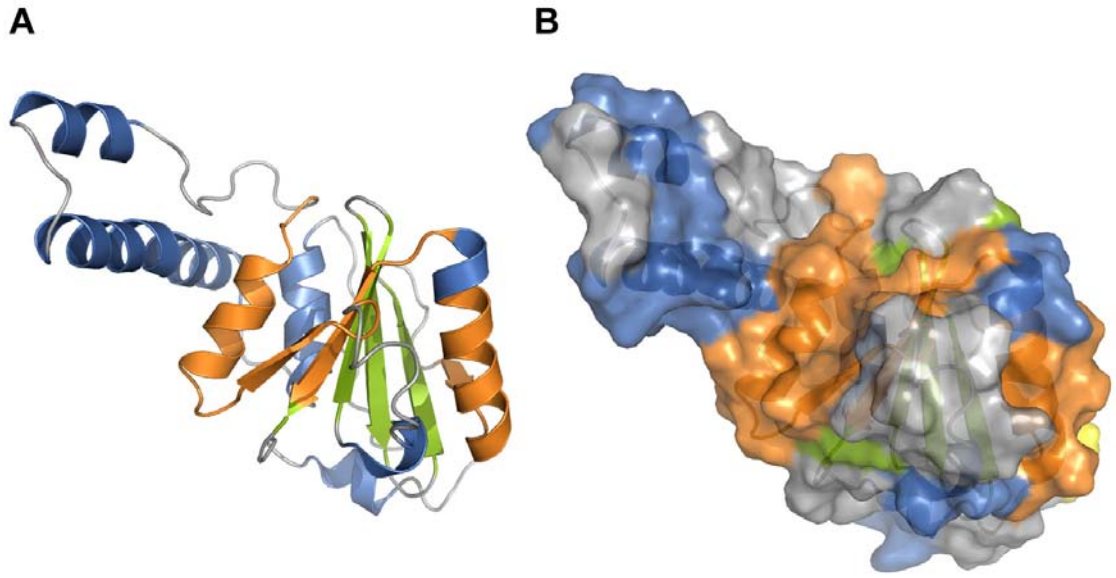

Figure 22 – Structure of the Josephin domain, exhibiting aggregation prone regions (orange), show as (**A)** cartoon view or (**B)** surface view. (The sequence regions at orange [aa 74-95; 146-155; 159-165] are presented in, at least, two algorithms. J1 without the purification tag: PDB ID:1YZB, Nicastro *et al.*, 2005))

All the algorithms used found aggregation-prone areas mainly on the Josephin domain (Fig. 23, aa 22-180). Results from Z_{tox} are very similar to Z_{agg}, however exhibiting less aggregation-prone spots, meaning that not all aggregation prone regions can form β-aggregates when in the native structure conformation. Zyggregator

also finds a highly aggregation-prone region on the hexahistidine tag (Fig. 23, aa 1-2). Together, these results reinforce the importance of other domains, other than the polyQ tract, that can be involved on protein aggregation.

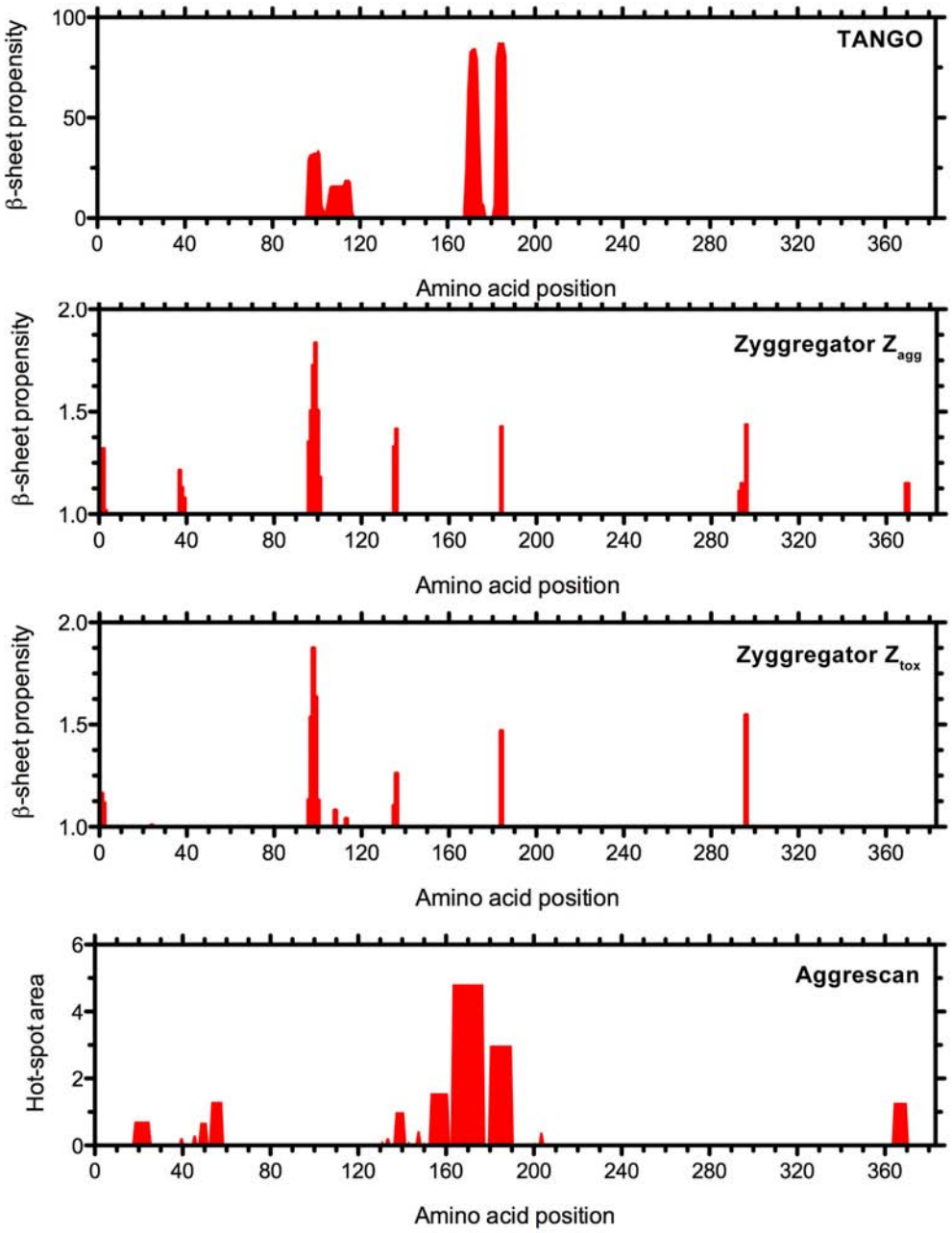

Figure 23 – Aggregation propensities calculated using different algorithms. TANGO, Zyggregator Z_{agg} and Aggrescan calculate the propensity of an unfolded protein to form β -sheet aggregates, while Zyggregator Z_{tox} calculates the propensity of a natively folded peptide to form those aggregates. (The sequence used was from the atx3 1-1N variant, with the purification tag [see Chapter 2, section 2.1.5, Fig. 5].)

There is a special interest on Josephin domain, since it has constitutes the catalytic cystein-protease domain of atx3 protein, is the smallest construct, exhibits alone amyloid-like characteristics as Congo red apple-green birefringence and, as shown by Masino and colleagues, forms fibrils (Masino *et al.*, 2004), and was shown to form dimmers conformationaly equivalent to wild type atx3 (Gales *et al.*, 2005).

3.2.2. – Ataxin-3 constructs form fibrils and exhibit Congo red birefringence

Throughout the oligomerization assays (section 3.1.4) conducted with 1-1N and J1 atx3 variants, we were able to detect the formation of protein pellets. We therefore stained these pellets with Congo red, a classic marker of amyloid fibrils (Nilsson, 2004), in search for amyloid-like characteristics.

At both 1-1N and J1 oligomerization assays, we observed the formation of pellets after incubations longer than 100h. As mentioned at section 3.1.4, we had a filtration by centrifugation step to prepare the samples for analytical size exclusion chromatography, and we observed that J1 formed a pellet after this step. This could be due to a high increase on local concentrations of protein, which might have lead to a rapid protein aggregation, and pellet formation.

The pellets formed were stained with Congo red and viewed under polarized light, revealing an apple-green birefringence (Fig. 24), characteristic of amyloid fibrils.

Apple-green birefringence was already shown for 1-1N variant (Gales *et al.*, 2005), but it had never been shown for Josephin domain alone. The Josephin domain alone has amyloid-like characteristics, since it can form fibrils under high temperature conditions (Masino *et al.*, 2004), and we now show that it precipitates, revealing apple-green birefringence (Fig. 24, B). However, this characteristic was only seen for the J1 that was submitted to a centrifugal filtering, since the pellets formed at 37ºC did not reveal the positive Congo red staining.

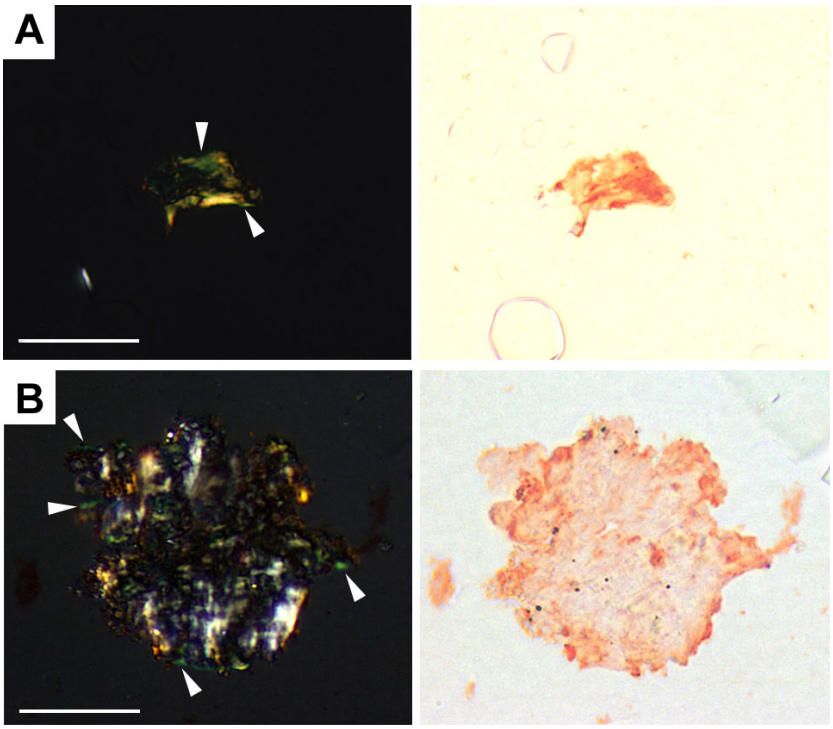

Figure 24 – Congo red birefringence of: **A**, 1-1N pellet and **B**, J1 pellet. The right images are the normal staining of Congo red while in the left is the apple-green birefringence, indicated on some spots with a white arrowhead. Scale bar represents 20μm.

On another experiment, but using ≈500μM of protein concentration, and incubation at 37ºC, we could observe the formation of gel-like pellets, as in close resemblance to Xue and colleagues (Xue *et al.*, 2010), for 1-1N, 1A and D1 variants and a mix of white and gel-like pellets for J1 variants. Those samples were stained with Congo red and did not reveal any birefringence, even so, electron micrographs of these pellets showed the existence of fibrils in 1-1N, 1A and D1 variants, and only amorphous aggregates on J1 (Fig. 25).

Full-length atx3 (1-1N variant) exhibits long fibrils (ranging from 100-250nm) with a diameter of 8-12nm, which were also observed, although smaller, on 1A and D1 fibrils. On the other hand, J1 formed large amorphous aggregates. The reason behind this is not clear, but might have to do with either specific protein regions that protect from the formation of amorphous aggregates directly, or by promoting an ordered aggregation (indirectly) that the Josephin domain alone lacks.

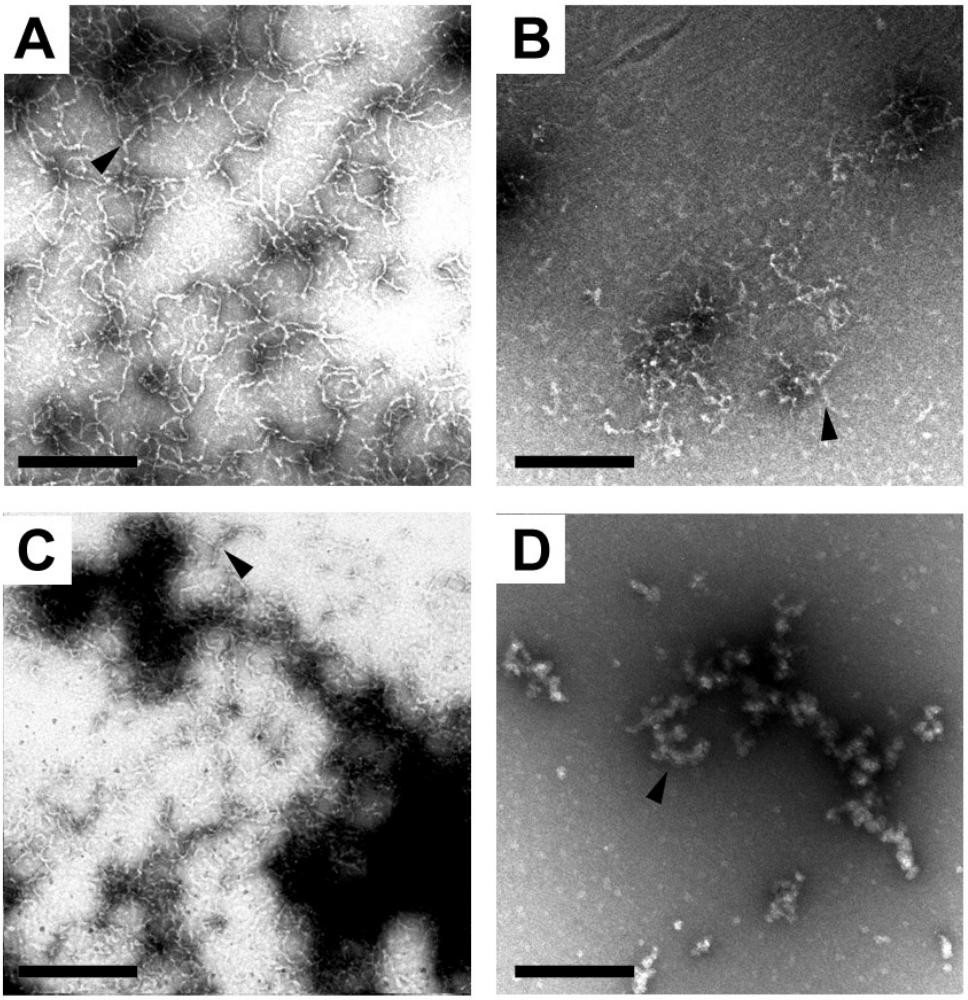

Figure 25 – Electron micrographs of fibrils of **A**, 1-1N; **B**, 1A; **C**, D1; **D**, amorphous aggregates of J1. Scale bar represents 300nm.

3.2.3. – Ataxin-3 variants aggregate at different rates

After demonstrating that 1-1N, 1A and D1 atx3 variants formed fibrils, while 1-1N and J1 variants exhibited Congo red positive staining, we were interested in exploring different aggregation conditions and how would they affect fibril formation, and compare the different variants in search for different aggregation profiles or aggregation rates.

Thioflavin-T is an extensively used probe to identify amyloid or amyloid-like structures. It is proposed that it binds to channels formed by the perpendicular cross-β

sheet structure along the fibrils (Fig. 26), greatly enhancing its fluorescence emission (Biancalana and Koide, 2010).

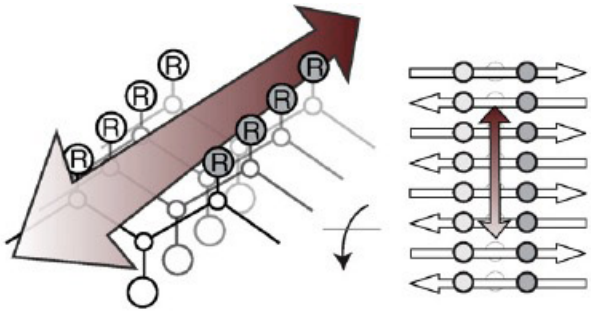

Figure 26 - Proposed model for Th-T binding to amyloid fibrils in which the ThT binds to a channel formed along the perpendicular cross-β sheet structure fibril. Adapted from (Biancalana and Koide, 2010).

Starting from previous work that showed increase aggregation rate for lower pHs (Macedo-Ribeiro *et. al*, unpublished data), we tested the influence of pH 7.5 and pH 7, and also different ionic strengths of the medium (with or without 200mM NaCl, that we will call “with salt” or “without salt” in future references). The results were fitted, when possible, to a Boltzmann sigmoidal type equation (Fig. 27, Equation 1), which was adapted to describe the voltage dependent activation of ion channels. However, the Bolztmann equation has been widely used to describe conformational changes of biological molecules involved in different mechanisms (Dubois *et al.*, 2009), and the sigmoidal curve has the stages seen for atx3 fibrillogenesis followed by ThT. These stages include the lag phase (nucleation event), a rapid growth phase (elongation event) and a final plateau (Gales *et al.*, 2005; Ellisdon *et al.*, 2006; Ellisdon *et al.*, 2007). Also, the Boltzmann fitting, allowed us to calculate the V_{50} (as we will call A_{50}), which, in our case, represents a 50% aggregation.

Equation 1 - Boltzmann equation adapted to describe the voltage depend activation of ion channels. (See Fig. 27)

$$y = Bottom + \frac{(Top - Bottom)}{1 + \exp\left(\frac{V_{50} - x}{Slope}\right)}$$

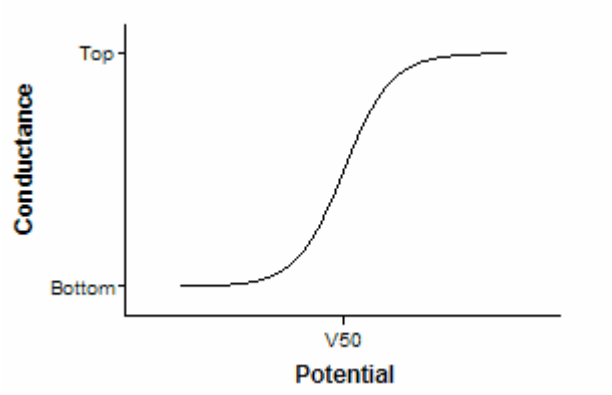

Figure 27 – Bolztmann sigmoidal type curve, adapted.

The assays exploring different salt concentrations for 1-1N variant (Fig. 28) reveals that it aggregates at the different rates. At pH 7.5 with/without salt the results fit a sigmoidal curve aggregation (R^2>0.98). On the other hand, at pH 7 we cannot observe a sigmoidal curve for both buffers, maybe due to an increase in fluorescence close to 400h, which might indicate a second step aggregation (Fig. 28, A and B, second green arrow). The calculated A_{50} (50% aggregation) shows a difference of ≈32h at pH 7.5 for the influence of salt (from 106.00h to 74.28h at pH 7.5 for no salt and salt, respectively). These results are also verified on other studies about the influence of ionic strength on aggregation, but for other amyloidogenic proteins, as mouse prion protein (Jain and Udgaonkar, 2010) and for Aβ-peptide (Klement *et al.*, 2007). Increase ionic strength seems to increase aggregation, and the morphology of the aggregates exhibits differences. Moreover, oligomers formed without salt exhibit less β -sheet content when compared to the ones formed with salts (Klement *et al.*, 2007; Jain and Udgaonkar, 2010). Aβ-peptide aggregates also in accordance with the precipitation power of ions of the Hofmeister series (Klement *et al.*, 2007). Atx3 D1 variant also revealed differences between salt and no salt (Fig. 29), aggregating slower in no salt conditions. It was also verified that D1 had a possible two stage aggregation (Fig. 29, second green and orange arrows), which is visible in both buffers, although in buffer with salt appears earlier than for buffer without salt.

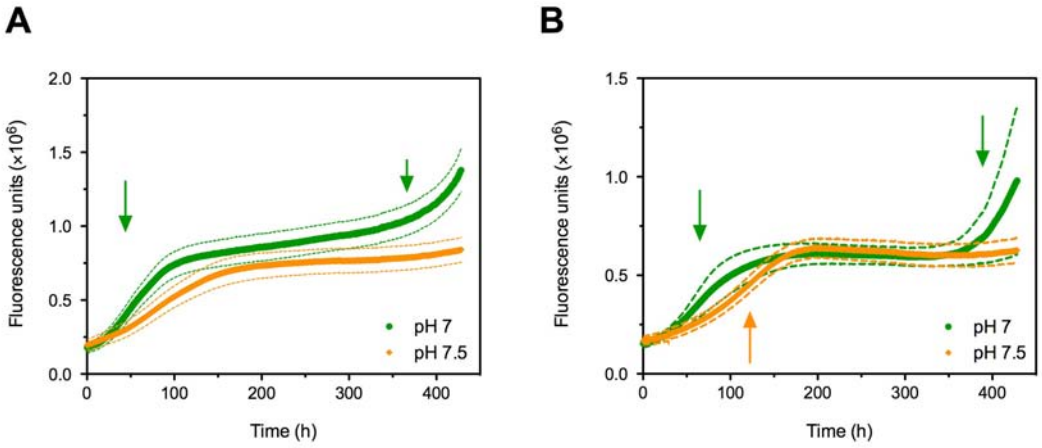

Figure 28 – ThT assays for 1-1N atx3 variant. **A**, Assay with salt. At pH 7 it is observable a faster aggregation, and a possible second step aggregation (second arrow). **B**, Assay without salt. At pH 7 it is also verified a faster aggregation, as well as a second step of aggregation (second green arrow). (Results are averages [±SE, dashed line] of, **A**: pH 7 and pH 7.5 6/8 [6 out of 8 replicates]; **B**: pH 7 7/8 and pH 7.5 8/8.)

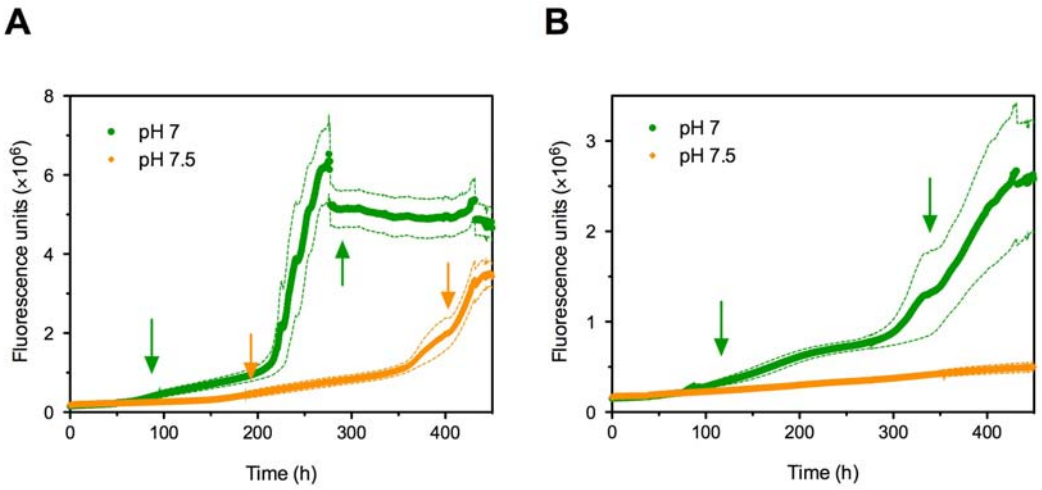

Figure 29 – ThT assays for D1 atx3 variant. **A**, Assay with salt. At pH 7 it is observable a faster aggregation, and a probable second stage of aggregation (second green and orange arrow). **B**, Assay without salt. At pH 7 it is also verified a faster aggregation, as well as a second step of aggregation (second green arrow). (Results are averages [±SE, dashed line] of, **A**: pH 7 and pH 7.5 6/8 [6 out of 8 replicates]; **B**: pH 7 7/8 and pH 7.5 8/8.)

Curiously, comparing 1-1N and D1 variants (buffer with salt), the possible second stage of aggregation for D1 variant appears almost two-fold earlier than for the

1-1N variant (Fig. 28 and 29, A). It seems that the presence of the third UIM, as well as the polyQ tract, of the 1-1N variant favours a faster first step aggregation, but do not favour a second step aggregation. The reason why we see this behaviour is unknown, but one could speculate that atx3 has different aggregation pathways, which can lead to different rates of aggregation that can probably exhibit the profiles showed.

As it was observed for these atx3 variants, at pH 7 they aggregate faster than at pH 7.5, in accordance with the influence of lower pH on increasing the partially unfolded states. The lower pH can act by decreasing the thermodynamic barrier for a protein to unfold, being therefore a condition more prone for aggregation (Jahn and Radford, 2008).

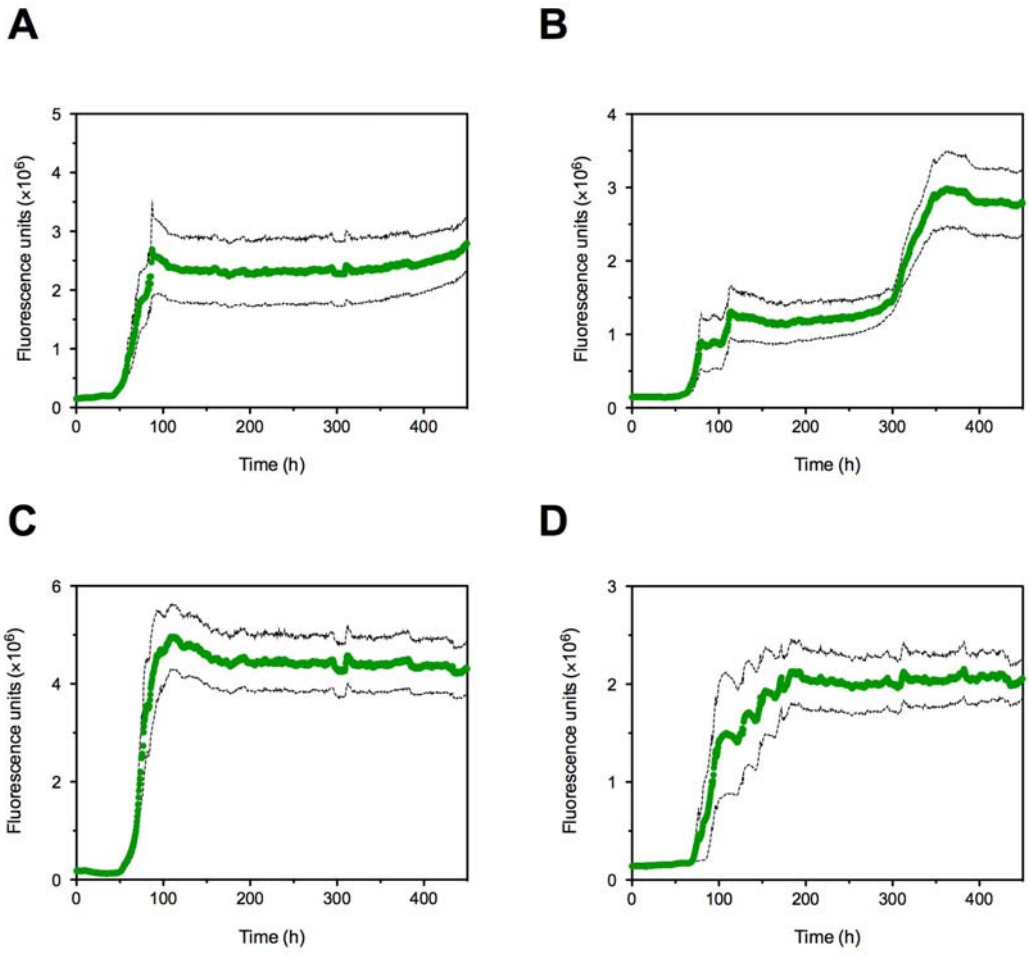

Figure 30 – ThT assay for 1-1N (A), 1A (B), D1 (C) and J1 (D) atx3 variants at pH 7. (Results are averages [±SE, dashed line] of, **A**: 6/10 [6 out of 10 replicates]; **B**: 9/10; **C**: 7/10; **D**: 7/10.)

In another assay we tested in the same 96-well plate the 1-1N, 1A, D1 and J1 variants (Fig. 31) as well as 1-1Nb (Fig. 32), at pH 7 and 37ºC. The results show good least squares fittings of 1-1N, D1 and robust fit for J1 (1-1N, D1, R^2>0.99; J1, Robust sum of squares 693.1). The 1A protein curiously shows a two-step aggregation (Fig. 30, B). Half of the replicates of 1A variant seem to show one pathway, and the other half, other pathway (further details on Appendix section II, Fig. 49).

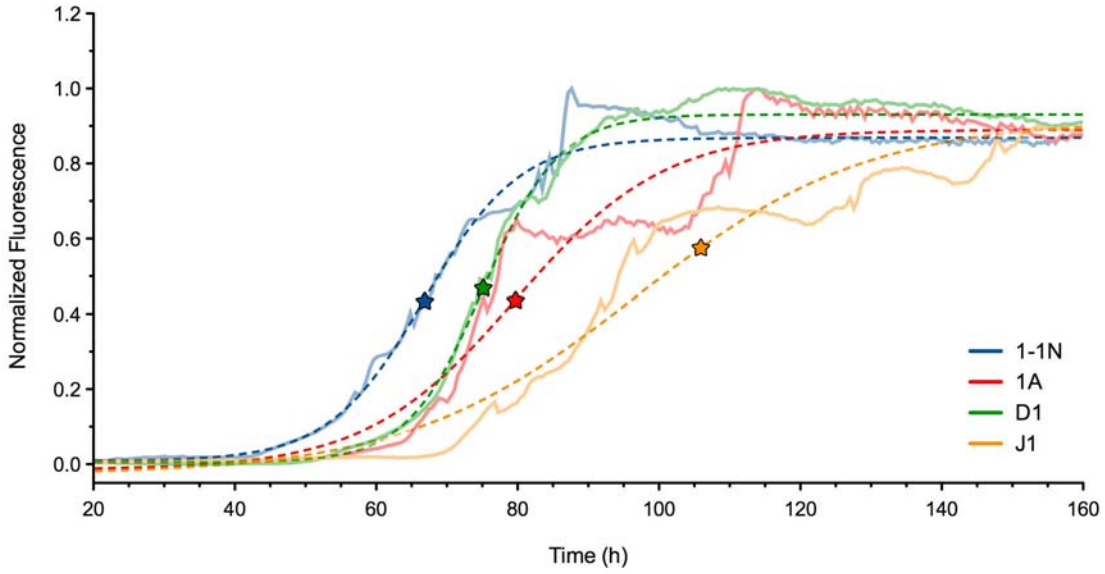

Figure 31 – Detailed view of ThT aggregation profiles of 1-1N, 1A, D1 and J1, at pH 7 in buffer with salt. J1 has the slowest aggregation while 1-1N has the fastest. D1 is very similar to 1-1N while 1A has a two-step aggregation. (ThT fluorescence: solid line; Curve fitting: dashed line. Stars indicate the A_{50}.)

The normalized fluorescence graph comparing the different variants for the time interval of 20-160h, shows the differences between aggregation rates on the rapid growth phase (Fig. 31). 1-1N variant (blue) aggregates the fastest, with an A_{50} of 66.8h, followed by D1 variant (green) with 75.2h and J1 variant (orange) with 105.9h. The 1A exhibited the two stage discussed above, still, the A_{50} of the combined stages is 79.7h. The aggregation rate series 1-1N>D1>1A>J1 can probably correlate with the thermal stability 1-1N<D1<1A<J1, as it seems that as more stable a variant is, it aggregates slower.

Curiously, the aggregation profile of 1-1Nb (Fig. 32) does not reveal a sigmoidal type curve and instead, it continuously increases fluorescence not reaching a plateau for the time interval measured. This important observation may point to an influence for the purification tag on the process of aggregation, being therefore essential for future studies the removal of the tag. Also Zyggregator Z_{agg} algorithm predicts for the first 2 residues in the purification tag (Methionine and Serine), a high propensity for aggregation, being a problem that we should not disregard. However, we should also take in account that these assay was performed only twice for 1-1Nb, and with the same protein batch.

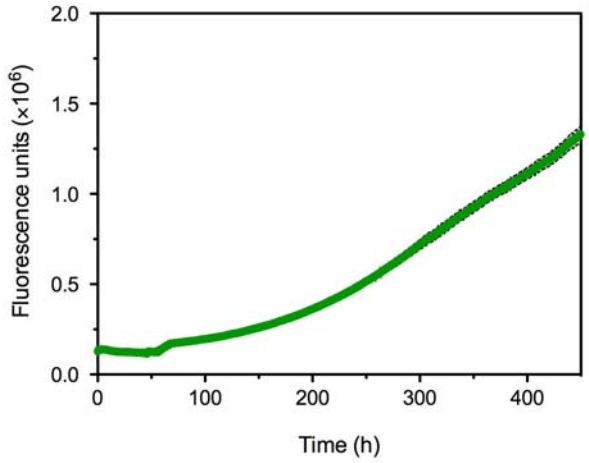

Figure 32 – ThT aggregation profile for 1-1Nb. The profile doesn't display a sigmoidal type aggregation; instead it concomitantly increases fluorescence not reaching a plateau in measured time interval. (Results are averages [±SE, dashed line] of 7 out of 10 replicates.)

Further assays were made, but this time with buffer B (10mM sodium phosphate, 140mM NaCl and 0,01% sodium azide), the same buffer used on the liposome leakage assays (but with sodium azide). An assay with 1-1N, 1A, D1, J1 (Fig. 33) and 1-1Nb atx3 variants (data not shown) was then performed on this buffer, at pH 7.

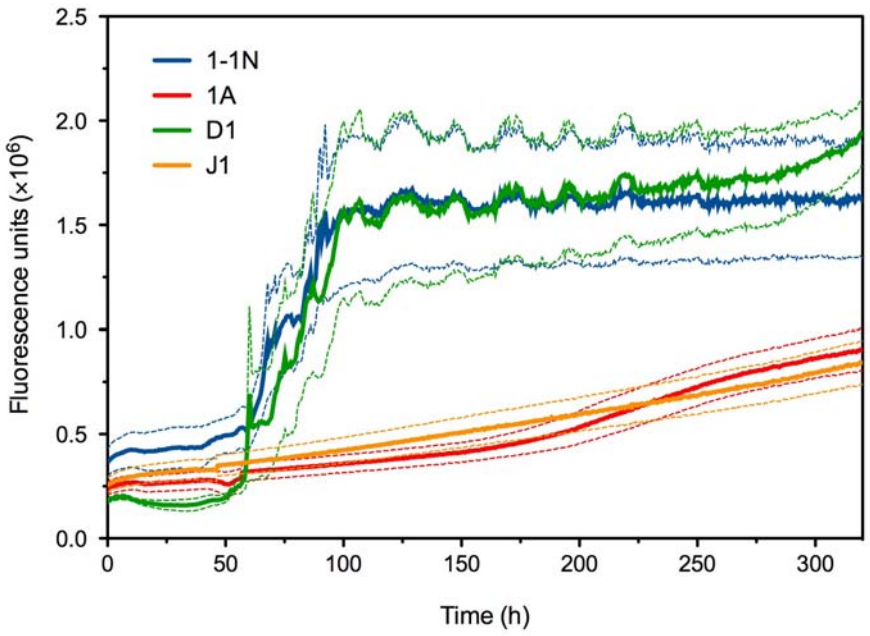

Figure 33 – Th-T aggregation assay for 1-1N, 1A, D1 and J1 in buffer B, pH 7. ThT fluorescence results show a normal aggregation for 1-1N and D1 variants, while 1A and J1 variants do not display a sigmoidal type curve. (Results are averages [±SE, dashed line] of: 1-1N: 6/6 [6 out of 6 replicates]; 1A: 4/6; D1: 6/6; J1: 6/6.)

The ThT assay in buffer B produces a slightly slower aggregation for 1-1N and D1, in contrast with buffer A. This observation correlates with the observation that increased salt concentration increases fibril formation (Klement *et al.*, 2007; Jain and Udgaonkar, 2010), since this buffer B has a salt concentration of 140mM NaCl, instead of 200mM from buffer A. 1-1N and D1 aggregation occurred 9h and 4h later (A_{50}), compared to the buffer containing 200mM NaCl. The 1A and J1 variants show different results when compared to the profiles obtained from buffer A (Fig. 30), which might be related with the either the conditions of aggregation or the protein preparations. The J1 previously used was suspected to have oligomers, since it formed pellets during concentration. This doubt was confirmed by electron microscopy (Fig. 34), which confirmed the presence of oligomeric structures.

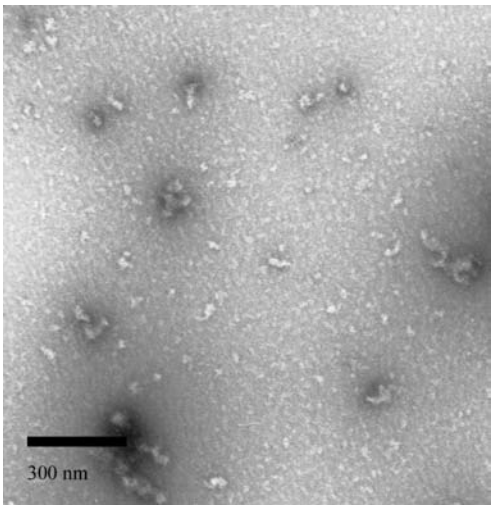

Figure 34 - Electron micrograph of J1 suspected of containing oligomers. Scale bar represents 300nm.

Having this in mind, J1 shows a profile similar to 1-1Nb, and the J1 used with buffer A (older batch) might have formed ThT positive fibrils simply because it already had the conditions for faster aggregation: the existence of possible nucleating cores (oligomers). Nevertheless, for this specific buffer (buffer B), the amount of time we measured ThT fluorescence could be insufficient to see any changes in either J1 or 1A variants. Finally, the 1-1Nb aggregation profile in this buffer was similar to the one using buffer A (data not shown).

We have so far studied the intrinsic protein physico-chemical properties of different atx3 variants, and the diversity of fibril forming rates and profiles. After this characterization, we were interested in determining the different capacities of monomers and oligomers to destabilize cell membrane, by using liposomes as a model for the membrane lipid bilayer.

3.3. – Ataxin-3 monomers do not destabilize liposome membranes

Liposomes with calcein inside were produced in order to assess changes membrane permeability by measuring the leakage of this fluorescent dye. Several

studies have revealed membrane destabilization properties for amyloid forming proteins (Zhu *et al.*, 2003; Quist *et al.*, 2005; Friedman *et al.*, 2009; Pieri *et al.*, 2009; Xue *et al.*, 2010), as well as atx3 (Ricchelli *et al.*, 2007). Previous studies (Macedo-Ribeiro, S. and Pedroso-Lima, M. C., unpublished data), showed that atx3 had the ability to destabilize liposomes, by inducing leakage, and the leakage was dependent on lipid compositions. For instance, liposomes containing just PS:PC (1:1 ratio) did not reveal any leakage, whether liposomes containing PS:PE:PC:Chol (1:1:1:1 ratio) had. The fluorescent dye used (calcein), in higher concentrations, self-quenches, since the excitation and emission spectra are partially overlapped. When calcein is release to aqueous media (and is therefore diluted), it greatly increases emission at 520nm. The liposome morphology was verified under electron microscopy (Fig. 35), and measurements revealed a size between 90-110nm in diameter, approximately the same size verified on their hydrodynamic radius (Faneca, H., unpublished data).

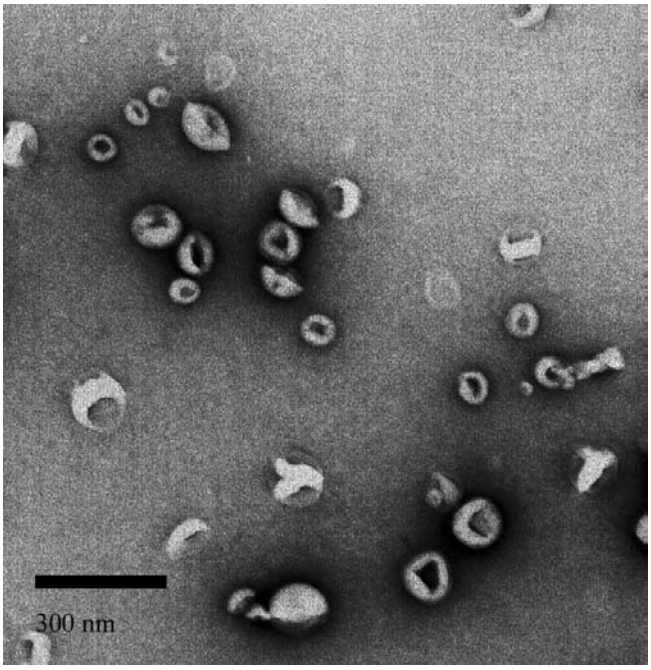

Figure 35 – Electron micrograph showing the prepared large unilamellar vesicles (LUVs). Average size of liposomes is ≈100nm. Scale bar represents 300nm.

With the purpose of testing the atx3 membrane destabilization properties we used 1-1N, 1A, D1, J1 and 1-1Nb monomers, as well as oligomers from 1-1N and J1 in leakage assay at pH 7.4 and pH 5.

Among the different results obtained we could observe one of three things, (a) the signal maintains during the assay (Fig. 36), (b) the signal increases (Fig. 37) or (c) the signal decreases (Fig. 38).

1-1N variant leakage kinetics at pH 7.4 (Fig. 36) doesn't display any observable leakage. 1A variant exhibits an unanticipated decrease in fluorescence (Fig. 37) while J1 clearly illustrates leakage of calcein (Fig. 38). Although allegedly monomeric J1 exhibited leakage, the protein batch was confirmed to have oligomers as discussed on section 3.2.3 (Fig. 34). Another batch of J1 was tested and did not reveal any significant calcein release.

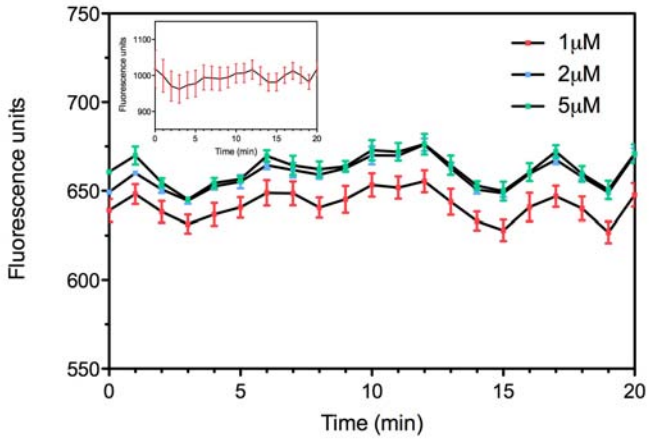

Figure 36 – Monomeric 1-1N calcein leakage kinetics at pH 7.4 showing no apparent alteration. In the upper left corner is displayed just liposomes.

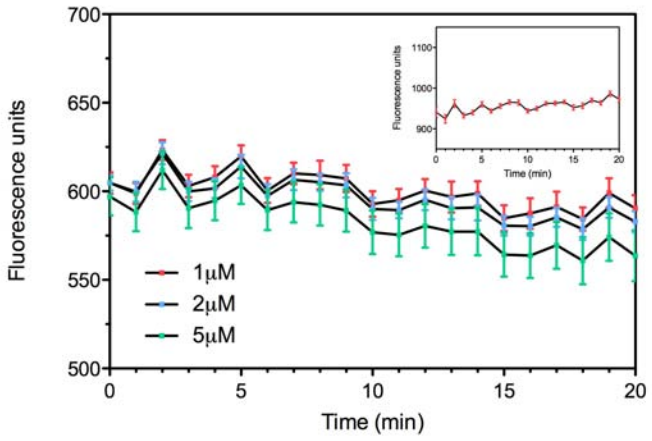

Figure 37 – Monomeric 1A calcein leakage kinetics at pH 7.4 showing a decrease in fluorescence. In the upper right corner is displayed just liposomes.

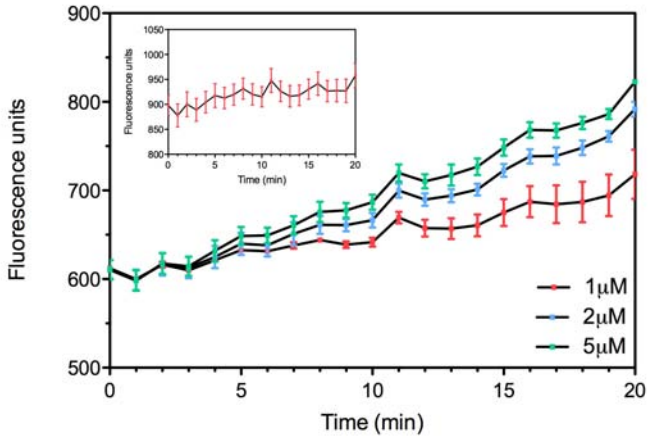

Figure 38 - J1 calcein leakage kinetics at pH 7.4, exhibiting leakage. This protein batch has oligomers, whose presence was confirmed by EM (Fig. 34). In the upper left corner is displayed just liposomes.

Calcein release form liposomes was quantified as a percentage of maximum, obtained by the addition of a surfactant (Triton-X100). The results present a high variability, and in several cases, the liposomes alone had more leakage than with protein. Also in numerous cases we verified a decrease in fluorescence, especially when using oligomers. Results from leakage assays using monomeric 1-1N (Fig. 39) reveal a high variability on the controls (liposome only), which was also observable on

monomeric 1A (Fig. 40), monomeric D1 (Fig. 41), monomeric J1 (Fig. 42), oligomers of 1-1N (Fig. 43), and J1 incubated for 6h at 37ºC (Fig. 44).

The monomeric 1-1N results seem to display a small leakage at pH 5 (Fig. 39, B), while compared to pH 7.4 (Fig. 39, A). There is no detectable and consistent linear alteration of leakage with the different concentrations used.

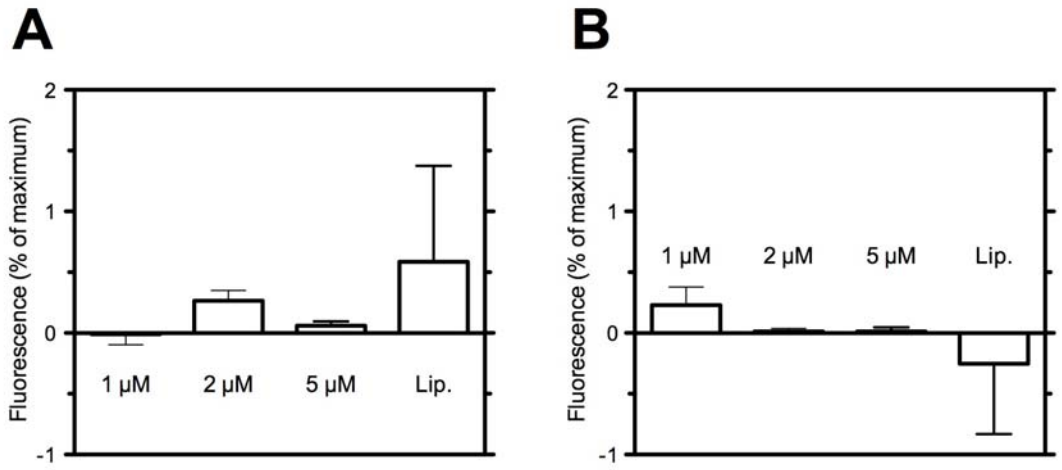

Figure 39 – Monomeric 1-1N calcein leakages at **A**, pH 7.4 and **B**, pH 5.

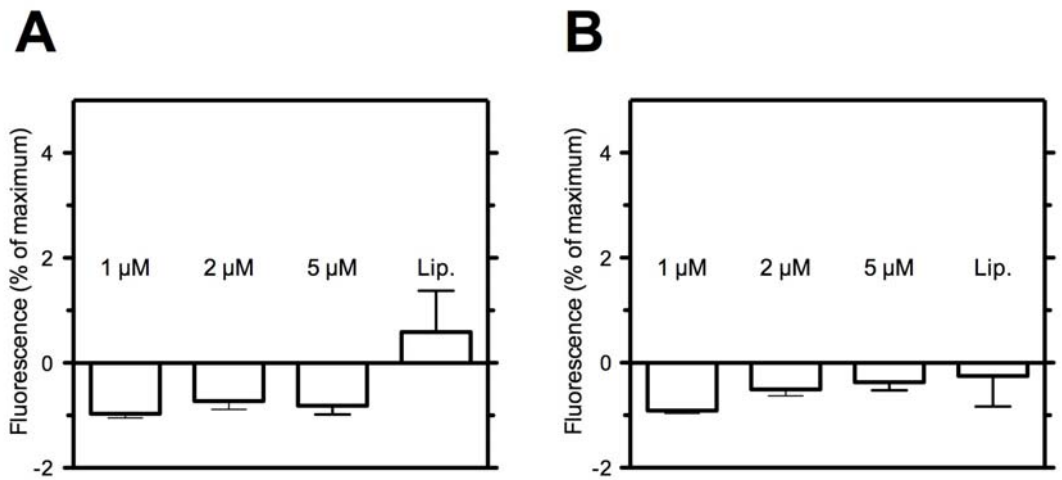

Figure 40 – Monomeric 1A calcein leakages at **A**, pH 7.4 and **B**, pH 5.

The monomeric 1A reveals a decrease in fluorescence for all concentrations at both pHs (Fig. 40). On monomeric D1 calcein leakages, the control (liposomes only)

greatly surpasses the leakages observed for protein, which inclusively decreases in fluorescence (Fig. 41).

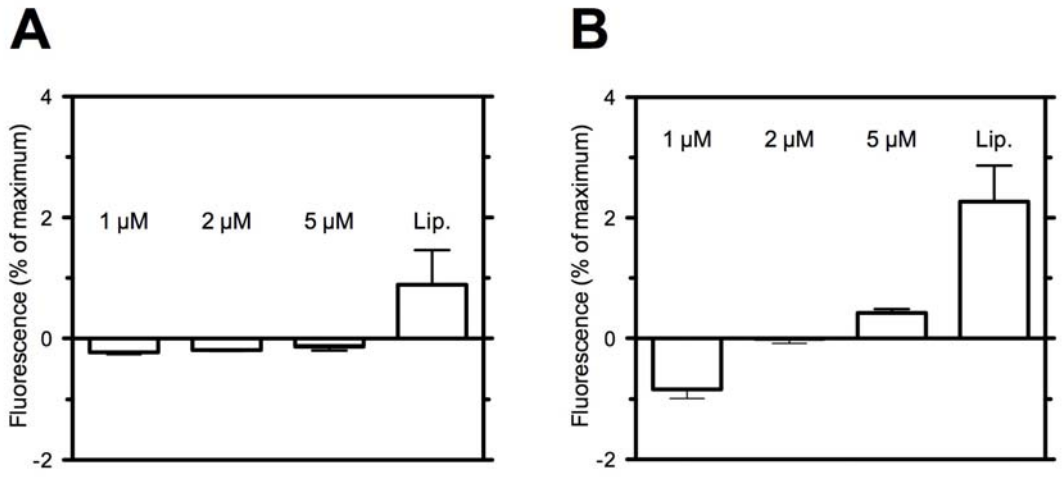

Figure 41 - Monomeric D1 calcein leakages at **A**, pH 7.4 and **B**, pH 5.

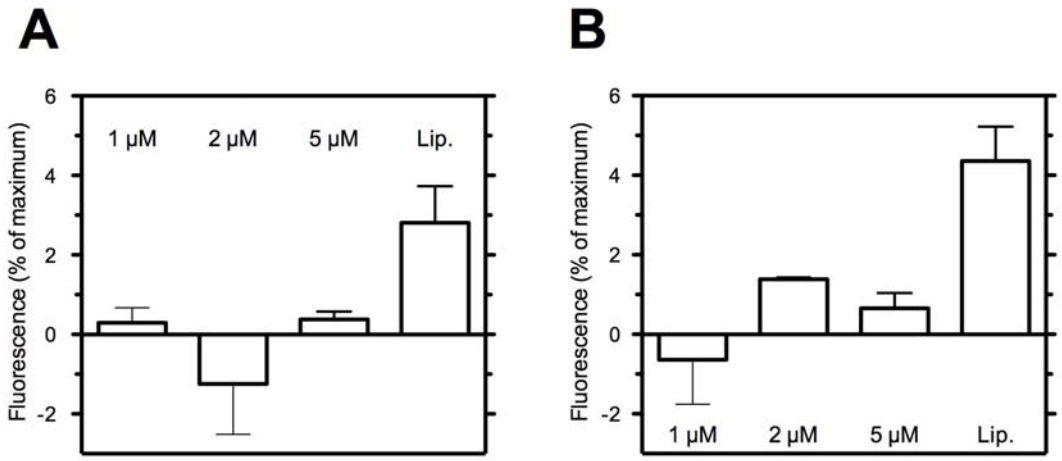

Figure 42 - Monomeric J1 calcein leakages at **A**, pH 7.4 and **B**, pH 5.

Overall, the monomeric forms of atx3 do not seem to cause any leakage on liposomes, since the subtraction of the controls (liposomes) will render either very small leakages (<0.4%) or negative results. Accordingly to the expected, monomers do not exhibit signs of destabilizing membranes, yet we should keep in mind that exposure of monomers to lipid interfaces might increase aggregation. A set of studies regarding lipid-protein interactions and protein aggregation show that lipid membranes can act as anti-chaperones, promoting aggregation (Lee *et al.*, 2002; Zhu *et al.*, 2002; Jensen and

Mouritsen, 2004; Zhao *et al.*, 2004; Gorbenko and Kinnunen, 2006; Hebda and Miranker, 2009; Relini *et al.*, 2009).

3.3.1. Ataxin-3 oligomers decrease calcein fluorescence

We further continued the leakage assays, but using the prepared oligomers of 1-1N (prepared by incubation in liposome assay buffer for 116h at 37ºC, section 3.1.4), as well a sample of J1 incubated 6h at 37ºC and readily used.

In resemblance to the monomer results, we verify high variability, and decrease in fluorescence compared to controls (liposomes). The major differences observed for two different assays performed (white bars versus black bars), is a proof of the high variability of these results, maybe indicating that small leakages cannot be measured, since they exceed the detection limit of the assay.

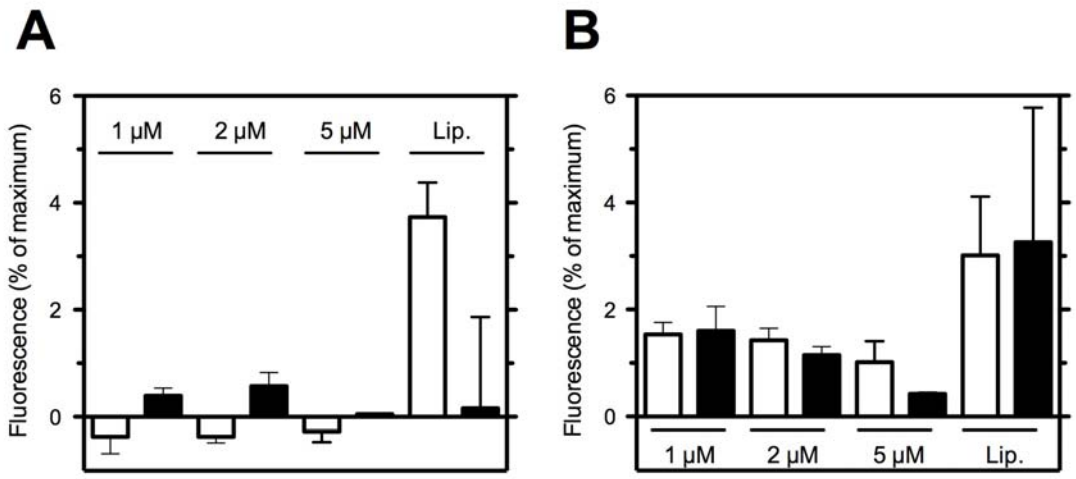

Figure 43 - Oligomers of 1-1N calcein leakages at **A**, pH 7.4 and **B**, pH 5. White and black bars represent two different assays.

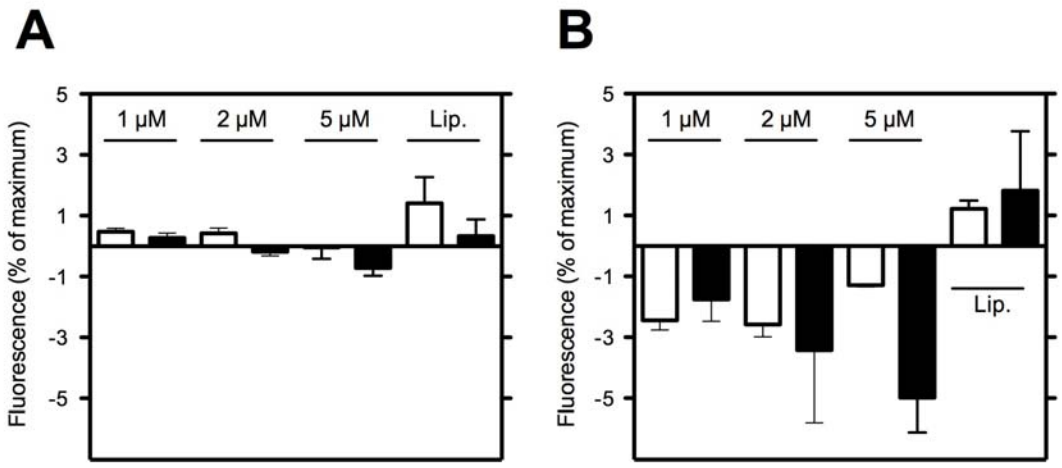

Figure 44 - Calcein leakage of a sample of J1 incubated at 37ºC for 6h. **A**, pH 7.4 and **B**, pH 5. White and black bars represent two different assays.

J1 that was incubated at 37ºC for 6h (in an attempt to produce oligomers without precipitating formation) shows a marked decrease in fluorescence for pH 5 (Fig. 44, B), while at pH 7.4 there is just a slight variation in fluorescence. Monomeric J1 reveals also an increased leakage from controls compared to the results with protein at different concentration (Fig. 42), rendering the leakage verified on those, not significant. Results from oligomers of 1-1N variant exhibit the same increased leakage on liposome controls (Fig. 43). At pH 5 (Fig. 43, B) it is possibly to observe increase leakage compared to pH 7.4 (Fig. 43, A) for the different protein concentrations, even though the controls are always higher.

The controls for the liposome leakage assay used were (a) leakage of liposomes in assay buffer alone, (b) proteins in assay buffer only and (c) only assay buffer. Buffer alone and protein on buffer exhibit almost zero fluorescence, while liposomes had frequently a starting fluorescence greater than liposomes plus protein.

In some particular experiments in which we measured the fluorescence in a continuous way, we verified that adding oligomers to the liposomes in the assay buffer decreased their fluorescence, and monomers did not exhibit this behaviour (data not shown). In an attempt to troubleshoot and overcome these problems we did emission

and absorbance spectra on calcein alone and with oligomers and monomers. The amount of free calcein used was adjusted in order to have the same fluorescence intensity as we see for liposomes treated with Triton X-100 (500nM calcein). We firstly thought that oligomers could partially absorb the emitted fluorescence of calcein, but the absorbance spectrum did not show any peak around 520nm (Fig. 45, B), meaning that the decrease of fluorescence is not due to absorbance by oligomers. Furthermore, oligomers do not exhibit any fluorescence with either excitation at 490nm (data not shown) or 520nm (Fig. 45, A; the peak observed is due to the excitation at 520nm, and because the fluorimeter lacks filters that block emission on the same excitation wavelength).

Finally, the spectra of oligomers plus calcein exhibits a decrease in the peak of fluorescence (Fig. 46, B), proving that it somehow interacts with the probe decreasing its fluorescence. On the other hand calcein plus monomers does not exhibit a decrease in fluorescence, but only a small shift in the emission maximum (Fig 46, A).

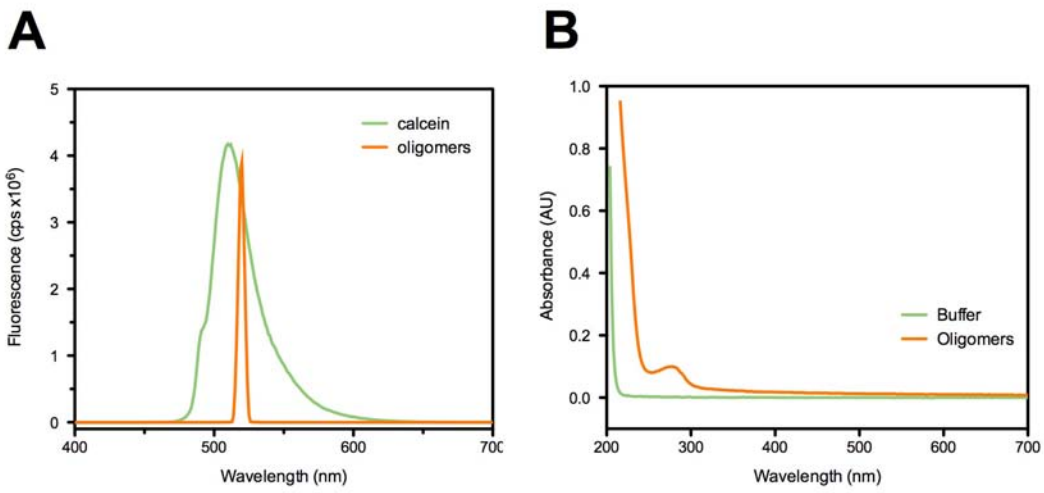

Figure 45 – Calcein and oligomer spectrofluorimetric properties. **A**, emission spectra of calcein (excitation at 490nm), and emission spectra of oligomers (excitation at 520nm). **B**, absorbance spectra for oligomers.

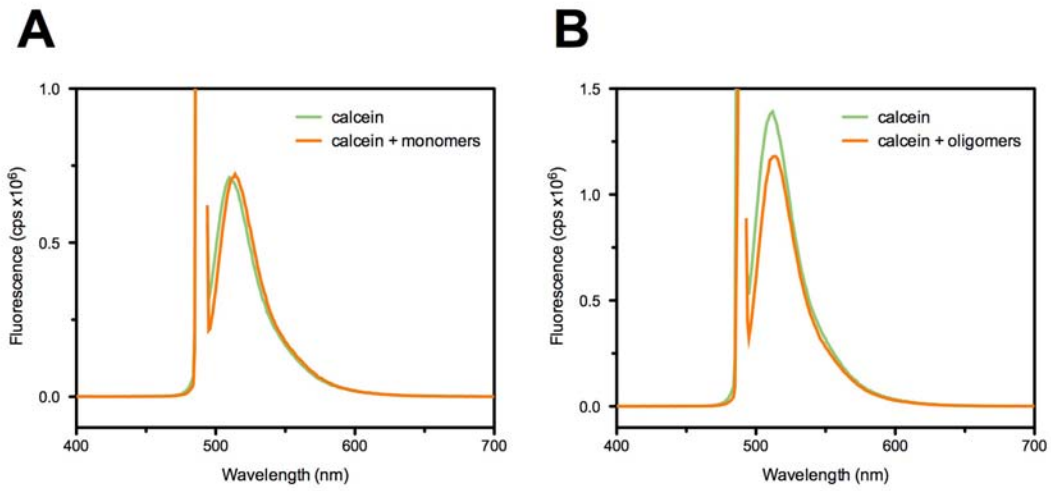

Figure 46 – Emission spectra (exct. 490nm) for either **A**, calcein plus monomers or **B**, calcein plus oligomers. (Monomer and oligomer concentrations were 2μM, calcein concentration 500nM).

Having this in mind, there are grounds for believing that calcein is not suitable for this kind of assay with atx3 oligomers, since we verify that oligomers decrease the probe's fluorescence, and therefore, will not give correct data on liposome membrane destabilization. To overcome this setback, we should use another probe that does not decrease its fluorescence with the contact with atx3 variants and oligomers. Another alternative would be using diphenylhexatriene (1-6-diphenyl-1,3,5-hexatriene, DPH) fluorescent dye, that has almost no fluorescence in water, but is highly fluorescent when intercalated in a lipid membrane. Ricchelli and colleagues used this fluorescent dye, and small liposomes (30nm diameter) of a synthetic derivative of phosphocholine, L-α-dimyristoylphosphoglycerocholine (DMPC), and measured the fluorescence anisotropy of DPH (Ricchelli *et al.*, 2007). They have successfully proven membrane destabilization by atx3 using this kind of system, which makes it a possible approach for future assays of membrane destabilization with atx3.

3.3.2. – Ataxin-3 oligomers appear to interact with liposomes

A leakage assay was performed with oligomers of 1-1N and liposomes, in order to verify by electron microscopy any visible interaction or consistent localization on

membrane. Protein oligomers were a mix of small fibrils and oligomers (Fig. 47, A), and the liposomes were consistently seen close to protein aggregates along the grid viewed by EM. This could have happened because of interaction of these aggregates with liposomes, but also because of a net effect of the fibrils that could have caught liposomes.

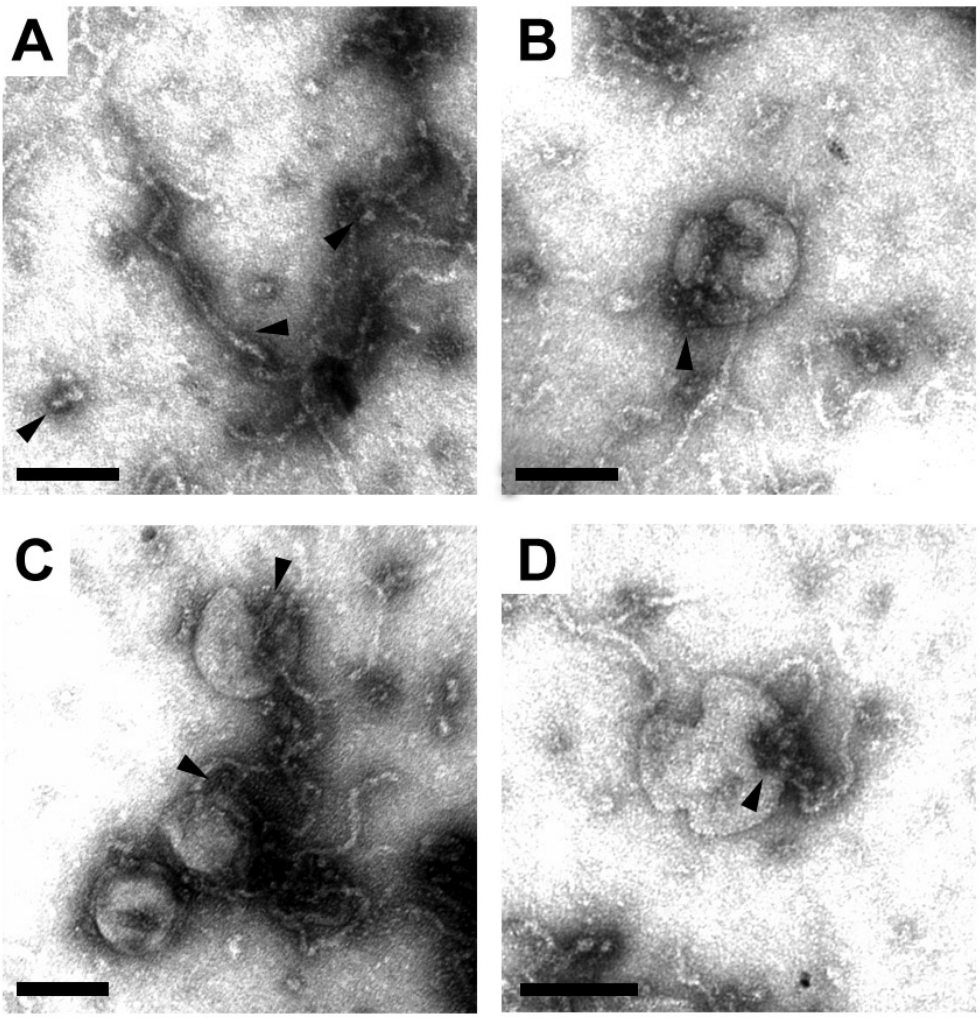

Figure 47 - Electron micrographs for a sample incubated with liposomes and 1-1N oligomers, exhibiting signs of interfering with liposomes. **A**, oligomer samples showing both fibrils and small oligomers. **B-D**, Both fibrils and oligomers are in close proximity to liposomes (almost no liposomes were seen alone). The micrographs seem to suggest some sort of membrane deformation, when in close proximity with either fibrils or oligomers.

Although there seems to be some sort of interaction between these aggregates and the liposomes, this kind of microscopy is not the most adequate. Techniques as

scanning electron microscopy could be very helpful on identifying any possible interaction of oligomers and liposome membranes, by scanning its surface. Furthermore, the affinity of these oligomers for the lipid membrane could be assessed with surface plasmon resonance, which allows to determine bind affinities.

Chapter 4 Conclusions

4.1. – Ataxin-3 domains influence the oligomerization process in different ways

Atx3 aggregation pathway is not yet fully characterised. The major works done so far, point to an aggregation via nucleation mechanism (Gales *et al.*, 2005; Ellisdon *et al.*, 2006; Ellisdon *et al.*, 2007), and the influence of the different domains is not completely clear. The presence of the polyQ tract in the full-length protein seems to induce a faster aggregation and a more severe phenotype (Chiti and Dobson, 2006; Bichelmeier *et al.*, 2007), while Josephin domain alone can aggregate (Masino *et al.*, 2004).

We have investigated the influence of atx3 protein domains in the aggregation process, by using atx3 variants: (i) containing all domains (1-1N); (ii) Josephin domain, two UIMs and polyQ (1A); (iii) Josephin domain and two UIMs (D1) and (iv) Josephin domain alone (J1). We found that, in near physiological conditions, the presence of the third UIM (1-1N) renders the protein a faster aggregation kinetics (compared to 1A), while the presence and absence of the polyQ tract (1A and D1 respectively) only induces only a slight variation. We have also concluded that Josephin domain alone aggregates in near physiological conditions, in accordance to the algorithm's predicted aggregate prone sequences in this domain. The influence of pH on aggregation kinetics was verified for 1-1N and D1 variants, and in both cases, lower pH favoured a faster aggregation process, which might correlate to the ability to increase protein partially unfolded states and therefore increased aggregation propensity (Jahn and Radford, 2008). Regarding the influence of ionic strength on protein aggregation, we verified that an increase in salt concentration produces a faster aggregation, as seen in other works (Klement *et al.*, 2007; Jain and Udgaonkar, 2010). We have also verified that in these aggregation conditions, all variants exhibited fibril morphology in EM, except for Josephin domain that exhibited amorphous aggregates. Moreover, 1-1N and J1 protein pellets exhibited Congo red birefringence, an amyloid characteristic.

It is reasonable to think that each domain can have a role in atx3 protein aggregation, and that the possible ways these domains interact *in vivo*, can modulate

how atx3 forms oligomers. Moreover, cells have quality control mechanisms that can eliminate these aggregates inhibiting their toxicity, and one might expect that, if the aggregation occurs faster than the capacity of cells to eliminate these species, the aggregates will accumulate and can be the cause of the toxic effects observed. Further assays should be made, following the aggregation of atx3 variants, as well as mutants that change a specific domain function, with ThT, intrinsic tryptophan fluorescence and circular dichroism (CD), in order to characterise the different role of each protein domain on the aggregation mechanism.

4.2. – Ataxin-3 oligomers, and not monomers, appear to be able to destabilise bilayer membranes

Lipid-protein interactions have been a recent studied subject, and there is an increased awareness that these interactions might have important cellular roles. Lipid membrane interface can promote protein misfolding, whereas cytotoxicity studies reveal a destabilization of cell membranes by oligomers (Demuro *et al.*, 2005; Gorbenko and Kinnunen, 2006; Takahashi *et al.*, 2008; Relini *et al.*, 2009). There are some studies that show the increased toxicity of oligomers over monomeric and fibrilar samples of amyloid-like proteins, by inducing membrane destabilization, in close correlation to the hypothesis that the oligomeric species are responsible for the toxicity (Demuro *et al.*, 2005; Ricchelli *et al.*, 2007).

We have adopted an experimental procedure using liposomes (specifically LUV containing PC:PE:PS:Chol. in 1:1:1:1 molar relation) with a fluorescent dye (calcein) inside, and determined the ability of atx3 monomeric variants and oligomers to destabilize the lipid bilayer membrane, by measuring the dye leakage. The results for monomeric atx3 variants showed a high variability, and no significant calcein release, in accordance to the hypothesis stating that monomeric and fibrilar species do not exhibit membrane destabilization properties. When using oligomeric species from the 1-1N atx3 variant, we found again high variability, rendering the results no significance,

and even a decrease in fluorescence. Noticing this effect, we further investigated the observed behaviour, to find out that oligomers decrease the fluorescence of the probe used. The monomeric 1-1N did not show a decrease in calcein fluorescence, but a slight shift in its emission maximum. Overcoming this step back, using the same experimental procedure principle, requires the use of another dye. Alternatively, we can use cell cultures, as Demuro and colleagues used (Demuro *et al.*, 2005), loaded with a fluorescent dye, and verify by fluorescence microscopy the decrease of fluorescence inside cells. This experimental procedure allows verifying destabilizations directly on a cellular membrane, and the degree of complexity and composition of these membranes is far from being matched by a liposome preparation. However, since specific lipids might have increased importance on membrane destabilization, the liposome preparation can be useful, allowing to test fewer lipids or lipid composition. Other possible approach would be to use dyes that intercalate in the lipid bilayer, as DPH. DPH was previously used to assess membrane destabilization induced by atx3 upon incubation with metal ions, by measuring fluorescence anisotropy (Ricchelli *et al.*, 2007).

Another interesting point is to study the influence of the lipid bilayer on how protein aggregates. There are clues that point to lipids behaving as anti-chaperones (Sparr *et al.*, 2004; Stefani, 2004; Zhao *et al.*, 2004), which might help to explain the aggregation process as it happens *in vivo*. If we take in account that these type of disorders are late onset, and the cellular membranes lipidic composition varies with age and organelle (Kleinig, 1970), one might speculate that lipid membranes can represent an important aspect for the development of these diseases. Although our approach was not able to confirm or deny membrane destabilization by oligomers, the electron micrographs done after the incubation period at 37ºC show close co localization of liposomes and protein aggregates. Moreover, the observed liposomes were almost always close to the aggregates, which appear to be penetrating the membrane. Still, transmission electron microscopy does not allow us to confirm any of

these apparent interactions. A possible approach would be to use a scanning electron microscope to scan the surface of liposomes obtaining a relief map, as it will allow to better see any possible interaction. Also, another interesting approach would be assessing the bind affinities of the monomeric, oligomeric and fibrilar forms of protein to lipid membranes, with surface plasmon resonance (SPR).

4.3. – Future remarks

The presented work has raised questions on the influence of specific domains on atx3 aggregation mechanism, as well as on the hypothesis of oligomers being the cause of cellular toxicity. The range of available tools will allow us to unveil new information about this protein pathway for aggregation, which can possibly create knowledge useful for other polyQ disorders, as well as to understand the mechanism behind protein misfolding. Furthermore, as lipid-protein interactions gains grounds as a possible modulator of cellular process, future work can uncover knowledge valuable to explain how oligomers can destabilize membranes, and how lipid interfaces can be a template for protein aggregation.

Finally, together with a growing body of information about post-translational modifications and interactions *in vivo*, these and future findings might give rise to valuable information, pragmatic on medical context of this type of neurodegenerative diseases.

References

Albi, E., M. L. Tomassoni and M. Viola-Magni (1997). "Effect of lipid composition on rat liver nuclear membrane fluidity." Cell Biochem Funct **15**(3): 181-90.

Albrecht, M., M. Golatta, U. Wullner and T. Lengauer (2004). "Structural and functional analysis of ataxin-2 and ataxin-3." Eur J Biochem **271**(15): 3155-70.

Audic, S., F. Lopez, J. M. Claverie, O. Poirot and C. Abergel (1997). "SAmBA: an interactive software for optimizing the design of biological macromolecules crystallization experiments." Proteins **29**(2): 252-7.

Bartlett, G. R. (1958). "Organization of red cell glycolytic enzymes; cell coat phosphorus transfer." Ann N Y Acad Sci **75**(1): 110-4.

Berke, S. J., Y. Chai, G. L. Marrs, H. Wen and H. L. Paulson (2005). "Defining the role of ubiquitin-interacting motifs in the polyglutamine disease protein, ataxin-3." J Biol Chem **280**(36): 32026-34.

Bevivino, A. E. and P. J. Loll (2001). "An expanded glutamine repeat destabilizes native ataxin-3 structure and mediates formation of parallel beta -fibrils." Proc Natl Acad Sci U S A **98**(21): 11955-60.

Biancalana, M. and S. Koide (2010). "Molecular mechanism of Thioflavin-T binding to amyloid fibrils." Biochim Biophys Acta **1804**(7): 1405-12.

Bichelmeier, U., T. Schmidt, J. Hubener, J. Boy, L. Ruttiger, K. Habig, S. Poths, M. Bonin, M. Knipper, W. J. Schmidt, J. Wilbertz, H. Wolburg, F. Laccone and O. Riess (2007). "Nuclear localization of ataxin-3 is required for the manifestation of symptoms in SCA3: in vivo evidence." J Neurosci **27**(28): 7418-28.

Bogdanov, M. and W. Dowhan (1995). "Phosphatidylethanolamine is required for in vivo function of the membrane-associated lactose permease of Escherichia coli." J Biol Chem **270**(2): 732-9.

Bokvist, M., F. Lindstrom, A. Watts and G. Grobner (2004). "Two types of Alzheimer's beta-amyloid (1-40) peptide membrane interactions: aggregation preventing transmembrane anchoring versus accelerated surface fibril formation." J Mol Biol **335**(4): 1039-49.

Bucciantini, M., E. Giannoni, F. Chiti, F. Baroni, L. Formigli, J. Zurdo, N. Taddei, G. Ramponi, C. M. Dobson and M. Stefani (2002). "Inherent toxicity of aggregates implies a common mechanism for protein misfolding diseases." Nature **416**(6880): 507-11.

Burnett, B., F. Li and R. N. Pittman (2003). "The polyglutamine neurodegenerative protein ataxin-3 binds polyubiquitylated proteins and has ubiquitin protease activity." Hum Mol Genet **12**(23): 3195-205.

Chai, Y., S. S. Berke, R. E. Cohen and H. L. Paulson (2004). "Poly-ubiquitin binding by the polyglutamine disease protein ataxin-3 links its normal function to protein surveillance pathways." J Biol Chem **279**(5): 3605-11.

Chiti, F. and C. M. Dobson (2006). "Protein misfolding, functional amyloid, and human disease." Annu Rev Biochem **75**: 333-66.

Chow, M. K., A. M. Ellisdon, L. D. Cabrita and S. P. Bottomley (2004). "Polyglutamine expansion in ataxin-3 does not affect protein stability: implications for misfolding and disease." J Biol Chem **279**(46): 47643-51.

Conchillo-Sole, O., N. S. de Groot, F. X. Aviles, J. Vendrell, X. Daura and S. Ventura (2007). "AGGRESCAN: a server for the prediction and evaluation of "hot spots" of aggregation in polypeptides." BMC Bioinformatics **8**: 65.

Crick, F. H. (1958). "On protein synthesis." Symp Soc Exp Biol **12**: 138-63.

Dai, R. M., E. Chen, D. L. Longo, C. M. Gorbea and C. C. Li (1998). "Involvement of valosin-containing protein, an ATPase Co-purified with IkappaBalpha and 26 S

proteasome, in ubiquitin-proteasome-mediated degradation of IkappaBalpha." J Biol Chem **273**(6): 3562-73.

Demuro, A., E. Mina, R. Kayed, S. C. Milton, I. Parker and C. G. Glabe (2005). "Calcium dysregulation and membrane disruption as a ubiquitous neurotoxic mechanism of soluble amyloid oligomers." J Biol Chem **280**(17): 17294-300.

Dobson, C. M. (2004). "Experimental investigation of protein folding and misfolding." Methods **34**(1): 4-14.

Doss-Pepe, E. W., E. S. Stenroos, W. G. Johnson and K. Madura (2003). "Ataxin-3 interactions with rad23 and valosin-containing protein and its associations with ubiquitin chains and the proteasome are consistent with a role in ubiquitin-mediated proteolysis." Mol Cell Biol **23**(18): 6469-83.

Dowhan, W., E. Mileykovskaya and M. Bogdanov (2004). "Diversity and versatility of lipid-protein interactions revealed by molecular genetic approaches." Biochim Biophys Acta **1666**(1-2): 19-39.

Dubois, J. M., G. Ouanounou and B. Rouzaire-Dubois (2009). "The Boltzmann equation in molecular biology." Prog Biophys Mol Biol **99**(2-3): 87-93.

Ellisdon, A. M., M. C. Pearce and S. P. Bottomley (2007). "Mechanisms of ataxin-3 misfolding and fibril formation: kinetic analysis of a disease-associated polyglutamine protein." J Mol Biol **368**(2): 595-605.

Ellisdon, A. M., B. Thomas and S. P. Bottomley (2006). "The two-stage pathway of ataxin-3 fibrillogenesis involves a polyglutamine-independent step." J Biol Chem **281**(25): 16888-96.

Fernandez-Escamilla, A. M., F. Rousseau, J. Schymkowitz and L. Serrano (2004). "Prediction of sequence-dependent and mutational effects on the aggregation of peptides and proteins." Nat Biotechnol **22**(10): 1302-6.

Friedman, R., R. Pellarin and A. Caflisch (2009). "Amyloid aggregation on lipid bilayers and its impact on membrane permeability." J Mol Biol **387**(2): 407-15.

Gales, L., L. Cortes, C. Almeida, C. V. Melo, M. do Carmo Costa, P. Maciel, D. T. Clarke, A. M. Damas and S. Macedo-Ribeiro (2005). "Towards a structural understanding of the fibrillization pathway in Machado-Joseph's disease: trapping early oligomers of non-expanded ataxin-3." J Mol Biol **353**(3): 642-54.

Gasteiger, E., C. Hoogland, A. Gattiker, S. Duvaud, M. R. Wilkins, R. D. Appel and A. Bairoch (2005). Protein Identification and Analysis Tools on the ExPASy Server. The Proteomics Protocols Handbook. J. M. Walker, Humana Press**:** 571-607.

Glabe, C. G. (2006). "Common mechanisms of amyloid oligomer pathogenesis in degenerative disease." Neurobiol Aging **27**(4): 570-5.

Gorbenko, G. P. and P. K. Kinnunen (2006). "The role of lipid-protein interactions in amyloid-type protein fibril formation." Chem Phys Lipids **141**(1-2): 72-82.

Gusella, J. F. and M. E. MacDonald (2000). "Molecular genetics: unmasking polyglutamine triggers in neurodegenerative disease." Nat Rev Neurosci **1**(2): 109-15.

Hashimoto, M., E. Rockenstein, L. Crews and E. Masliah (2003). "Role of protein aggregation in mitochondrial dysfunction and neurodegeneration in Alzheimer's and Parkinson's diseases." Neuromolecular Med **4**(1-2): 21-36.

Hebda, J. A. and A. D. Miranker (2009). "The interplay of catalysis and toxicity by amyloid intermediates on lipid bilayers: insights from type II diabetes." Annu Rev Biophys **38**: 125-52.

Hubener, J. and O. Riess (2010). "Polyglutamine-induced neurodegeneration in SCA3 is not mitigated by non-expanded ataxin-3: conclusions from double-transgenic mouse models." Neurobiol Dis **38**(1): 116-24.

Ichikawa, Y., J. Goto, M. Hattori, A. Toyoda, K. Ishii, S. Y. Jeong, H. Hashida, N. Masuda, K. Ogata, F. Kasai, M. Hirai, P. Maciel, G. A. Rouleau, Y. Sakaki and I. Kanazawa (2001). "The genomic structure and expression of MJD, the Machado-Joseph disease gene." J Hum Genet **46**(7): 413-22.

Inoue, H., H. Nojima and H. Okayama (1990). "High efficiency transformation of Escherichia coli with plasmids." Gene **96**(1): 23-8.

Jahn, T. R. and S. E. Radford (2005). "The Yin and Yang of protein folding." FEBS J **272**(23): 5962-70.

Jahn, T. R. and S. E. Radford (2008). "Folding versus aggregation: polypeptide conformations on competing pathways." Arch Biochem Biophys **469**(1): 100-17.

Jain, S. and J. B. Udgaonkar (2010). "Salt-Induced Modulation of the Pathway of Amyloid Fibril Formation by the Mouse Prion Protein." Biochemistry.

Jensen, M. O. and O. G. Mouritsen (2004). "Lipids do influence protein function-the hydrophobic matching hypothesis revisited." Biochim Biophys Acta **1666**(1-2): 205-26.

Kawaguchi, Y., T. Okamoto, M. Taniwaki, M. Aizawa, M. Inoue, S. Katayama, H. Kawakami, S. Nakamura, M. Nishimura, I. Akiguchi and et al. (1994). "CAG expansions in a novel gene for Machado-Joseph disease at chromosome 14q32.1." Nat Genet **8**(3): 221-8.

Kayed, R., E. Head, J. L. Thompson, T. M. McIntire, S. C. Milton, C. W. Cotman and C. G. Glabe (2003). "Common structure of soluble amyloid oligomers implies common mechanism of pathogenesis." Science **300**(5618): 486-9.

Kleinig, H. (1970). "Nuclear membranes from mammalian liver. II. Lipid composition." J Cell Biol **46**(2): 396-402.

Klement, K., K. Wieligmann, J. Meinhardt, P. Hortschansky, W. Richter and M. Fandrich (2007). "Effect of different salt ions on the propensity of aggregation and on the structure of Alzheimer's abeta(1-40) amyloid fibrils." J Mol Biol **373**(5): 1321-33.

Lee, H. J., C. Choi and S. J. Lee (2002). "Membrane-bound alpha-synuclein has a high aggregation propensity and the ability to seed the aggregation of the cytosolic form." J Biol Chem **277**(1): 671-8.

Macedo-Ribeiro, S., L. Cortes, P. Maciel and A. L. Carvalho (2009). "Nucleocytoplasmic shuttling activity of ataxin-3." PLoS One **4**(6): e5834.

Maciel, P., C. Gaspar, A. L. DeStefano, I. Silveira, P. Coutinho, J. Radvany, D. M. Dawson, L. Sudarsky, J. Guimaraes, J. E. Loureiro and et al. (1995). "Correlation between CAG repeat length and clinical features in Machado-Joseph disease." Am J Hum Genet **57**(1): 54-61.

Mao, Y., F. Senic-Matuglia, P. P. Di Fiore, S. Polo, M. E. Hodsdon and P. De Camilli (2005). "Deubiquitinating function of ataxin-3: insights from the solution structure of the Josephin domain." Proc Natl Acad Sci U S A **102**(36): 12700-5.

Marchal, S., E. Shehi, M. C. Harricane, P. Fusi, F. Heitz, P. Tortora and R. Lange (2003). "Structural instability and fibrillar aggregation of non-expanded human ataxin-3 revealed under high pressure and temperature." J Biol Chem **278**(34): 31554-63.

Masino, L., G. Nicastro, R. P. Menon, F. Dal Piaz, L. Calder and A. Pastore (2004). "Characterization of the structure and the amyloidogenic properties of the

Josephin domain of the polyglutamine-containing protein ataxin-3." J Mol Biol **344**(4): 1021-35.

Mattson, M. P. (1995). "Degenerative and protective signaling mechanisms in the neurofibrillary pathology of AD." Neurobiol Aging **16**(3): 447-57; discussion 458-63.

Murphy, R. M. (2007). "Kinetics of amyloid formation and membrane interaction with amyloidogenic proteins." Biochim Biophys Acta **1768**(8): 1923-34.

Nakano, K. K., D. M. Dawson and A. Spence (1972). "Machado disease. A hereditary ataxia in Portuguese emigrants to Massachusetts." Neurology **22**(1): 49-55.

Nicastro, G., R. P. Menon, L. Masino, P. P. Knowles, N. Q. McDonald and A. Pastore (2005). "The solution structure of the Josephin domain of ataxin-3: structural determinants for molecular recognition." Proc Natl Acad Sci U S A **102**(30): 10493-8.

Nilsson, M. R. (2004). "Techniques to study amyloid fibril formation in vitro." Methods **34**(1): 151-60.

Orr, H. T. (2001). "Beyond the Qs in the polyglutamine diseases." Genes Dev **15**(8): 925-32.

Paulson, H. L., M. K. Perez, Y. Trottier, J. Q. Trojanowski, S. H. Subramony, S. S. Das, P. Vig, J. L. Mandel, K. H. Fischbeck and R. N. Pittman (1997). "Intranuclear inclusions of expanded polyglutamine protein in spinocerebellar ataxia type 3." Neuron **19**(2): 333-44.

Perez, M. K., H. L. Paulson, S. J. Pendse, S. J. Saionz, N. M. Bonini and R. N. Pittman (1998). "Recruitment and the role of nuclear localization in polyglutamine-mediated aggregation." J Cell Biol **143**(6): 1457-70.

Perutz, M. F. (1999). "Glutamine repeats and neurodegenerative diseases: molecular aspects." Trends Biochem Sci **24**(2): 58-63.

Perutz, M. F. and A. H. Windle (2001). "Cause of neural death in neurodegenerative diseases attributable to expansion of glutamine repeats." Nature **412**(6843): 143-4.

Pieri, L., M. Bucciantini, P. Guasti, J. Savistchenko, R. Melki and M. Stefani (2009). "Synthetic lipid vesicles recruit native-like aggregates and affect the aggregation process of the prion Ure2p: insights on vesicle permeabilization and charge selectivity." Biophys J **96**(8): 3319-30.

Pozzi, C., M. Valtorta, G. Tedeschi, E. Galbusera, V. Pastori, A. Bigi, S. Nonnis, E. Grassi and P. Fusi (2008). "Study of subcellular localization and proteolysis of ataxin-3." Neurobiol Dis **30**(2): 190-200.

Quist, A., I. Doudevski, H. Lin, R. Azimova, D. Ng, B. Frangione, B. Kagan, J. Ghiso and R. Lal (2005). "Amyloid ion channels: a common structural link for protein-misfolding disease." Proc Natl Acad Sci U S A **102**(30): 10427-32.

Ranum, L. P., J. K. Lundgren, L. J. Schut, M. J. Ahrens, S. Perlman, J. Aita, T. D. Bird, C. Gomez and H. T. Orr (1995). "Spinocerebellar ataxia type 1 and Machado-Joseph disease: incidence of CAG expansions among adult-onset ataxia patients from 311 families with dominant, recessive, or sporadic ataxia." Am J Hum Genet **57**(3): 603-8.

Ravikumar, B., C. Vacher, Z. Berger, J. E. Davies, S. Luo, L. G. Oroz, F. Scaravilli, D. F. Easton, R. Duden, C. J. O'Kane and D. C. Rubinsztein (2004). "Inhibition of mTOR induces autophagy and reduces toxicity of polyglutamine expansions in fly and mouse models of Huntington disease." Nat Genet **36**(6): 585-95.

Relini, A., O. Cavalleri, R. Rolandi and A. Gliozzi (2009). "The two-fold aspect of the interplay of amyloidogenic proteins with lipid membranes." Chem Phys Lipids **158**(1): 1-9.

Ricchelli, F., P. Fusi, P. Tortora, M. Valtorta, M. Riva, G. Tognon, K. Chieregato, S. Bolognin and P. Zatta (2007). "Destabilization of non-pathological variants of ataxin-3 by metal ions results in aggregation/fibrillogenesis." Int J Biochem Cell Biol **39**(5): 966-77.

Rodrigues, A. J., M. D. Costa, T. L. Silva, D. Ferreira, F. Bajanca, E. Logarinho and P. Maciel (2010). "Absence of ataxin-3 leads to cytoskeletal disorganization and increased cell death." Biochim Biophys Acta.

Rousseau, F., J. Schymkowitz and L. Serrano (2006a). "Protein aggregation and amyloidosis: confusion of the kinds?" Curr Opin Struct Biol **16**(1): 118-26.

Rousseau, F., L. Serrano and J. W. Schymkowitz (2006b). "How evolutionary pressure against protein aggregation shaped chaperone specificity." J Mol Biol **355**(5): 1037-47.

Saitoh, T., K. Horsburgh and E. Masliah (1993). "Hyperactivation of signal transduction systems in Alzheimer's disease." Ann N Y Acad Sci **695**: 34-41.

Scheel, H., S. Tomiuk and K. Hofmann (2003). "Elucidation of ataxin-3 and ataxin-7 function by integrative bioinformatics." Hum Mol Genet **12**(21): 2845-52.

Schmitt, I., M. Linden, H. Khazneh, B. O. Evert, P. Breuer, T. Klockgether and U. Wuellner (2007). "Inactivation of the mouse Atxn3 (ataxin-3) gene increases protein ubiquitination." Biochem Biophys Res Commun **362**(3): 734-9.

Schubert, D., C. Behl, R. Lesley, A. Brack, R. Dargusch, Y. Sagara and H. Kimura (1995). "Amyloid peptides are toxic via a common oxidative mechanism." Proc Natl Acad Sci U S A **92**(6): 1989-93.

Shehi, E., P. Fusi, F. Secundo, S. Pozzuolo, A. Bairati and P. Tortora (2003). "Temperature-dependent, irreversible formation of amyloid fibrils by a soluble human ataxin-3 carrying a moderately expanded polyglutamine stretch (Q36)." Biochemistry **42**(49): 14626-32.

Shoffner, J. M. (1997). "Oxidative phosphorylation defects and Alzheimer's disease." Neurogenetics **1**(1): 13-9.

Singer, S. J. and N. N. Dewji (2006). "Evidence that Perutz's double-beta-stranded subunit structure for beta-amyloids also applies to their channel-forming structures in membranes." Proc Natl Acad Sci U S A **103**(5): 1546-50.

Sparr, E., M. F. Engel, D. V. Sakharov, M. Sprong, J. Jacobs, B. de Kruijff, J. W. Hoppener and J. A. Killian (2004). "Islet amyloid polypeptide-induced membrane leakage involves uptake of lipids by forming amyloid fibers." FEBS Lett **577**(1-2): 117-20.

Stefani, M. (2004). "Protein misfolding and aggregation: new examples in medicine and biology of the dark side of the protein world." Biochim Biophys Acta **1739**(1): 5-25.

Tait, D., M. Riccio, A. Sittler, E. Scherzinger, S. Santi, A. Ognibene, N. M. Maraldi, H. Lehrach and E. E. Wanker (1998). "Ataxin-3 is transported into the nucleus and associates with the nuclear matrix." Human Molecular Genetics **7**(6): 991-997.

Takahashi, T., S. Kikuchi, S. Katada, Y. Nagai, M. Nishizawa and O. Onodera (2008). "Soluble polyglutamine oligomers formed prior to inclusion body formation are cytotoxic." Hum Mol Genet **17**(3): 345-56.

Tartaglia, G. G., A. P. Pawar, S. Campioni, C. M. Dobson, F. Chiti and M. Vendruscolo (2008). "Prediction of aggregation-prone regions in structured proteins." J Mol Biol **380**(2): 425-36.

Tartaglia, G. G. and M. Vendruscolo (2008). "The Zyggregator method for predicting protein aggregation propensities." Chem Soc Rev **37**(7): 1395-401.

Todi, S. V., B. J. Winborn, K. M. Scaglione, J. R. Blount, S. M. Travis and H. L. Paulson (2009). "Ubiquitination directly enhances activity of the deubiquitinating enzyme ataxin-3." EMBO J **28**(4): 372-82.

Warrick, J. M., L. M. Morabito, J. Bilen, B. Gordesky-Gold, L. Z. Faust, H. L. Paulson and N. M. Bonini (2005). "Ataxin-3 suppresses polyglutamine neurodegeneration in Drosophila by a ubiquitin-associated mechanism." Mol Cell **18**(1): 37-48.

Xue, W. F., A. L. Hellewell, W. S. Gosal, S. W. Homans, E. W. Hewitt and S. E. Radford (2009). "Fibril fragmentation enhances amyloid cytotoxicity." J Biol Chem **284**(49): 34272-82.

Xue, W. F., A. L. Hellewell, E. W. Hewitt and S. E. Radford (2010). "Fibril fragmentation in amyloid assembly and cytotoxicity: when size matters." Prion **4**(1): 20-5.

Yamada, M., T. Sato, S. Tsuji and H. Takahashi (2008). "CAG repeat disorder models and human neuropathology: similarities and differences." Acta Neuropathol **115**(1): 71-86.

Zhao, H., E. K. Tuominen and P. K. Kinnunen (2004). "Formation of amyloid fibers triggered by phosphatidylserine-containing membranes." Biochemistry **43**(32): 10302-7.

Zhu, M., J. Li and A. L. Fink (2003). "The association of alpha-synuclein with membranes affects bilayer structure, stability, and fibril formation." J Biol Chem **278**(41): 40186-97.

Zhu, M., P. O. Souillac, C. Ionescu-Zanetti, S. A. Carter and A. L. Fink (2002). "Surface-catalyzed amyloid fibril formation." Journal of Biological Chemistry **277**(52): 50914-50922.

Appendix

I – Cleavage of 1-1Nb hexahistidine tag

The cleavage of the purification tag of 1-1Nb was obtained by incubation overnight at 4ºC with 2µg of TEV protease (Fig. 48) to 10µg of protein (the best condition found, Fig. 48, A).

The best condition showed an almost complete cleavage of protein (Fig. 48, A), and the same was verified on the entire protein batch cleavage (Fig. 48, B).

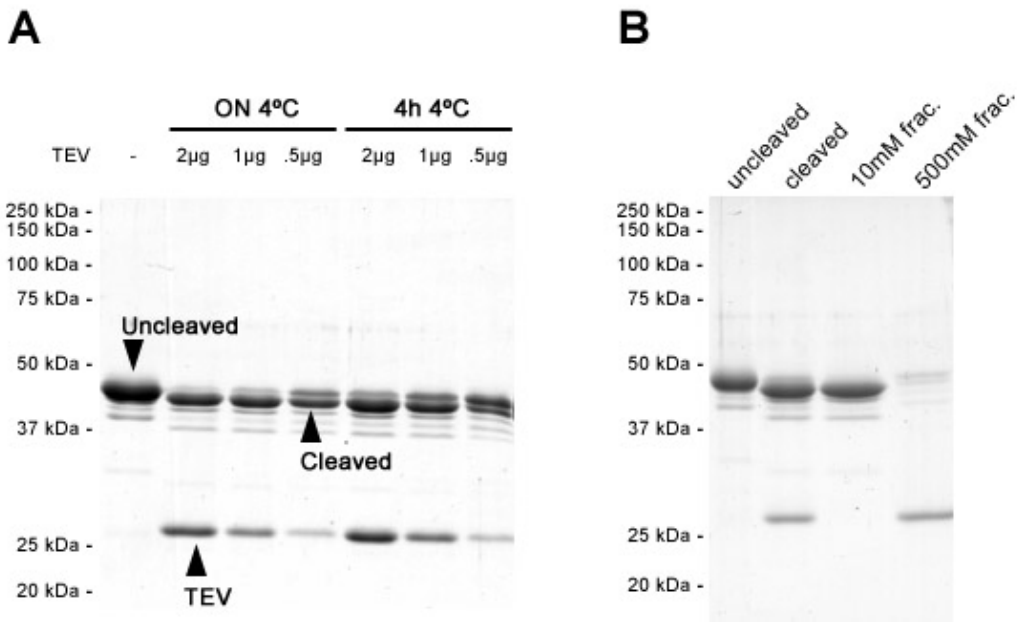

Figure 48 – TEV cleavage assay. **A**, Two different conditions tested, were it is possible to see the uncleaved protein, cleaved protein and the TEV protein. An almost complete cleavage is seen on the best condition. **B**, Cleavage of the entire protein batch. 10mM imidazole eluted the cleaved protein and 500mM imidazole fraction eluted the hexahistidine tag, uncleaved protein as well as the TEV protein

II – 1A ThT aggregation profiles exhibit a two step aggregation

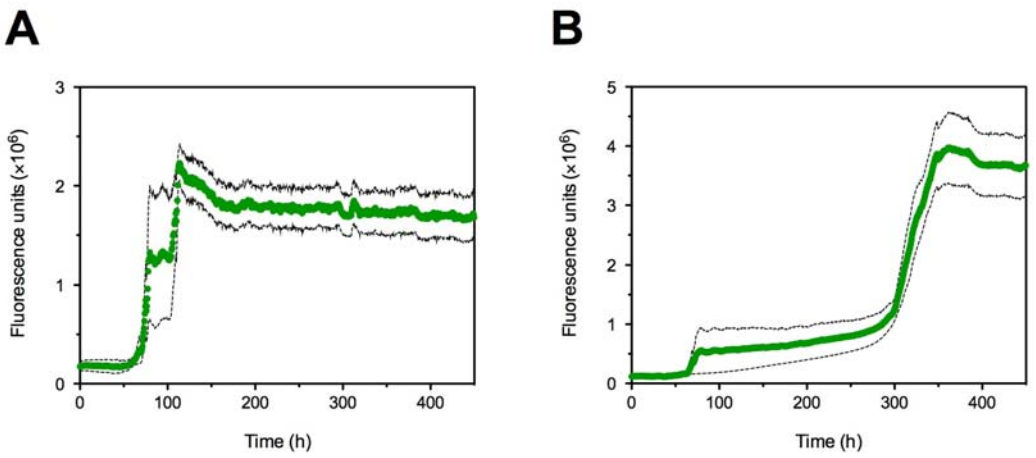

Figure 49 – Two distinct aggregation profiles for 1A. **A**, Profile for 4 out of 10 replicates, showing only one aggregation step. **B**, Profile for 5 out of 10 replicates, showing two distinct aggregation events.

As it was discussed at Chapter 3, section 3.2.3, the 1A exhibited a two-stage aggregation profile. From 10 replicates, 4 exhibited one profile and 5 exhibited a different one (Fig. 49). On Fig. 49, A, it appears that there is only one step aggregation and on Fig. 49, B, there are two. The first step on the Fig. 49, B, is at the same position as in the one step aggregation profile (Fig. 49, A). Accordingly to the least square fittings on the first step and the second step (Fig. 49, A and B respectively), the A_{50} is 80.9h, and 314h, being separated by almost 233h.

The motive behind this apparent two-stage mechanism can be related to possible more than one aggregation mechanism. For instance, the protein, at pH 7 may have two competing pathways for aggregation, since almost 50%-50% of the replicates has either on single step aggregation or a two stage steps.

III – Protein analytical size exclusion profiles, concentration and yield

The purified proteins concentration is summarized on Table 4, which is complement with the analytical size exclusion profiles (Fig. 51-53), and the SDS-PAGE analysis (Fig. 50).

Table 4 – Summary of atx3 variants concentration, yield and size exclusion profiles.

Code	Atx3 variant	Concentration		Yield[i]	Size exclusion profile
		μM	mg/mL		
#a	1-1N	903	39.71	≈ 4.0	Fig. 51, A
#b	D1	469	15.49	≈ 1.5	Fig. 51, B
#c	1A	494	21.05	≈ 1.3	Fig. 51, C
#d	1-1N	1060	46.69	≈ 4.7	Fig. 51, D
#e	J1	395	9.39	≈ 0.9	Fig. 52, A
#f	1A	1000	42.60	≈ 5.6	Fig. 52, B
#g	J1	1635	38.86	≈ 3.1[ii]	Fig. 52, C
#h	1-1Nb	332	13.7	≈ 2.0[iii]	Fig. 52, D
#i	D1	679	22.40	≈ 2.0	Fig. 53, A
#j	J1	1844	43.82	≈ 5.8	Fig. 53, B
#k	1-1N	626	27.58	≈ 8.6	Fig. 53, C

(i, yield represents the amount of concentrated protein obtained per liter of culture media used; ii, this preparation had precipitates that were filtered through a 0.22μm PVDF centrifugal filter; iii, yield after the cleavage of the purification tag.)

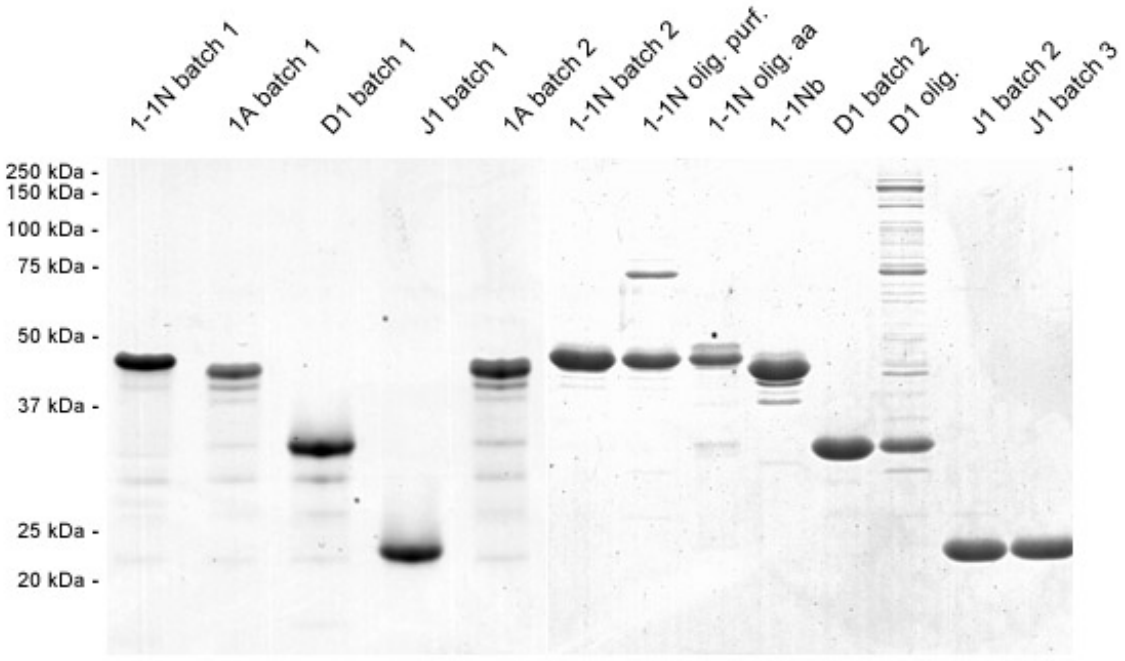

Figure 50 - SDS-PAGE analysis of purified proteins. (1-1N batch 1, *code #d*; 1A batch 1, *code #c*; D1 batch 1, *code #b*; J1 batch 1, code #*e*; 1A batch 2 *code #f*; 1-1N batch 2, *code #k*; 1-1Nb, *code #h*; D1 batch 2, *code #i*; J1 batch 2, *code #g*; J1 batch 3, *code #j*.)

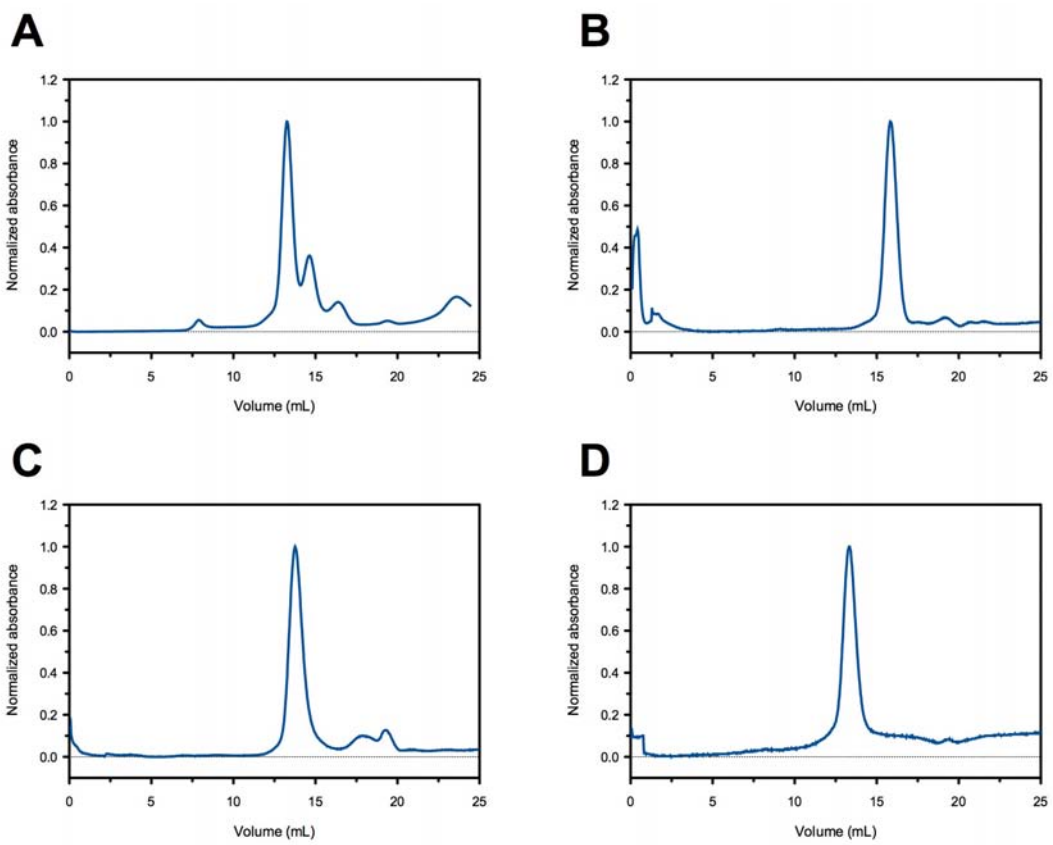

Figure 51 – Analytical size exclusion profile for: **A**, 1-1N; **B**, D1; **C**, 1A; **D**, 1-1N.

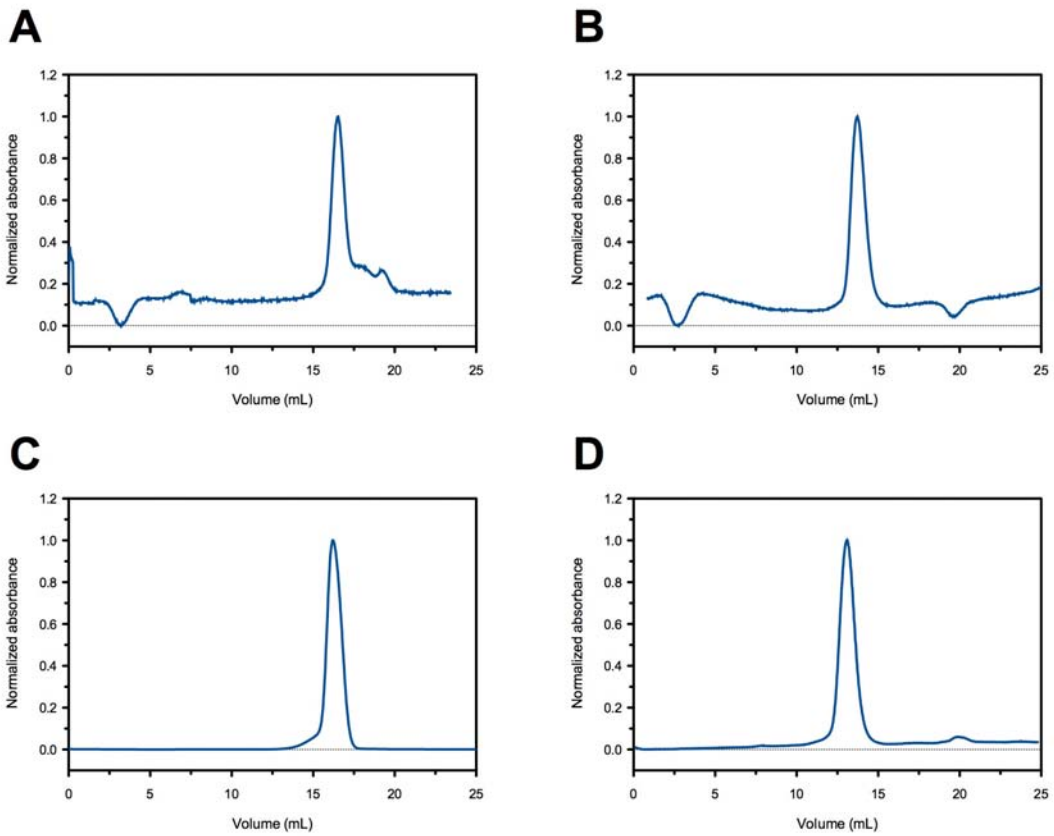

Figure 52 – Analytical size exclusion profile for: **A**, J1; **B**, 1A; **C**, J1; **D**, 1-1Nb.

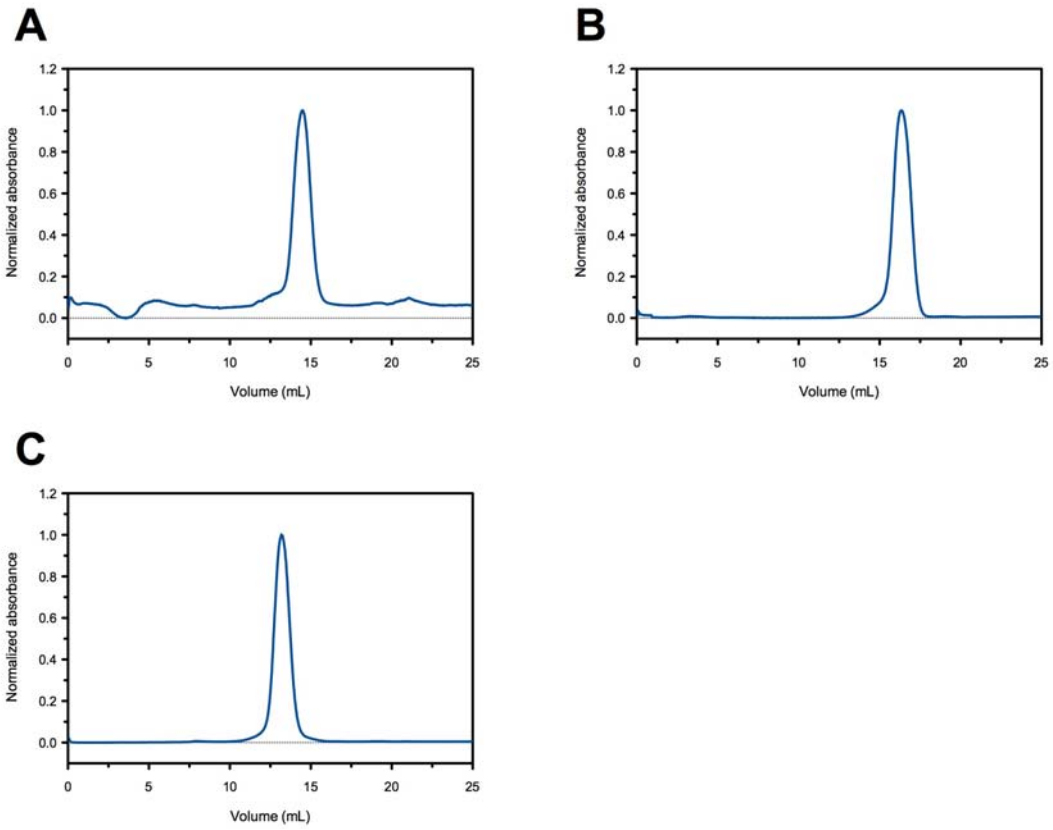

Figure 53 – Analytical size exclusion profile for: **A**, D1; **B**, J1; **C**, 1-1N.